Turun yliopisto
University of Turku

NEW [^{18}F]TRACERS FOR ALZHEIMER'S

DISEASE IMAGING

Labeling synthesis and biological testing.

Johanna Rokka

University of Turku

Faculty of Medicine
Department of Clinical Physiology and Nuclear Medicine
Turku PET Centre
Turku Doctoral Programme of Molecular Medicine TuDMM

Supervised by

Professor Olof Solin, PhD
Turku PET Centre
University of Turku
Turku, Finland

Adj. Professor Merja Haaparanta-Solin, PhD
Turku PET Centre
University of Turku
Turku, Finland

Professor Juha O. Rinne, MD, PhD
Turku PET Centre
University of Turku
Turku, Finland

Reviewed by

Professor
Jari Yli-Kauhaluoma, PhD
Faculty of Pharmacy
University of Helsinki
Helsinki, Finland

Dr. Jordi Llop, PhD
Molecular Imaging – Radiochemistry
CIC biomaGune
San Sebastian, Spain

Opponent

Professor Sharon Stone-Elander, PhD
Department of Clinical Neuroscience
Karolinska Institutet
Stocholm, Sweden.

Raila-mammalle ja Marjatta-mummille

ABSTRACT

Johanna Rokka

NEW [^{18}F]TRACERS FOR ALZHEIMER'S DISEASE IMAGING. LABELING SYNTHESIS AND BIOLOGICAL TESTING.

University of Turku
Faculty of Medicine
Department of Clinical Physiology and Nuclear Medicine, Turku PET Centre
Turku Doctoral Programme of Molecular Medicine TuDMM

Alzheimer's disease (AD) is the most common form of dementia. Characteristic changes in an AD brain are the formation of β-amyloid protein (Aβ) plaques and neurofibrillary tangles, though other alterations in the brain have also been connected to AD. No cure is available for AD and it is one of the leading causes of death among the elderly in developed countries.

Liposomes are biocompatible and biodegradable spherical phospholipid bilayer vesicles that can enclose various compounds. Several functional groups can be attached on the surface of liposomes in order to achieve long-circulating target-specific liposomes. Liposomes can be utilized as drug carriers and vehicles for imaging agents.

Positron emission tomography (PET) is a non-invasive imaging method to study biological processes in living organisms. In this study using nucleophilic ^{18}F-labeling synthesis, various synthesis approaches and leaving groups for novel PET imaging tracers have been developed to target AD pathology in the brain. The tracers were the thioflavin derivative [^{18}F]flutemetamol, curcumin derivative [^{18}F]treg-curcumin, and functionalized [^{18}F]nanoliposomes, which all target Aβ in the AD brain. These tracers were evaluated using transgenic AD mouse models. In addition, ^{18}F-labeling synthesis was developed for a tracer targeting the S1P$_3$ receptor.

The chosen ^{18}F-fluorination strategy had an effect on the radiochemical yield and specific activity of the tracers. [^{18}F]Treg-curcumin and functionalized [^{18}F]nanoliposomes had low uptake in AD mouse brain, whereas [^{18}F]flutemetamol exhibited the appropriate properties for preclinical Aβ-imaging. All of these tracers can be utilized in studies of the pathology and treatment of AD and related diseases.

Keywords: Alzheimer's disease, β-amyloid, Functionalized nanoliposomes, Positron emission tomography (PET), PET tracer, Nucleophilic ^{18}F-labeling, S1P$_3$ receptor

TIIVISTELMÄ

Johanna Rokka

UUSIEN ALZHEIMERIN TAUDIN [^{18}F]MERKKIAINEIDEN LEIMAUSSYNTEESI JA
BIOLOGINEN TESTAUS

Turun yliopisto
Lääketieteellinen tiedekunta
Kliininen fysiologia ja isotooppilääketiede, Valtakunnallinen PET-keskus
Molekyylilääketieteen tohtoriohjelma TuDMM

Annales Universitatis Turkuensis Sarja - ser. D osa - tom. 1156
Suomen Yliopistopaino Oy, Juvenes Print - Turku, Suomi 2015

Alzheimerin tauti on yleisin dementiasairaus. Tyypillisimmät Alzheimerin taudin aiheuttamat muutokset ovat β-amyloidi(Aβ)proteiinista koostuvien plakkien sekä hermosäievyyhteiden muodostuminen aivoihin. Alzheimerin tautiin on liitetty myös muita aivomuutoksia. Tällä hetkellä Alzheimerin tautiin ei ole parantavaa hoitoa. Ikääntyneiden keskuudessa Alzheimerin tauti on yksi tavallisimmista kuolemaan johtavista syistä.

Liposomit ovat biologisesti yhteensopivia, luontaisesti hajoavia, pallomaisia kaksoisfosfolipidikerroksellisia vesikkeleitä, jotka voivat sulkea sisälleen erilaisia yhdisteitä. Liposomin pintaan voidaan liittää useita erilaisia funktionaalisia ryhmiä, jotta saadaan elimistössä pitkään kiertäviä, tarkoin kohdennettuja liposomeja. Liposomeja voidaan käyttää lääkeaineiden ja kuvantamisaineiden kuljettimina.

Positroniemissiotomografia (PET) on kuvantamismenetelmä, jonka avulla voidaan tutkia biologisia prosesseja elävässä eliössä. Tässä tutkimuksessa nukleofiiliseen ^{18}F-fluorileimaukseen perustuvien synteesireittien avulla kehitettiin uusia merkkiaineita Alzheimerin taudin aivomuutosten tutkimiseen. Kehitetyt merkkiaineet olivat tioflaviinijohdos [^{18}F]flutemetamoli, kurkumiinijohdos [^{18}F]treg-kurkumiini sekä funktionalisoituja [^{18}F]nanoliposomeja. Kaikki nämä yhdisteet kohdistuivat Alzheimerin taudin Aβ plakkeihin. Merkkiaineet evaluoitiin käyttäen Alzheimerin tautia mallintavia siirtogeenihiiriä. Lisäksi kehitettiin S1P₃-reseptoriin kohdentuvan merkkiaineen ^{18}F-leimaussynteesi.

Valitulla ^{18}F-leimaussynteesistrategialla on vaikutusta merkkiaineen radiokemialliseen saantoon ja ominaisaktiivisuuteen. [^{18}F]Treg-kurkumiini sekä funktionaaliset [^{18}F]nanoliposomit kertyivät vain vähän koe-eläimen aivoihin, kun taas [^{18}F]flutemetamoli osoittautui sopivan käyttökelpoiseksi prekliiniseen kuvantamiseen. Kaikkia tässä työssä kehitettyjä merkkiaineita voidaan käyttää tutkittaessa Alzheimerin taudin ja samanlaisten sairauksien patologiaa ja hoitoa.

Avainsanat: Alzheimerin tauti, β-amyloidi, funktionalisoidut nanoliposomit, positroniemissiotomografia (PET), PET-merkkiaine, nukleofiilinen ^{18}F-leimaus, S1P₃-reseptori

6

CONTENTS

ABBREVIATIONS

AD	Alzheimer's disease
Aβ	β-amyloid
ApoE	Apolipoprotein E
BBB	Blood-brain barrier
CNS	Central nervous system
CT	Computed tomography
DMF	*N,N*-Dimethyl formamide
DMSO	Dimethyl sulfoxide
DLS	Dynamic light scattering
EOB	End of bombardment
EOS	End of synthesis
HPLC	High performance liquid chromatography
LC	Liquid chromatography
LDLrs	Low-density lipoprotein receptors
MR	Magnetic resonance
MS	Mass spectrometry
NIR	Near infrared spectroscopy
PdI	Polydispersity index
PEG	Polyethyleneglycol
PET	Positron emission tomography
PLGA	Polylactic-co-glycolic acid
PSL	Photo-stimulated luminescence
RAC	Radioactive concentration
RCC	Radiochemical conversion
RCP	Radiochemical purity
RCY	Radiochemical yield
RES	Reticulo-endothelial system
S1P	Sphingosine-1-phosphate
S1PR	Sphingosine-1-phosphate receptor
SphK	Sphingosine kinase
SA	Specific activity
SPR	Surface plasmon resonance
SUV	Standard uptake value
THF	Tetrahydrofuran
TLC	Thin layer chromatography
UV	Ultraviolet

LIST OF ORIGINAL PUBLICATIONS

This thesis is based on the following original publications, which are referred to in the text by their Roman numerals.

I.   Rokka J, Federico C, Jurttila J, Snellman A, Rinne JO, Haaparanta M, Solin O: *$^{19}F/^{18}F$ exchange synthesis for a novel [^{18}F]S1P$_3$ –radiopharmaceutical* J Label Compd Radiopharm 2013;56:385-391.

II.   Snellman A, Rokka J, Lopez-Picon FR, Eskola O, Wilson I, Farrar G, Scheinin M, Solin O, Rinne JO, Haaparanta-Solin M: *Pharmacokinetics of [^{18}F]flutemetamol in wild-type rodents and its binding to beta amyloid deposits in a mouse model of Alzheimer's disease* Eur J Nucl Med Mol Imaging 2012;39:1784-1795.

III.   Rokka J, Snellman A, Zona C, La Ferla B, Nicotra F, Salmona M, Forloni G, Haaparanta-Solin M, Rinne JO, Solin O: *Synthesis and evaluation of a ^{18}F-curcumin derivate for β-amyloid plaque imaging* Bioorg Med Chem. 2014;22(9):2753-2762.

IV.   Rokka J, Snellman A, Kaasalainen M, Salonen J, Zona C, La Ferla B, Nicotra F, Re F, Masserini M, Forsback S, Lopez-Picon F, Rinne JO, Haaparanta-Solin M, Solin O: *^{18}F-labeling syntheses and preclinical evaluation of functionalized nanoliposomes tailored for theranostics of Alzheimer´s disease.* Submitted

1. INTRODUCTION

Alzheimer's disease (AD) is the most common form of dementia (Duthey, 2013). Several alterations in the brain are connected to AD, the characteristics of which are the formation of β-amyloid protein (Aβ) plaques and neurofibrillary tangles in AD brain (Nordberg et al., 2010, Serrano-Pozo et al., 2011). These characteristic changes were first observed by Professor Alois Alzheimer in 1906 when he examined his patient's brain after her death (Mauer et al., 1997). Although knowledge about AD has grown during the last century, the underlying causes are still unknown. Currently, there are approximately 36.5 million AD patients in the world and no curative treatment is available (Duthey, 2013, Alzheimer's Association, 2014).

Nanoliposomes are closed phospholipid bilayer structures that can both encapsulate compounds and have functional groups attached on the surface (Torchilin, 2006, Allen and Cullis, 2013). Liposomes can be applied in medicine and cosmetics (Torchilin, 2006, Liu and Welchs, 2012, Allen and Cullis, 2013). In medicine, functionalized nanoliposomes are used in drug delivery and offer an interesting platform for combining therapy and multimodality imaging agents (Torchilin, 2006, Liu and Welchs, 2012, Allen and Cullis, 2013). The biggest drawback of nanoliposomes has been fast opsonin recognition and clearance from the blood to the reticulo-endothelial system (RES) (Moghimi et al., 2001, Trochilin, 2006). Several approaches have been developed to create long-circulating stealth liposomes, polyethylene glycol (PEG) functionalization being one of the most commonly used (Moghimi et al., 2001, Trochilin, 2006, Allen and Cullis, 2013). Nanoliposome surface functionalization is also used to enhance liposome entry into the tissue of interest and target-specific binding, as well as to attach imaging agents (Torchilin, 2006, Liu and Welchs, 2012, Allen and Cullis, 2013). Research on functional groups and functionalized liposomes aiming at developing long-circulating target-specific functionalized nanoliposomes for medicinal applications (Torchilin, 2006, Liu and Welchs, 2012, Allen and Cullis, 2013) is currently being carried out by many research groups.

Positron emission tomography (PET) is a non-invasive imaging technique that can be used to study biological processes in living organisms. For a PET study, the tracer (a compound labeled with a positron-emitting nuclide) is administered to the subject under

investigation. Several positron emitters can be used for labeling the PET tracers, and the most commonly used are ^{11}C, ^{13}N, ^{15}O, ^{18}F, and ^{68}Ga. These positron emitters decay primarily by positron emission (β^+) followed by annihilation, which results in two 511 keV γ rays that can be detected with the PET camera.

Before PET imaging can be used as a diagnostic tool in a clinical setting, the PET tracer needs to be synthesized and evaluated (Figure 1.1). First, the positron emitter is produced with a cyclotron or radionuclide generator, and is then attached to a molecule during PET tracer synthesis. The tracer binding properties and specificity for the target are studied in vitro using cell cultures, peptide extracts, or post-mortem tissue sections. The pharmacokinetic properties of the tracer are then studied in experimental animals using in vivo or ex vivo methods (Figure 1.1.).
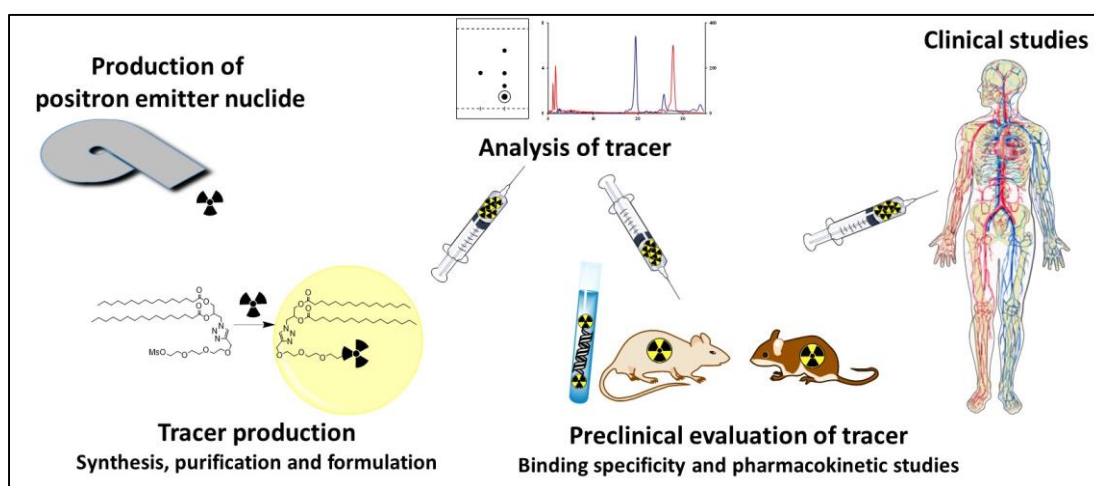
Figure 1.1. Chart of new tracer production and evaluation. The PET tracer is synthesized and analyzed, and then evaluated preclinically before it can be administered to humans.

This thesis describes the development of new PET tracers for imaging in AD (Figure 1.2.). The studied tracers were thioflavin and curcumin derivatives (study II-III) and functionalized nanoliposomes (study IV) targeting Aβ, and a derivative of indole-3-carboxylic acid amide targeting S1P$_3$ receptors (study I) in the AD brain. The tracers were labeled via nucleophilic ^{18}F-fluorination and the Aβ-tracers preclinically evaluated using transgenic mouse models of AD.
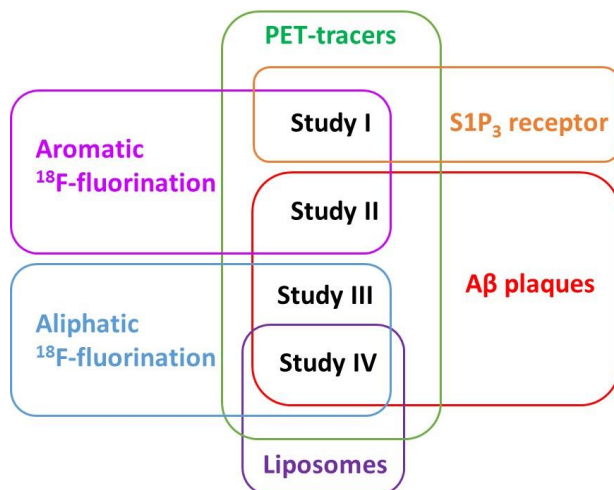
Figure 1.2. Relationships between studies I - IV, ^{18}F-fluorination methods, and targets in the AD brain.

2. REVIEW OF THE LITERATURE

2.1. Synthesis of ^{18}F-labeled PET tracers

2.1.1. Nucleophilic labeling

Fluorine-18 (^{18}F) is a positron emitter that has a half-life of 109.8 min and decays mainly by positron emission. Due to its relatively long half-life and positron decay properties, ^{18}F is one of the most commonly used radionuclides for PET studies. Nucleophilic ^{18}F-fluorination is the most common method for synthesizing ^{18}F-labeled PET tracers. In nucleophilic reactions, the ^{18}F-fluoride ion (^{18}F$^-$) substitutes the leaving group from the precursor molecule. This reaction is suitable both for aliphatic and aromatic nucleophilic ^{18}F-substitutions. Nucleophilic ^{18}F-fluorination is an efficient reaction that can produce large quantities of tracer with high specific activity (SA).

^{18}F$^-$ is usually produced via the ^{18}O(p,n)^{18}F nuclear reaction; ^{18}O-enriched water is irradiated with cyclotron-accelerated high energy protons in the cyclotron target chamber (Figure 2.1., Solin et al., 1988). The resultant ^{18}F$^-$ is in aqueous solution and needs to be transformed into a more reactive form. This is achieved by (i) replacing the countercation and (ii) removing excess water via the acetonitrile assisted azeotropic distillation. Because of the nature of fluoride, the spontaneously formed ion bond between ^{18}F$^-$ and the countercation in aqueous solution is very strong, hampering the nucleophilic ^{18}F-labeling reaction. Thus, ^{18}F$^-$ requires a countercation that allows ^{18}F-fluoride to react with a precursor molecule. In addition, the introduction of a suitable countercation increases the solubility of ^{18}F$^-$ in organic solvents; this is important because nucleophilic ^{18}F-fluorination is usually performed in organic media (Cai et al., 2008). Suitable countercations for ^{18}F$^-$ are heavy alkali metals, such as cesium and rhodium, both of which have been used successfully in nucleophilic ^{18}F-fluorination reactions (Figure 2.1., Tewson et al., 1978, Levy et al., 1982, Attina et al., 1983, Berridge et al., 1983, Pascali et al., 1990, Mu et al., 2012). Currently, the most commonly used countercations for ^{18}F$^-$ are tetraalkyl ammonium ions (Figure 2.1., Culbert et al., 1995) and macrocyclic aminopolyether-potassium complexes; among these, the complex of potassium and Kryptofix 2.2.2 is the most widely used (Figure 2.1., Lehn and Sauvage, 1971, Spitznagle and Marino, 1977, Hamacher et al., 1986). All countercations are usually introduced to aqueous ^{18}F-solution as carbonates, bicarbonates, hydroxides, or oxalates. Concurrently

weakly basic conditions are generated, preventing the protonation of ^{18}F-fluoride and increasing the reactivity of ^{18}F$^-$ (Cai et al., 2008).
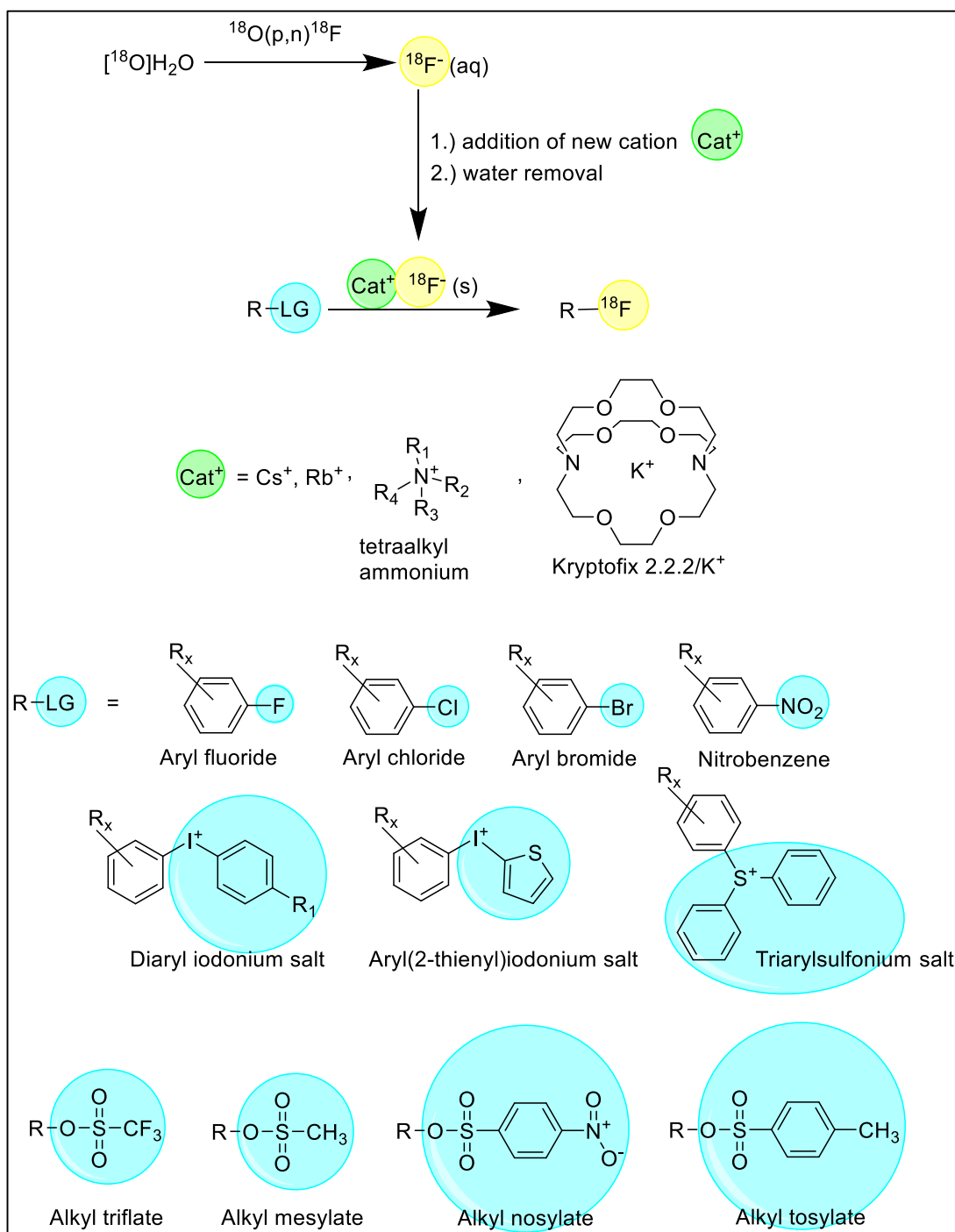
Figure 2.1. The nucleophilic ^{18}F-labeling reaction. The structures and names of countercations (Cat$^+$) and leaving groups (LG) that are commonly used in nucleophilic ^{18}F-labeling reactions are given underneath the reaction scheme.

The leaving group of the precursor molecule is chosen to support the selected labeling route. Several leaving groups can be used (Figure 2.1., Cai et al., 2008). The main task of the leaving group is to balance the electron density during the nucleophilic ^{18}F-

fluorination reaction. The leaving group should also be easily displaced from the precursor molecule. As the leaving group has a clear impact on the reaction kinetics, it must be selected carefully. The ^{18}F-labeling strategy and the structure of the precursor molecule will designate the most suitable leaving group for the reaction.

In aromatic nucleophilic ^{18}F-fluorination reactions, ^{18}F is attached directly to the aromatic ring (Figure 2.1.). This reaction usually requires a long reaction time at an elevated temperature. The nitro group has been the classic choice as a leaving group. The ^{18}F-substitution of the nitro group is effective, especially if there is a nitro or cyano group at the *ortho* or *para* positions of the aryl ring (Attina et al., 1983). High radiochemical yields (RCYs) have also been achieved in one-step ^{18}F-labeling of benzaldehydes and methoxybenzaldehydes if a nitro group is used as a leaving group (Shen et al., 2009). Several radiotracers have been synthesized using ^{18}F-substitution of a nitro group, including Aβ imaging agents [^{18}F]flutemetamol (Storey et al., 2007) and [^{18}F]AZD4694 (Swahn et al., 2012).

Halides, mainly chlorine and bromine, have also been widely used as the leaving group of nucleophilic ^{18}F-labeling reactions. Using *p*-halideacetophenone as a model compound, chlorine was found to be the best leaving group, followed by bromine, whereas iodine is the worst leaving group within halides (Hashizume et al., 1997). A nitro, cyano, or aldehyde group at the *para* position of the aryl ring assists in aromatic halide substitution by [18]F$^-$ (Cai et al., 2008). PET tracers such as [^{18}F]haloperidol, [^{18}F]PK 14105, and [^{18}F]flutemetamol, have been produced from chlorine derivative precursors (Pascali et al., 1990, Hashizume et al., 1997, Mathis et al., 2003a). ^{18}F-labeling of several [3,2-*c*]pyrazolo steroids has also been performed using 2-chloropyridyl and 2-chloropyrimidyl derivatives as precursor molecules (Hoyte et al., 2002, Kahn et al., 2006). In the two-step synthesis of [^{18}F]-(S)-fluoxetine, ^{18}F-fluorination was performed by substituting bromine from 1-[bromo(difluoro)methyl]-4-chlorobenzene (Hammadi and Crouzel, 1993).

Aryliodonium and arylsulfonium salts are used for aromatic ^{18}F-fluorination under mild conditions. Diaryliodonium salts have been used as precursor molecules for one-step nucleophilic ^{18}F-labeling of electron-deficient aryl rings (Pike and Aigbirhio, 1995). In this reaction [18]F$^-$ is selectively attached to the more electron-deficient aryl ring. Aryl(2-thienyl)iodonium salt has been used for one-step ^{18}F-fluorination of electron-rich aryl

rings (Ross et al., 2007). Ortho-substituents in aryl rings enhance the reaction between iodonium salts and [18]F⁻. Triarylsulfonium salts can be used for nucleophilic ^{18}F-fluorination of non-activated aromatic compounds with high RCY (Mu et al., 2012).

For aliphatic nucleophilic ^{18}F-fluorination, several sulfonates (e.g., triflates, tosylates, mesylates, and nosylates) can act as favourable leaving groups (Figure 2.1.). ^{18}F-substitution of sulfonates is efficient, especially if the leaving group is attached to the primary carbon atom (Cai et al., 2008). These ^{18}F-labeling reactions can be performed under mild conditions, as only moderate and short heating is required to achieve high RCY (Cai et al., 2008). Triflate is an excellent leaving group and has been used, for example, in the nucleophilic ^{18}F-fluorination of glucose [^{18}F]derivatives (Tewson et al., 1978, Gatley et al., 1980, Levy et al., 1982, Hamacher et al., 1986). Indeed, triflate precursor is currently utilized worldwide for the production of the well known radiotracer [^{18}F]FDG (Hamacher et al., 1986). Mesylate is used, for example, in the synthesis of 21-[^{18}F]fluoroprogesterone (Spritznagle and Marino, 1977), 6- and 7-[^{18}F]fluoropalmitate acids (Berridge et al., 1983), and [^{18}F]florbentaben (Zhang et al., 2005). Nosylate has been used as a leaving group in nucleophilic ^{18}F-fluorination of nucleoside derivatives (Grierson et al., 2000, Oh et al., 2004, Kang et al., 2006) and [^{18}F]curcumin derivative (Lee et al., 2011). Tosylate has been used in the synthesis of [^{18}F]fluoroalkyl reagents (Cai et al., 2008) and for direct ^{18}F-labeling of amyloid imaging agents [^{18}F]FDDNP (Agdeppa et al., 2001), [^{18}F]florpentapir (Choi et al., 2009), and [^{18}F]fluoropropoxycurcumin (Ruy et al., 2006).
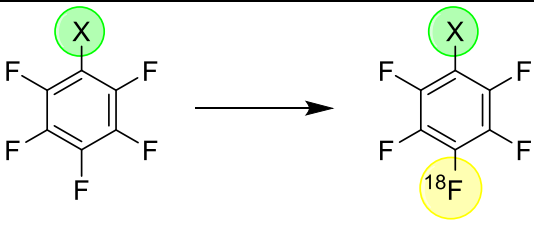
2.1.2.   *[19]F/^{18}F isotope exchange reaction*

The ^{19}F/^{18}F isotope exchange reaction relies on the nucleophilic aromatic substitution mechanism (Cacace et al., 1982). Several studies have examined the effects of the molecular structure of the precursor compound and the kinetic parameters of the ^{19}F/^{18}F isotope exchange reaction to optimize the RCY and increase the specific radioactivity SA of the end product (Cacace et al., 1981, Cacace et al., 1982, Kilbourn and Subramaian, 1990, Blom et al., 2009, Malik et al., 2011).

With polyfluorobenzenes, the rate of the ^{19}F/^{18}F isotope exchange reaction is highly dependent on the other substituents in the ring, and the exchange rate increases as a function of the reaction temperature (Table 2.1., Cacace et al., 1982, Blom et al., 2009).

For hexafluorobenzene and for pentafluorobenzene substituted with the trifluoromethyl, the nitro or the formyl group the isotope exchange reaction occurs at room temperature with good yields (Blom et al., 2009). In pentafluorobenzenes, bromo and chloro substituents accelerate the exchange rate compared to unsubstituted pentafluorobenzene and hexafluorobenzene (Cacace et al., 1982). However, ^{18}F-substitution on the chloro or bromo positions has been observed as a side reaction (Cacace et al., 1982). In fluorobenzophenones, the yield of the ^{19}F/^{18}F isotope exchange reaction is dependent on the position of fluorine atoms on the aryl ring (Blom et al., 2009). The exchange reaction occurs preferentially at the fluorine atom located in the *para* or *ortho* position of the carbonyl group, and to a much lower extent at the *meta* position. With electron-donating substituents such as amino, *N*-methylamino, hydroxide-substituted pentafluorobenzenes, and *N*-(pentafluorophenyl)formamide or *N*-(pentafluorophenyl)benzamide only minor reaction has been observed, even if the reaction solution is heated (Blom et al., 2009). With 2-fluoropyridine, the ^{19}F/^{18}F isotope exchange reaction requires elevated temperatures (Malik et al., 2011). Methoxy and methyl substituents at the pyridine ring decrease the reaction yield (Malik et al., 2011).
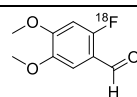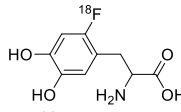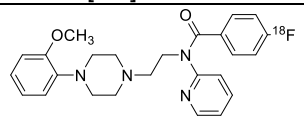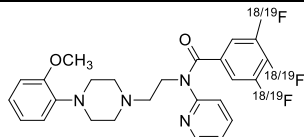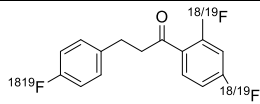
Table 2.1. ^{19}F/^{18}F isotope exchange reactions of polyfluorobenzenes and the substituents that increase or decrease the exchange reaction rate.
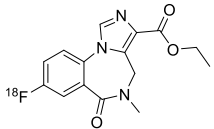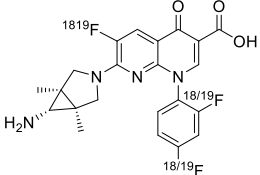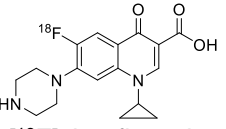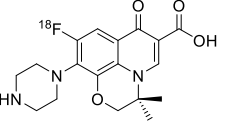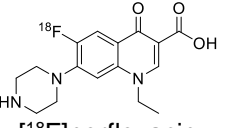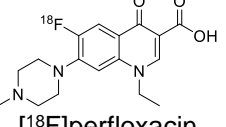
X		Reference
F	Increase the exchange reaction rate	Blom et al., 2009, Cacade et al., 1982
H		Cacade et al., 1982
Cl		
Br		
CHO		Blom et al., 2009
NH$_2$	Decrease the exchange reaction rate	Blom et al., 2009
NHCH$_3$		
OH		
NHCHO		
NHCOC$_6$H$_5$		

The $^{19}F/^{18}F$ isotope exchange reaction has not been observed with multifluoroalkylbenzenes or multifluoroalkanes (Blom et al., 2009), but moderately high yields have been achieved with 1,1-difluoro-2,2-dichloroethyl aryl ethers (Kilbourn and Subramanian, 1990). This reaction is dependent on the substituents on the aryl ring, reaction temperature, and reaction time (Kilbourn and Subramanian, 1990). A nitro group at the *meta* position of the phenyl ring contributes to the isotope exchange reaction and increases the yield compared to phenyl ether, but the yields of *para*-fluorophenyl ethers are decreased by the effect of fluorine. Higher reaction temperature, greater precursor concentration, and prolonged reaction time increase the yield.

Several PET tracers have been produced using the $^{19}F/^{18}F$ isotope exchange reaction, including 6-[^{18}F]fluoroverataldehyde, a labeling block for 6-[^{18}F]fluoro-L-DOPA synthesis (Al-Labadi et al., 2006), 6-[^{18}F]fluoro-L-DOPA (Wagner et al., 2009), 4-[^{18}F]fluorophenyl and 3,4,5-tri[^{18}F]fluorophenyl derivatives of WAY-100635 (Blom et al., 2009), *N*-methyl-[^{18}F]flumazenil (Ryzhikov et al., 2004), and the antibiotics [^{18}F]trovafloxacin ([^{18}F]CP 99,219, Babich et al., 1996), [^{18}F]ciprofloxacin (Langer et al., 2003a), [^{18}F]levofloxacin, [^{18}F]norfloxacin, and [^{18}F]pefloxacin (Langer et al., 2003b) (Table 2.2).

Table 2.2. ^{18}F-labeled tracers produced using the $^{19}F/^{18}F$ isotope exchange reaction. Tracer name and structure, initial ^{18}F-activity (A_0), $^{19}F/^{18}F$ isotope exchange reaction temperature (Δ), radiochemical conversion (RCC) after the ^{18}F-fluorination reaction, number of reaction steps after ^{18}F-fluorination, and the RCY and specific activity (SA) at the end of the synthesis (EOS) are listed. A dash (–) indicates that the information was not provided in the article.

Tracer	A_0 [GBq]	Δ [˚C]	RCC after [^{18}F]fluorination [%]	Reaction steps after [^{18}F]fluorination	RCY @ EOS [%]	SA @ EOS[µmol/ GBq]	Reference
6-[^{18}F]fluoroveratraldehyde	10 -20	140	85 ± 5	0	-	-	Al-Labadi et al., 2006
6-[^{18}F]-L-DOPA	-	110	50	3	22	1.5	Wagner et al., 2009
[^{18}F]4-fluorophenyl derivative of WAY-100635	0.5	150	8 ± 1	0	-	0.01	Blom et al.,. 2009
[^{18}F]3,4,5-trifluorophenyl derivative of WAY-100635	1	150	35 ± 3	0	-	0.58	Blom et al., 2009
[^{18}F]1-(2,4-difluorophenyl)-3-(4-fluorophenyl)propan-1-one	5.3	150	60 ± 5	0	-	1	Blom et al., 2009

Structure							
N-methyl-[18F]flumazenil	7.4	130	62 ± 8	-	47 ± 3	0.37	Ryzhikov et al., 2004
[18F]trovafloxacin	-	160	---	0	15 - 30	-	Babich et al., 1996
[18F]ciprofloxacin	52.5 ± 11.3	180	23 ± 7	1	2.5	0.43 ±0.20	Langer et al., 2003a
	60 -65	180	78 ± 7	1	-	-	Langer et al., 2003b
[18F]levofloxacin	60 - 65	180	59 ± 7	1	-	-	Langer et al., 2003b
[18F]norfloxacin	57.6	180	29 ± 4	1	3.5	0.303	Langer et al., 2003b
[18F]perfloxacin	50.55	180	29 ± 4	1	3.8	0.909	Langer et al., 2003b

2.1.3. *Click chemistry*

Click chemistry is a method used to introduce the ^{18}F label to a complex molecule under mild aqueous conditions. In a first step, a small molecule is labeled with [^{18}F]fluoride, and then the [^{18}F]compound is clicked with a larger molecule to obtain the desired [^{18}F]molecule. The first click approaches utilized copper-catalyzed 1,3-dipolar Huisgen cycloaddition, in which copper(I) catalyzed the reaction of one azide and one alkyne, yielding a 1,2,3-triazole ring at room temperature (Figure 2.2, Huisgen, 1963, Pretze et al., 2013). In this reaction, either the azide or alkyne compound can be ^{18}F-labeled before the click reaction. Copper-catalyzed 1,3-dipolar Huisgen cycloaddition was first exploited in ^{18}F-labeling of peptide derivatives (Marik et al., 2006, Glaser and Årstad, 2007), but it has also been adapted for the synthesis of various ^{18}F-tracers, such as glucose derivatives, nanoparticles, and markers of apoptosis (Pretze et al., 2013, Devaraj et al., 2009).

One of the pitfalls of copper-catalyzed 1,3-dipolar Huisgen cycloaddition is the cytotoxicity of copper. To overcome this problem, copper-free click chemistry was developed. The most commonly used 1,3-dipolar Huisgen cycloaddition-related copper-free click approach is the reaction of cyclooctyne with an azide group, which yields a triazole ring (Figure 2.2, Baskin et al., 2007, Pretze et al., 2013). A similar copper-free reaction is the tetrazine-click in which a strained cyclooctene reacts with tetrazine in an inverse electron-demand Diels-Alder reaction (Figure 2.2, Blackman et al., 2008). These reactions are as effective as 1,3-dipolar Huisgen cycloaddition under physiological conditions (Baskin et al., 2007, Blackman et al., 2008, Campbell-Verduyn et al., 2011, Pretze et al., 2013).
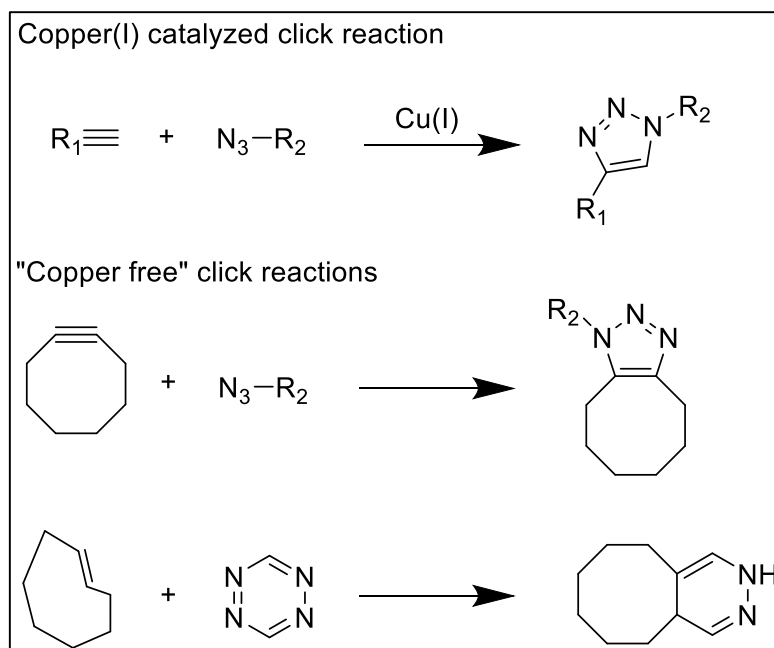
Figure 2.2. General reaction of the copper(I) catalyzed click reaction and copper-free click reactions.

Copper-free click reactions can be performed in vivo (Carpenter et al., 2011, Campbell-Verduyn et al., 2011, Devaraj et al., 2012, Emmetiere et al., 2013, Zeglis et al., 2013, Pretze et al., 2013, Knight and Cornelissen, 2014). The general idea behind in vivo click chemistry is to perform the bioorthogonal cyclization reaction in the tissue of interest. The first reaction component is administered to the experimental animal and allowed to accumulate in the tissue of interest (Knight and Cornelissen, 2014) before the radiolabeled component is administered to the same experimental animal. When the radiolabeled compound reaches the tissue of interest, a spontaneous condensation reaction occurs, resulting in selective trapping of the radioactivity in the tissue of interest. Using a pre-targeting strategy, long circulating, unlabeled compounds targeting specific tissues (e.g., monoclonal antibodies) can be used. If the labeled compound (able to undergo the *in vivo* click reaction with the first compound) has a fast clearance, shorter lived positron emitters can be used, resulting in a lower radiation dose to the subject under investigation and enhanced signal-to-noise ratio. Bioorthogonal pre-targeting approaches have been used in PET imaging for, for example, peptide, antibody, and liposome labeling (Baskin et al., 2007, Blackman et al., 2008, Campbell-Verduyn et al., 2011, Emmetiere et al., 2013, Pretze et al., 2013).

2.1.4. Analysis of [^{18}F]tracers

[^{18}F]tracers are analyzed using chromatographic methods, mainly high performance liquid chromatography (HPLC) and thin layer chromatography (TLC). HPLC and TLC methods can be used to assess reaction kinetics or to determine the quality of the purified tracer. Usually the identity, RCY, radiochemical purity (RCP), and SA of the tracer are measured with these chromatographic methods.

The HPLC method usually employs a UV detector in series with a radioactivity detector in the outflow of the HPLC column. The radioactivity detector in HPLC systems is usually a scintillation detector that detects γ radiation, but β radiation detectors are also used. To increase the sensitivity, γ-γ- and β-γ-γ-coincidence detectors can be used (Nickles et al., 1992). HPLC is used to determine SA because the concentration and radioactivity of the sample can be measured using the same HPLC run. HPLC can also be used to determine the identity, RCY, and RCP of [^{18}F]tracer. If the [^{18}F]tracer does not have UV absorption properties, LC/MS combined with a radioactivity detector (radioLC/MS method) can be used to identify the [^{18}F]tracer. RadioLC/MS and radioLC/MS/MS are also excellent techniques for identifying related [^{18}F] substances or isomers of [^{18}F]tracer in reaction mixtures (Kirjavainen et al., 2013). Alternativelly to the MS, refraction index or conductometric detectors, among others, can be used.

Photo-stimulated luminescence (PSL) digital autoradiography is a method that detects positron emission using storage phosphorimaging plates. This method is useful for detecting radioactivity distribution on a TLC plate, as the method is very sensitive and has a broad linear range from 0.2 Bq to 2 kBq (Haaparanta et al., 2006, Kämäräinen et al., 2006). TLC combined with PSL digital autoradiography is especially useful for reaction kinetic analysis because only small aliquots of sample are needed and several samples can be analyzed simultaneously in a short period of time. In addition, identity, RCC, and RCP can be determined with the combined TLC/PSL digital autoradiography method. Besides PSL digital autoradiography also film autoradiography or different TLC scanners which detect the radioactivity direct from TLC plate can be used (Solin, 1983, Kämäräinen et al., 2006).

2.2. Liposomes

2.2.1. *General*

Liposomes are spontaneously forming, spherical phospholipid bilayer vesicles found in aqueous systems (Allen and Chonn, 1987, Torchilin, 2005, Phillips et al., 2009). Liposomes ares composed of naturally occurring components or their derivatives (Allen and Chonn, 1987, Torchilin, 2005, Phillips et al., 2009). Thus, liposomes are biocompatible and biodegradable. The structure of liposomes is flexible and easy to modify, which allows easy adjustment of a liposome's size from a few nanometers to several micrometers (Jesorka and Orwar, 2008, Torchilin, 2005, Allen and Chonn, 1987). Liposomes can enclose hydrophilic and hydrophobic compounds. In medicinal applications, liposomal encapsulation can be utilized to protect the drug from early metabolic breakdown, minimize the adverse effects of the drug, and increase the rate of intracellular delivery (Torchilin, 2005, Immordino et al., 2006, Li and Huang, 2008, Jesorka and Orwar, 2008, Allen and Cullis, 2013). This use is especially interesting in the pharmaceutical and medical fields, as liposomal drugs can reduce the dose of the drug without compromising its effect. Currently, several biomedical liposome applications are in use and the research in this field is undergoing fast progress (Torchilin, 2005, Jesorka and Orwar, 2008, Allen and Cullis, 2013).

One of the major disadvantages of liposomes is the fast recognition by opsonins and elimination from the blood to the reticulo-endothelial system (RES) (Moghimi et al., 2001, Torchilin, 2005). Liposomes ranging from 50 to 250 nm show decreased uptake by the RES (Allen and Chonn, 1987, Levchenko et al., 2002, Li and Huang, 2008). Thus, nanoliposomes that are less than 300 nm are the focus of research. To overcome early clearance, the lipid composition of liposomes has been optimized and different functional groups attached to the liposome surface have been tested (Allen and Chonn, 1987, Webb et al., 1995, Moghimi et al., 2001, Torchilin, 2005, Allen and Cullis, 2013). For example, liposomes that consist of a mixture of cholesterol and sphingomyelin have shown longer circulation times in the blood and slow accumulation in the liver and the spleen of mice (Allen and Chonn, 1987, Webb et al., 1995, Levchenko et al., 2002). The size and lipid composition of liposomes have also been shown to affect liposome distribution in the rat brain (MacKay et al., 2005).

Polyethyleneglycol (PEG) functionalization has been shown to decrease liposome elimination to the RES (Klibanov et al., 1990, Levchenko et al., 2002); hence, pegylation is one of the most widely used methods for the preparation of long-circulating liposomes (Moghimi et al., 2001, Torchilin, 2005). Liposomes can also be functionalized to favour accumulation in the tissue of interest and specifically bind to the target (Moghimi et al., 2001, Torchilin 2005). The high surface area-to-volume ratio also enables the multifunctionalization of liposomes with various ligands to obtain long-circulating target-specific liposomes.

2.2.2. *Preparation of liposomes*

Liposomes were first introduced by Bangham et al. in 1965, when they reported the synthesis of close packed lipid-containing membranes (Bangham et al., 1965). Using the method called thin film hydration, or the Bangham method (Figure 2.3). In this method, organic solutions of lipids are mixed together and the organic solvent evaporated to dryness using a rotary evaporator (Bangham et al., 1965). An aqueous solution, usually buffer or salt solution, is added to the vessel in order to rehydrate the lipids to obtain a solution of liposomes. Since then, several more advanced procedures have been developed for liposome production (Deamer and Bangham, 1976, Szoka and Papahadjopoulos, 1978, Kikuchi et al., 1991, Pons et al., 1993, Buboltz and Feigenson, 1999, Otake et al., 2001, Wagner et al., 2002, Stark et al., 2010, Zhigaltsev et al., 2012).
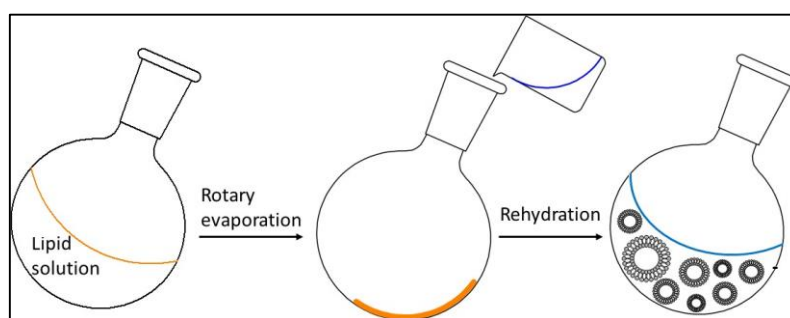
Figure 2.3. Scheme of liposome preparation by Bangham's thin film hydration.

Although the rehydration method generally affects the liposome particle size, any method by itself cannot yield a uniform size distribution (Woodbury et al., 2006). Extrusion is a method used to unify the size of liposomes in a solution (Olson et al., 1979). To extrude the liposome solution, it is pushed through a filter membrane. Polycarbonate membranes with a pore size fixed to that of the desired liposomes are commonly used (Olson et al.,

1979, Jesorka and Orwar, 2008). After extrusion the liposome solution needs to be purified, usually by column chromatography.

Several methods can be utilized for liposome functionalization (Aubin-Tam and Hamad-Schifferli, 2008). Functional groups can be covalently bound to the core lipid before liposome synthesis; alternatively, they can also be covalently or electrostatically bound on the surface of liposome after liposome preparation. To encapsulate the drug inside the liposome, the drug can be dissolved in the aqueous solution used for during liposome preparation; alternatively, the drug can be trapped inside the liposome after liposome preparation using, for example, a pH gradient (Torchilin, 2005, Allen and Cullis, 2013). This process is called remote loading.

2.2.3.   *Functionalized liposomes for passing the blood-brain barrier*

To enhance the passing of liposomes through the blood-brain barrier (BBB), various functional groups targeting different BBB receptors, such as transferrin, low-density lipoproteins, and glucose transport receptors (Lai et al., 2013, Xu et al., 2013) have been used. Cell penetrating peptides have also been used to enhance liposome BBB penetration (Lai et al., 2013, Xu et al., 2013). The functional groups used for BBB receptor targeting are often derived from natural receptor ligands (Lai et al., 2013, Xu et al., 2013).

Apolipoprotein E (ApoE) binds to the low-density lipoprotein receptors (LDLrs) on brain capillary endothelial cells and is transported through the BBB (Sauer et al., 2005, Lai et al., 2013). To utilize LDLrs as a transport route across the BBB liposomes have been functionalized with monomer ApoE 133-149 (COG 133) or with monomer and dimer ApoE 141-150 (Sauer et al., 2005, Re et al., 2011a, Re et al., 2011b, van Rooy et al., 2011, Bana et al., 2013). In vitro cell studies and studies in healthy mice have shown that COG 133 functionalization does not improve the BBB penetration of liposomes; thus, COG 133 is not a suitable ligand to improve BBB penetration of the liposomes (van Rooy et al., 2011). Liposomes functionalized with monomer or dimer ApoE 141-150 have shown higher uptake into human and rat brain capillary cells than non-functionalized liposomes (Sauer et al., 2005, Re et al., 2011a, Re et al., 2011b, Markoutsa et al., 2014). In vitro BBB model studies have also shown that liposomes functionalized with monomer ApoE 141-150 (mApoE) can cross the BBB better than non-functionalized liposomes (Re et al., 2011a, Bana et al., 2013, Markoutsa et al., 2014). Enhanced brain uptake has been observed in healthy mice with mApoE-liposomes compared to plain liposomes (Bana et

al., 2013, Markoutsa et al., 2013), suggesting that mApoE functionalized liposomes may use the LDL transport system to reach the brain (Sauer et al., 2005, Re et al., 2011a, Re et al., 2011b, Bana et al., 2013, Markoutsa et al., 2014).

Glucose transporter 1 (GLUT1) is expressed primarily in endothelial cells of the BBB and to varying extents in different regions of the brain (Hao et al., 2013). To enhance the BBB penetration of liposomes through GLUT1, p-aminophenyl-α-D-manopyranoside (MAN) and multivalent glucosides have been incorporated on the surface of liposomes (Ying et al., 2010, Hao et al., 2013). Based on preclinical evaluations using BBB cell models and biodistribution studies in mice, MAN increases the BBB penetration of liposomes (Ying et al., 2010, Hao et al., 2013). In vivo studies with healthy mice have shown that multivalent glucosides enhance liposome penetration of the BBB (Qu et al., 2014).

Transferrin receptors are also located on the endothelial cells of the BBB. To enhance liposomal BBB penetration, several ligands have been developed to target the transferrin receptor (van Rooy et al., 2011, Salvati et al., 2013, Markoutsa et al., 2012, Markoutsa et al., 2014, Huang et al., 2013). Antibodies OX-26 and RI7217 have been used for liposome transport via BBB transferrin receptors (van Rooy et al., 2011, Markoutsa et al., 2012, Markoutsa et al., 2014, Salvati et al., 2013). Surface plasmon resonance (SPR) and immunoblotting studies have confirmed that RI7212-decorated liposomes bind to transferrin receptors (Salvati et al., 2013). In vitro cell culture studies have shown that neither RI7212 nor OX-26 have cytotoxic effects, and they both increase the cellular uptake of liposomes (van Rooy et al., 2011, Markoutsa et al., 2012, Markoutsa et al., 2014, Salvati et al., 2013). In vivo and ex vivo studies in healthy mice reported increased brain uptake of OX-26 antibody-functionalized liposomes compared to liposomes without OX-26 antibody (Markoutsa et al., 2014). RI7212 functionalized liposomes are found in significantly greater amounts in the cerebrum, cerebellum, parenchyma, and capillaries of healthy mouse brain compared to plain liposomes, although the total mouse brain uptake is low (van Rooy et al., 2011).

Lactoferrin is a glycoprotein belonging to the transferrin family and utilizes receptor-mediated transcytosis to penetrate the BBB (Huang et al., 2013). In vitro studies with rat endothelial cells and in vivo studies with healthy mice have revealed that lactotransferrin-

functionalized liposomes show higher BBB penetration than plain liposomes, although the total brain uptake in mice was low (Huang et al., 2013).

Transferrin-functionalized liposomes have also shown improved BBB penetration properties. Studies have also been carried out with other short chained cell-penetrating peptides: trans-activator of transcription (TAT) peptide, penetratin, mastoparan, and poly-L-arginine (Sharma et al., 2012, Sharma et al., 2014). All of these peptides increase BBB penetration in vitro (in cells), but they also increase liposome toxicity. This toxicity decreases if transferrin is used as a functional group of liposomes. These dual-functionalized liposomes have exhibited higher BBB penetration in vitro using cells (Sharma et al., 2012) and ex vivo in healthy rats (Sharma et al., 2014) compared to non-functionalized or only transferrin-functionalized liposomes.

2.2.4. *Functionalized liposomes targeting β-amyloid plaques*

Different targeting compounds, including lipid derivatives integrated in the liposome lipid bilayer or compounds covalently bound to the liposome surface have been used to bind liposomes to β-amyloid (Aβ) plaques (Figure 2.4).
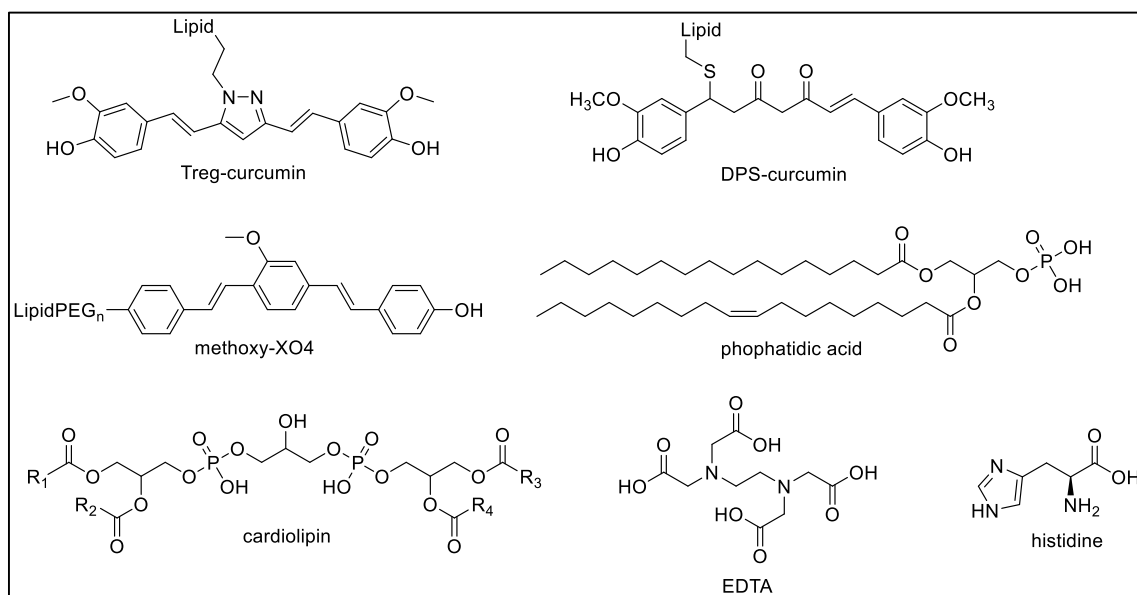
Figure 2.4. Liposome functional groups targeting Aβ.

Congo red derivative methoxy-XO4 (1,4-bis(4'-hydroxystyryl)-2-methoxybenzene) has been shown to bind Aβ plaques with nanomolar affinity (Klunk et al., 2002). Stealth liposomes have been functionalized with methoxy-XO4 in order to target Aβ plaques

(Tanifum et al., 2012). Methoxy-XO4 has a dual role in the liposome; it targets Aβ plaques and acts as a fluorescent marker. In vitro studies using synthetic Aβ(1-40) fibrils have shown that these liposomes have high Aβ binding (Tanifum et al., 2012). Methoxy-XO4-functionalized stealth nanoliposomes have shown improved BBB penetration and specific binding to parenchymal plaques and cerebral amyloid angiopathy in transgenic AD mice (Tanifum et al., 2012).

Curcumin is a neuroprotective compound that inhibits the formation of Aβ oligomers and Aβ aggregation, and binds to Aβ plaques (Yang et al., 2005, Garcia-Alloza et al., 2007, Begum et al., 2008). Curcumin derivatives have been attached to the surface of liposomes in order to target Aβ plaques (Mourtas et al., 2011, Taylor et al., 2011, Lazar et al., 2013). Two different derivatives have been studied: curcumin-phospholipid conjugate (DPS-curcumin) and the lipidic pyrazole derivative of curcumin (treg-curcumin). SPR studies with Aβ(1-42) fibrils and immunoassay studies with Aβ(1-42) aggregates have revealed that treg-curcumin-functionalized liposomes bind Aβ fibrils and inhibit aggregation, whereas the results for DPS-curcumin-functionalized liposomes did not differ much from those for plain liposomes (Mourtas et al., 2011, Taylor et al., 2011). Preclinical evaluation of DPS-curcumin-functionalized liposomes has shown that these bind to Aβ plaques in human and transgenic mouse brain sections in vitro (Lazar et al., 2013), but do not pass the BBB. However, DPS-curcumin liposomes directly injected into the transgenic mouse brain were shown to bind Aβ plaques, with low binding to diffuse Aβ plaques (Lazar et al., 2013).

Liposomes functionalized with anionic phospholipids (i.e., phosphatidic acid or cardiolipin) have been shown to bind Aβ(1-42) fibrils in vitro (Gobbi et al., 2010, Re at al., 2011). Studies with brain capillary endothelial cells have shown that phosphatidic acid or cardiolipin do not enhance liposomal uptake into the brain (Re et al., 2011). Phosphatidic acid-functionalized liposomes were further functionalized with RI7212 (Salvati et al., 2013) or mApoE (Bana et al., 2013, Re et al., 2011) in order to enhance brain uptake; this did not interfere with phosphatidic acid binding of Aβ(1-42) fibrils but improved liposome BBB penetration, which was confirmed by in vitro studies (Salvati et al., 2013, Bana et al., 2013, Re et al., 2011) and ex vivo studies in healthy mice (Bana et al., 2013).

Copper and zinc interact with β-amyloid peptides and create insoluble amyloid plaques (Mufamadi et al., 2012). These metals and the metal chelating ligands histidine and EDTA have been used as functional groups on liposomes developed to resolubilize the β-amyloid peptides in amyloid plaques and reduce the number of amyloid plaques (Mufamadi et al., 2012). In vitro studies done with Aβ(1-42) plaques and neuronal cells have shown that these functionalized liposomes decrease the number of Aβ plaques and the neurotoxicity resulting from their presence (Mufamadi et al., 2012).

2.2.5. *Nanoparticles targeting Aβ*

In addition to liposomes, other nanoparticles have been developed to target Aβ in AD. Nanoparticles produced by emulsifying wax were functionalized by covalently bonding D-penicillamine (Cui et al., 2005). D-penicillamine has been shown to chelate metals, especially copper(I). Using this feature of D-penicillamine, these nanoparticles are capable of resolubilizing copper-Aβ(1-42) aggregates in vitro (Cui et al., 2005).

A similar approach was used to create curcumin-loaded polylactic-co-glycolic acid (PLGA) nanoparticles (Mathew et al., 2012). These PLGA particles were functionalized with Tet-1 peptide in order to enhance BBB penetration and neuron affinity. In vitro studies performed with protein aggregates and glioma cells have shown that these nanoparticles disaggregate Aβ proteins and show uptake in glioma cells (Mathew et al., 2012).

Quinoline-*n*-butylcyanoacrylate-based nanoparticles have also been developed to target Aβ plaques in the AD brain (Kulkarni et al., 2009). In these particles, clioquinol is used to enhance brain uptake and Aβ binding (Kulkarni et al., 2009). These particles are prepared using a polymerization technique and a surface coating of 1% Tween-80. Using ^{125}I-labeling, binding to amyloid plaques in postmortem human brain sections was shown. These particles also quickly enter the healthy mouse brain with fast wash out (Kulkarni et al., 2009). The total in vivo brain uptake one hour after tracer injection was reported to be higher in transgenic AD mice than healthy mice, suggesting specific binding to Aβ plaques (Kulkarni et al., 2009).

IgG4.1 is an antibody against human fibrillar Aβ42 peptide that has been shown to have specific affinity towards fibrillar Aβ (Poduslo et al., 2011). Iron oxide particles coated with pegylated phospholipids have been further functionalized with antibody IgG4.1 to

target cerebrovascular amyloid proteins in the brain (Poduslo et al., 2011, Jaruszewski et al., 2014). Preclinical evaluation of these nanoparticles has shown that they enter the brain and bind specifically to amyloid plaques in the cerebrovascular wall (Poduslo et al., 2011, Jaruszewski et al., 2014).

2.2.6.   *Analysis of nanoliposomes*

During liposome analysis, the size, zeta potential (ζ potential), and lipid composition are measured (Edwards and Baeumner, 2006, Jesorka and Orwar, 2008). The exact liposome size can be measured using transmission electron microscopy (TEM). With TEM methods, the diameter, polydispersity, and size distribution of liposomes can be determined accurately (Edwards and Baeumner, 2006, Jesorka and Orwar, 2008). Gel exclusion chromatography is used to determine the hydrodynamic radius of liposomes (Jesorka and Orwar, 2008). Using commercial gel columns, liposomes between 30 and 300 nm can be separated. This method can also be used to purify the liposome mixture after extrusion. The disadvantage of gel exclusion chromatography is that the gel material can interact with liposomes, causing blocking or precipitation (Jesorka and Orwar, 2008).

Dynamic light scattering (DLS) is the most common method for determining the size distribution of liposomes. In this method, the hydrodynamic diameter of the liposome is determined (Edwards and Baeumner, 2006). The hydrodynamic diameter is the diameter of the liposome covered with solvent molecules, which is slightly larger than the true diameter of the liposome (Doane et al., 2012). With this method individual sizes cannot be determined, but the results show the size distribution (Jesorka and Orwar, 2008). The polydispersity index (PdI) indicates the variation in distribution and is usually calculated using the Cumulant algorithm. PdI values can range between 0 and 1, with values close to zero indicating that the liposomes are very monodisperse and values close to 1 indicating that the liposomes have polydisperse hydrodynamic diameters.

The ζ potential is the potential of the liposome surface (Doane et al., 2012 Jesorka and Orwar, 2008). When the ζ potential is measured, two approximations can be used: Hückel approximation is used for small liposomes and low dielectric constant solutions, and the Smoluchowski approximation is used for larger liposomes and moderately high dielectric constant solutions (Doane et al., 2012). If the ζ potential is known, the quality of the liposomes can be predicted; a value close to zero implies that the liposomes may

aggregate rapidly; extremely stable liposomes have ζ potentials >60 mV (Hanaor et al., 2012). With cationic liposomes the surface charge is positive, whereas anionic liposomes have a negative surface charge. Factors affecting ζ potential are pH and the ion concentration of the solution. The isoelectric point of a liposome is the pH at which the ζ potential of the liposome is zero. Therefore, if the surface charge of the liposome is zero, the stability of the liposome decreases and liposome aggregation increases.

The lipid content of the liposomes is measured to ensure that no lipid oxidation or degradation occurred during preparation or storage (Edwards and Baeumner, 2006). The amount of lipid and, eventually, the liposome encapsulation efficiency (i.e., the amount of encapsulated compound) are usually determined by chromatographic or spectrometric methods (Edwards and Baeumner, 2006, Jesorka and Orwar, 2008).

2.2.7.   *Nanoliposomes and PET*

Nanoliposomes have also been developed as PET imaging agents. The high surface area-to-volume ratio of liposomes allows the production of multifunctional and target-specific liposomes for imaging (Devaraj et al., 2009, Welch et al., 2009, Liu and Welch, 2012, 2009, Abou et al., 2013, Li et al., 2012, Qin et al., 2013). Liposomes differ from the traditional small molecule PET tracers in that they usually need a longer time to accumulate in the tissue of interest than small molecules. Thus, PET-liposomes are usually labeled with ^{18}F, ^{64}Cu, ^{89}Zr, or ^{124}I due to the relatively long half-life of these radioactive nuclides (Phillips et al., 2009, Liu and Welch, 2012). PET-liposomes have been used to study the in vivo behavior of functionalized liposomes and for tumor imaging (Phillips et al., 2009, Welch et al., 2009, Lammers et al., 2010, Qin et al., 2013).

Many possibilities exist for radiolabeling liposomes (Figure 2.5.). The radiolabeling can be done before liposome synthesis. In this case, the core-forming compound is radiolabeled first, and then the actual liposomes are produced (Phillips et al., 2009). The radiolabeled core-forming compound is usually a diacylglycerol derivative (Marik et al., 2007, Emmetiere et al., 2013), pegylated alkoxybenzene derivative (Urakami et al., 2007, Devaraj et al., 2009), or cholesteryl ether derivative (Jensen et al., 2012), and ^{18}F-labeling is achieved using nucleophilic ^{18}F-fluorination. When the core-forming compound is radiolabeled, the radiolabel is in the lipid bilayer or very close to it. An alternative radiolabeling method consists of encapsulation of the PET tracer inside the liposome

(Phillips et al., 2009, Hatakana et al., 2010, Medina et al., 2011, Oku et al., 2011, Benezra et al., 2012). Liposomes can also be labeled after they are produced by applying the remote loading method; this labeling strategy is preferred when using radiometals (Phillips et al., 2009). In remote loading, the radiometal either forms a chelate with adjacent lipid phosphate heads on the core of the liposome (Abou et al., 2013), or is trapped in the chelator, which has been coupled to the surface of the liposome or trapped inside the liposome during preparation (Seo et al., 2008, Petersen et al., 2011, Seo et al., 2011, Locke et al., 2012, Petersen et al., 2012, Kang et al., 2013, Li et al., 2012, Mitchell et al., 2013).
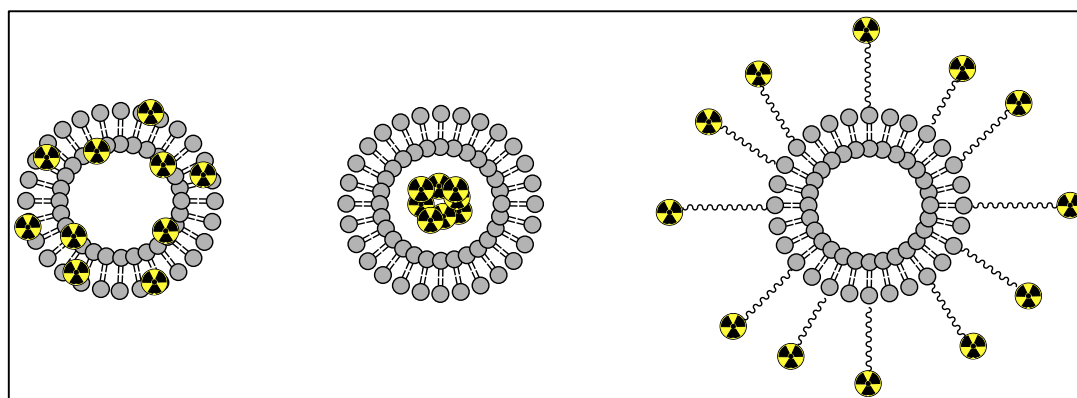
Figure 2.5. Labeling approaches for PET-liposomes. The radionuclide can be found on the core of the liposome (left), inside the liposome (middle), or attached to the end of the functional group (right).

All the aforementioned labeling strategies have advantages and disadvantages. Liposomes do not tolerate high temperatures or large quantities of organic solutions. If the labeling is done before the liposomes are produced, the liposomes will not restrict the labeling circumstances or purification methods. On the other hand, the RCY of the labeled product has to be reasonably high, especially when ^{18}F is used as the radionuclide, because the total synthesis time from the start of labeling to the end of liposome synthesis is relatively long with respect to the half-life of the positron emitter. Therefore, the remote loading method of labeling is more beneficial, though the labeling must occur in aqueous solution and only minor variance from room temperature is allowed. In addition, the radiolabeled liposomes have to be purified from the reaction mixture after incorporating the radioactivity, which limits the utilization of remote loading labeling.

Studies of PET-liposomes in healthy mice have shown that the lipid composition and functionalization of liposomes affect the biodistribution of the liposomes (Marik et al.,

2007, Urakami et al., 2007, Devaraj et al., 2009). PET-liposomes accumulate ultimately in the liver, spleen, lungs, and kidneys. For tumor imaging, several liposomes have been developed (Seo et al., 2008, Medina et al., 2011, Petersen et al., 2011, Seo et al., 2011, Jensen et al., 2012, Benezra et al., 2012, Petersen et al., 2012, Locke et al., 2012, Abou et al., 2013, Kang et al., 2013, Li et al., 2012, Mitchell et al., 2013, Emmetiere et al., 2013). Although the labeling strategies and functional groups for these liposomes differ, biodistribution studies in tumor-bearing mice have shown that all liposomes are excreted primarily through the liver and spleen, but relatively high accumulation in tumors has been observed due to the functional group on the liposome surface (Seo et al., 2008, Seo et al., 2011, Medina et al., 2011, Petersen et al., 2011, Jensen et al., 2012, Benezra et al., 2012, Petersen et al., 2012, Locke et al., 2012, Abou et al., 2013, Emmetiere et al., 2013, Kang et al., 2013, Li et al., 2012, Mitchell et al., 2013).

Multimodal liposomes have also been developed. These liposomes are PET and CT (Devaraj et al., 2009), PET and MR (Abou et al., 2013), or PET, MR, and NIR (Li et al., 2012) imaging agents coupled in the same liposome. These liposomes have been designed for tumor imaging and preclinical studies have shown promising results (Abou et al., 2013, Devaraj et al., 2009, Li et al., 2012).

2.3. Alzheimer's disease and PET imaging

2.3.1. Alzheimer's disease

AD is a neurological disease that causes neuronal loss, dementia, and cognitive impairment. The severity of AD is classified using Braak stages; early onset AD is Braak stage I and fully developed AD is Braak stage VI (Braak and Braak, 1997). In addition to memory loss, common symptoms related to AD are apathy, disorientation, behavioral changes, and confusion (Alzheimer Association, 2014).

The main hallmarks of AD in the brain tissue are Aβ plaques and neurofibrillary tangles, which Prof. Alois Alzheimer recognized in 1906 (Mauer et al., 1997, Serrano-Pozo et al., 2011). Much research focusing on the cause and treatment of AD has been carried out since that discovery. Currently, the symptoms and progression of AD are well known, but the underlying cause is still a mystery (Braak and Braak, 1997, Nordberg et al., 2010, Serrano-Pozo et al., 2011). Several different hypotheses address AD (Figure 2.6.); the most commonly accepted are the amyloid and tau cascades, but neuroinflammation,

oxidative stress, alterations in glucose and fatty acid metabolism, and changes in vascular and receptor activity in the brain have also been connected to AD (Karran et al., 2011, Nordberg et al., 2010, Serrano-Pozo et al., 2011 Swomley et al., 2013). Although knowledge of AD has increased, no curative treatment is available.
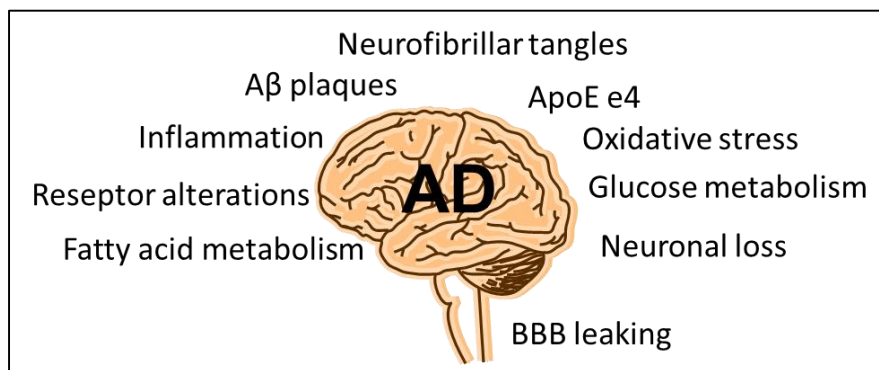
Figure 2.6. Pathogeneses related to Alzheimer's disease.

2.3.2.   *β-amyloid plaques and the amyloid cascade*

Aβ plaques are the primary markers of AD. Aβ plaques are insoluble, diffuse, or compact plaques of Aβ peptides. According to the amyloid cascade hypothesis, Aβ plaques trigger the cascade that eventually leads to AD (Hardy and Selkoe, 2002, Karran et al., 2011). Aβ peptides originate from amyloid precursor protein (APP) (Karran et al., 2011, Serrano-Pozo et al., 2011). Sequential cleavage of APP by β-cleaving amyloid precursor protein enzyme (β-secretase) and γ-secretase leads to the formation of Aβ peptides of varying lengths, with 40 or 42 amino acids being the most predominant length (Figure 2.7., Karran et al., 2011).
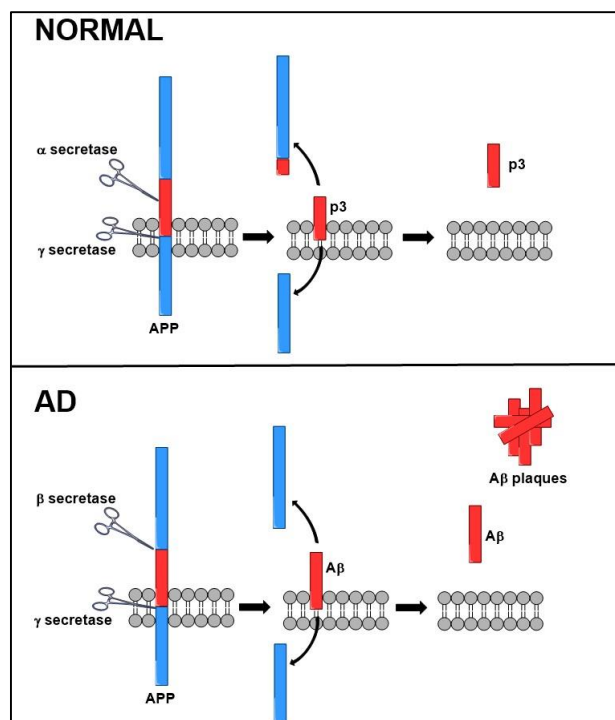
Figure 2.7. Formation of Aβ plaques. Top, normal APP cleavage. Bottom, APP cleavage and Aβ plaque formation.

Amyloid plaques are formed when abnormal quantities of Aβ peptides accumulate in extracellular areas. There are two types of amyloid plaques: diffuse and dense-core plaques (Serrano-Poze et al., 2011). Dense-core plaques are thioflavine T-positive and are associated with several harmful effects related to neuronal death. Dense-core amyloid plaques are more often found in the brains of AD patients, whereas diffuse amyloid plaques are more common in the brains of elderly non-Alzheimer's patients (Serrano-Poze et al., 2011). The amount of Aβ plaques varies in different regions of the AD brain. Small amounts are usually found in the cerebellum, whereas a high plaque density can be found in the cortical areas of the brain (Braak and Braak, 1997, Nordberg et al., 2010). The total amount of Aβ plaques in the AD brain is in the low milligram range (Karran et al., 2011, Serrano-Pozo et al., 2011). One of the prevalent therapeutic aims is to reduce the amount of Aβ plaques by decreasing production, facilitating clearance, and inhibiting the aggregation of Aβ peptides in the AD brain.

Transgenic mouse models of AD have been developed to study the Aβ cascade in experimental animals. These mice over-express a human APP, which leads to the spontaneous formation of Aβ plaques in the brains of these mice (Figure 2.7.). Commonly used AD mouse models are tg2576 (Hsiao et al., 1996), tgCRND8 (Chrishti et al., 2001),

APP23 (Sturchler-Pierrat et al., 1997), and APPswe-PS1dE9 (Jankowsky et al., 2004). Tg2576 mice over-express the Swedish human Aβ precursor protein APP_{695} (K670N-M671L), which has two mutations at amino acid positions 670 and 671 (Hsioa et al., 1996). Tg2576 mice develop classic senile plaques and diffuse plaques, and cognitive deficits begin at 5 months of age (Hsioa et al., 1996, Webster et al., 2014). TgCRND8 mice over-express the Swedish APP_{695} and the Indiana mutation V717F in the human precursor protein (Chrishti et al., 2001). Amyloid plaques and memory deficit are seen in TgCRND8 mice starting at the age of 3 months (Chrishti et al., 2001, Webster et al., 2014). The APP23 mouse model has human precursor protein mutations Swedish APP_{695} and London mutation V7171 (Sturchler-Pierrat et al., 1997). In this model, the first cognitive deficits are seen at 3 months of age and Aβ plaques from 6 months of age (Sturchler-Pierrat et al., 1997, Webster et al., 2014). APPswe-PS1dE9 mice also express the Swedish APP_{695} together with the presenilin 1 (PS1)dE9 mutation, which has been seen in early onset familial AD patients (Jankowsky et al., 2004). The memory deficit can be observed at 3 months of age, and at the age of 6 months the animals have Aβ plaques in the brain (Jankowsky et al., 2004, Webster et al., 2014).

2.3.3.   *Sphingosine-1-phosphate and sphingosine-1-phosphate receptors*

Sphingosine-1-phosphate (S1P) is a lysophospholipid that plays an important role as a cellular mediator (Marsolais and Rosen, 2009, Hla and Brinkmann, 2011, Maceyka et al., 2012). S1P is produced enzymatically from ceramide via *N*-deacylation and phosphorylation (Figure 2.8.). The phosphorylation reaction is catalyzed by two sphingosine kinases, SphK1 and SphK2. In plasma, S1P is mainly bound to high density lipoprotein and albumin in nanomolar concentrations and widely distributed throughout the body. Several enzymes regulate the S1P concentrations by degrading excess amounts of this phospholipid. S1P is involved in various signaling and regulatory functions in the cardiovascular system, immune system, and central nervous system (CNS) (Marsolais and Rosen, 2009, Hla and Brinkmann, 2011, Milstien et al., 2007, Sim-Silley et al., 2009, Soliven et al., 2011, Maceyka et al., 2012). S1P modulates activity through five different receptor subtypes ($S1P_1$ – $S1P_5$) belonging to the G-protein-coupled receptor family. Because of the multiple roles of S1P, the S1P receptors (S1PRs) are responsible for differentiating S1P regulatory and signaling tasks (Marsolais and Rosen, 2009, Hla and Brinkmann, 2011, Maceyka et al., 2012).
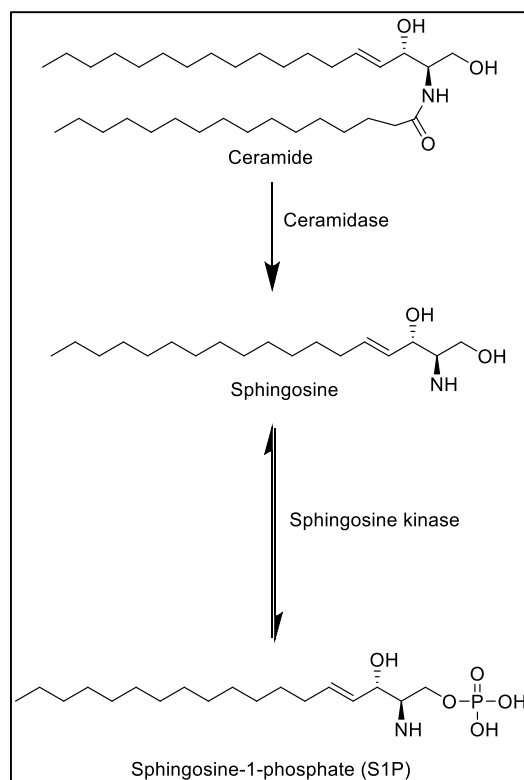
Figure 2.8. The formation of sphingosine-1-phosphate.

In the CNS, all S1PRs are extensively expressed on various cells (Marsolais and Rosen, 2009, Hla and Brinkmann, 2011, Milstien et al., 2007, Sim-Silley et al., 2009, Soliven et al., 2011). The functions of S1P and S1PRs in the CNS are not fully understood, but they have been connected to several cell responses, including cell signaling, neuronal proliferation, cell survival, and the regulation of BBB permeability (Marsolais and Rosen, 2009, Hla and Brinkmann, 2011, Milstien et al., 2007, Sim-Silley et al., 2009, Soliven et al., 2011). The receptor subtype $S1P_3$ is supposed to be expressed in astrocytes, oligodendrocytes, neurons, and microglia, and it is also related to the regulation of transcellular transport, hearing, and balance (Marsolais and Rosen, 2009, Soliven et al., 2011). $S1P_3$ receptor is also involved in inflammation and dendritic cell sequestration in lymph nodes, heart rate regulation, vasodilation, and vasoconstriction (Marsolais and Rosen, 2009, Nakamura et al., 2012, Sanna et al., 2004, Koide et al., 2007).

Various compounds have been developed to study S1PRs (Huwiler and Pfeilschifter, 2008, Marsolais and Rosen, 2009, Maceyka et al., 2012). FTY-720P is one of the first compounds developed for S1PRs (Figure 2.9, Mandala et al., 2002). FTY-720P is a non-specific agonist for S1PRs and has been widely used in studies of S1PRs. Also, more selective S1PR subtype agonists and antagonists have been developed (Marsolais and

Rosen, 2009, Mandala et al., 2002, Huwiler and Pfeilschifter, 2008, Murakami et al., 2010, Buzard et al., 2012, Nakamura et al., 2012, Maceyka et al., 2012). TY-52156, a chlorophenylhydrazone derivative, is an S1P$_3$ receptor antagonist (Murakami et al., 2010). Cell culture studies and animal experiments with healthy rats have shown that TY-52156 binds specifically to the S1P$_3$ receptors and regulates cardiovascular phenomena in vivo (Figure 2.9, Murakami et al., 2010). According to a database search and cell culture studies, 3,4-dialkoxybenzophenone derivatives VPC23019 and BLM-241 are also antagonists for the S1P$_3$ receptors (Figure 2.9, Davis et al., 2005, Koide et al., 2007). A family of 6-substituted indole-3-carboxylic acid amide compounds has been described to have high agonist or antagonist biological behavior for S1P$_3$ receptor (Figure 2.9, Beard et al., 2008). The biological behavior of other S1P$_3$ receptor-specific compounds has not yet been evaluated.
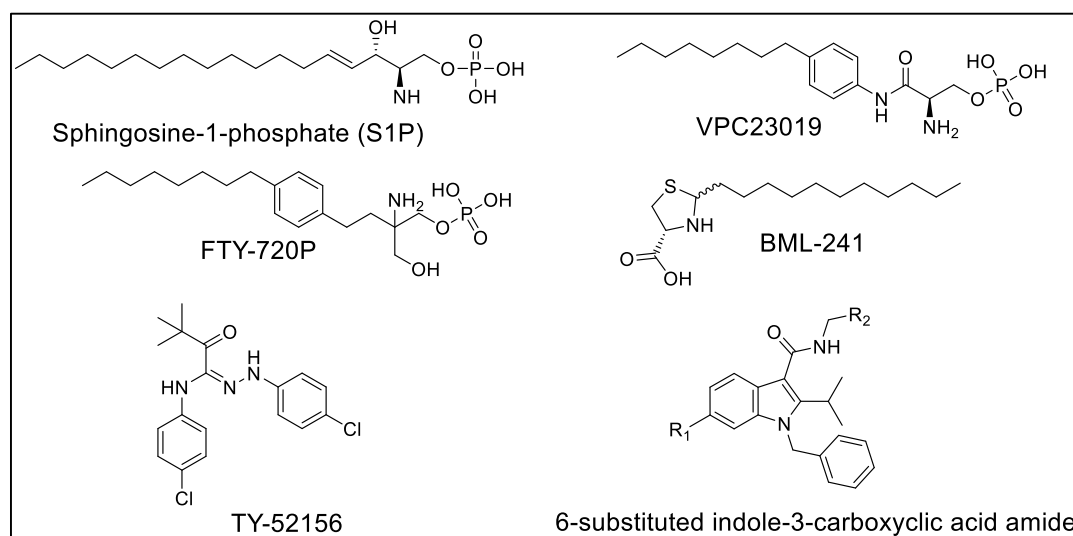
Figure 2.9. Compounds that have shown an affinity toward S1P$_3$ receptors.

Although knowledge of S1PR involvement in health and disease remains limited, the expression of S1PRs and level of S1P have been suggested to be related to CNS disorders (Marsolais and Rosen, 2009, Hla and Brinkmann, 2011, Milstien et al., 2007, Sim-Silley et al., 2009, Soliven et al., 2011). In the sporadic AD brain, the activity of phosphorylating sphingosine kinase SphK2 is elevated compared to healthy controls even though the amount of SphK2 is decreased (Takasugi et al., 2011). Cell studies revealed that Aβ fibrils increase the SphK2 activity (Takasugi et al., 2011). In neurons, increased S1P levels cause a variety of issues, including proteolytic activity of β-secretase 1 and overproduction of Aβ (Takasugi et al., 2011). Inhibition of SphK2 enzyme activity reduces Aβ formation in

the transgenic mouse brain (Takasugi et al., 2011). On the other hand, S1P levels are decreased in the human AD brain compared to healthy controls, and this loss correlates with the Braak stage of AD (Couttas et al., 2014).

2.3.4.   *Positron emission tomography*

PET is a sensitive in vivo imaging technique that enables the study of processes in living organisms (Phelps, 2000) by using positron emitter-labeled tracers (PET tracers) to measure biochemical processes in the tissues of interest. A PET tracer is designed to specifically bind or interact with the target of interest. PET tracers decay by positron emission (β^+-emission); the nucleus of the positron emitter emits a short-lived positron (e^+). Subsequently, the positron is annihilated by an electron, creating two 511 keV γ rays which are emitted 180° from each other (Figure 2.10), with the gamma energies representing the masses of the annihilated β-particles. The PET camera detects these γ rays in γ-γ-coincidence in detectors on opposite sides of the organ of interest, forming an image of the distribution of the radioactivity (Figure 2.10). Because PET images do not provide morphological information, CT and MR images are commonly used for anatomical reference. With PET and a suitable tracer, biological processes and abnormalities can be identified and studied (Phelps, 2000). In AD patients, PET imaging can be utilized as a diagnostic tool and to study the pathophysiology of the disease.
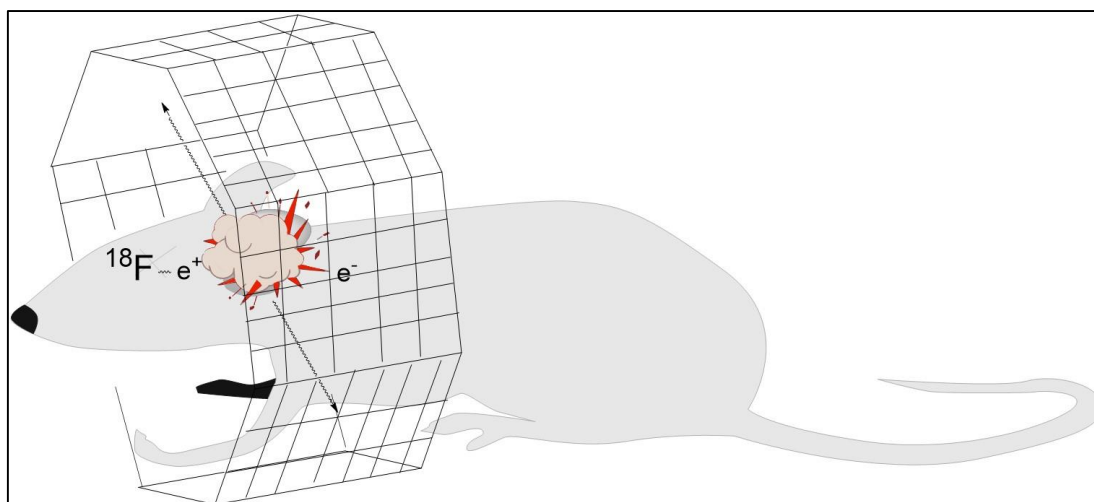
Figure 2.10. The principle of PET imaging using an ^{18}F-labeled tracer.

2.3.5.   *PET tracers for β-amyloid imaging of Alzheimer's disease*

Several PET tracers have been developed for Aβ imaging in AD (Nordberg et al., 2010, Rowe and Villemagne, 2013). [^{11}C]PIB and [^{18}F]FDDNP are the most widely used PET

tracers for clinical imaging of Aβ in AD, but the ^{18}F-labeled tracers [^{18}F]flutemetamol, [^{18}F]florbentaben, [^{18}F]florbentapir, and [^{18}F]AZD4694 are potential new PET tracers for clinical and diagnostic AD imaging in humans (Figure 2.11, Nordberg et al., 2010, Rowe and Villemagne, 2013). In addition, several [^{18}F]curcumin derivatives have shown potential as new amyloid markers (Figure 2.11, Cai et al., 2011, Lee et al., 2011, Ruy et al., 2006).
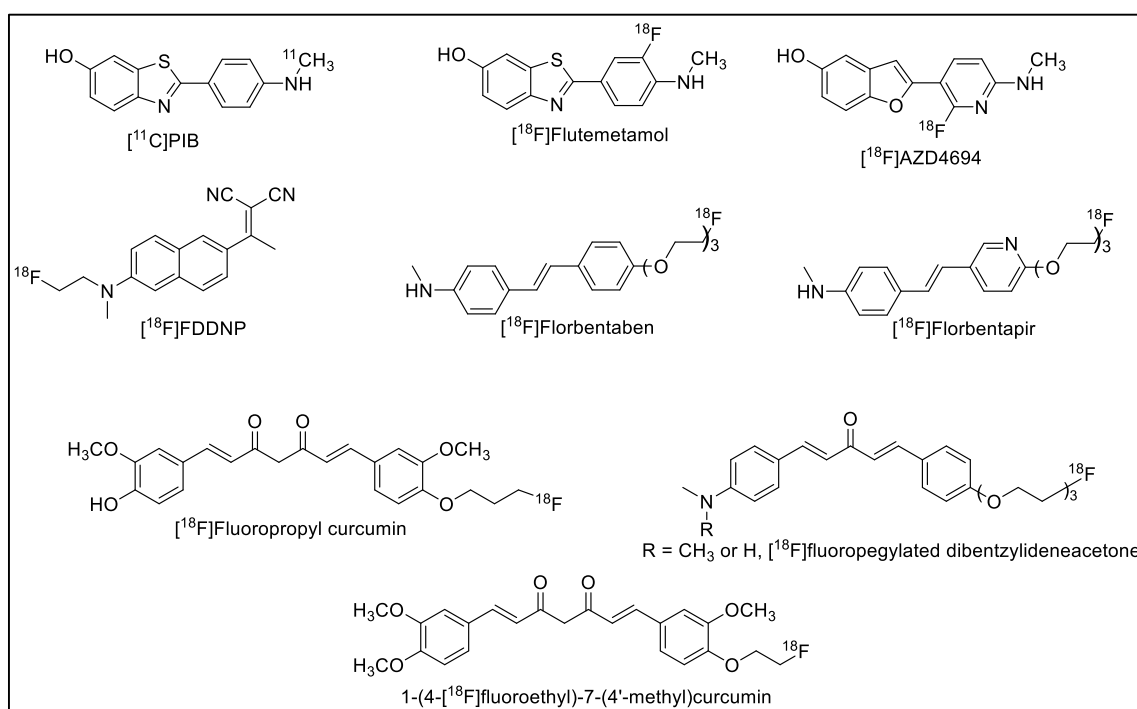
Figure 2.11. Molecular structures of [^{11}C]PIB and [^{18}F]amyloid tracers for Aβ imaging in AD.

Naphthalene derivative 2-(1-{6-[(2-[^{18}F]fluoroethyl)(methyl)amino]-2-naphtyl}ethylidene)malononitrile ([^{18}F]FDDNP) was the first tracer developed for AD PET imaging (Agdeppa et al., 2001, Shoghi-Jadid et al., 2002). [^{18}F]FDDNP is synthesized using nucleophilic ^{18}F-fluorination and the tosyl derivative of FDDNP (Agdeppa et al., 2001). [^{18}F]FDDNP is highly lipophilic and has a measured logP value of 3.92 (Agdeppa et al., 2001). Studies of Aβ fibrils have shown that [^{18}F]FDDNP has two binding sites in fibrils with affinity in the low nanomolar range (Agdeppa et al., 2001). In vitro binding studies done with human AD brain sections have shown that [^{18}F]FDDNP binds to dense core and diffuse Aβ plaques, and weakly to the neurofibrillary tangles (Agdeppa et al., 2001). The Aβ binding of [^{18}F]FDDNP is displaced effectively with non-steroidal anti-inflammatory drugs, such as naproxen and ibuprofen (Agdeppa et al., 2003). These in vitro findings were confirmed in a preclinical

in vivo study with the triple-transgenic AD rat model tg478/tg1116/tg11587 (Teng et al., 2011). Studies of the displacement of Aβ binding with [^{18}F]FDDNP and Congo Red or thioflavin T, as well as [^{3}H]PIB and FDDNP, indicate that the binding site of FDDNP is different from the binding site of Congo Red, thioflavin T, or PIB (Agdeppa et al., 2003, Ni et al., 2013). In a study of the tg2576 mouse model, [^{18}F]FDDNP did not show appropriate behavior for preclinical Aβ imaging of the AD mouse model (Kuntner et al., 2009). Clinical studies have shown that [^{18}F]FDDNP is suitable for in vivo imaging of Aβ plaques in the human brain (Shoghi-Jadid et al., 2001), and it has been used in several clinical studies (Nordber et al., 2010, Rowe and Villemagne, 2013). In addition, [^{18}F]FDDNP has been used to image neurofibrillary tangles in AD (Kepe et al., 2013).

Thioflavin derivative [^{11}C]2-(4'-(methylamino)phenyl)-6-hydroxybenzothiazole ([^{11}C]PIB, [^{11}C]6-OH-BTA-1) is the most commonly used clinical tracer for imaging Aβ burden in the brains of AD patients (Mathis et al., 2003b, Nordber et al., 2010, Rowe et al., 2013, Rowe and Villemagne, 2013). Several methods have been developed to produce [^{11}C]PIB (Mathis et al., 2003b, Philippe et al., 2011, Shao et al., 2011). The easiest method is to use [^{11}C]methyl triflate as a labeling agent and to label the 6-OH-BTA-0 using a one-step synthesis.

Studies done with postmortem human brain sections have shown that PIB specifically binds Aβ plaques (Klunk et al., 2004, Ikonomovic et al., 2008). The binding of [^{11}C]PIB to Aβ fibrils is in the low nanomolar range (Mathis et al., 2003b, Klunk et al., 2005, Ikonomovic et al., 2008, Ni et al., 2013). These binding studies also showed that PIB has two binding sites: one high-affinity site and one low-affinity site. Structure-activity relationship studies revealed that Aβ fibrils have two high-affinity binding sites and one low-affinity binding site for PIB (Lockhart et al., 2005, Wu et al., 2008, Reinke and Gestwicki, 2011). The important structural features of PIB for Aβ binding are planar and linear hydrophobic ring systems that fit between the Aβ fibril axes and are bound to the two parallel high-affinity binding sites. The *N*-methyl group of aniline can also form hydrogen bonds with a nearby hydrophobic pocket of the Aβ fibril (Lockhart et al., 2005, Wu et al., 2008). The overall hydrophobicity of the compound is important for binding, and in the structure of PIB the polar hydroxyl group at the benzothiazole ring is tolerated due to the *N*-methyl group of aniline, which preserves the overall hydrophobicity of PIB (Lockhart et al., 2005, Wu et al., 2008, Reinke and Gestwicki, 2011). [^{11}C]PIB has a

measured logP of 1.2 (Mathis et al., 2003b). In humans and mice, [^{11}C]PIB has been shown to undergo moderately fast peripheral metabolism (Mathis et al., 2003b, Klunk et al., 2004). Studies with transgenic AD mice have shown that the transgenic mouse model affects the results because, with some transgenic mouse models, the Aβ plaques probably do not have a proper binding site for [^{11}C]PIB (Klunk et al., 2005, Toyama et al., 2005, Maeda et al., 2007, Snellman et al., 2013). In humans, [^{11}C]PIB has been shown to specifically bind Aβ plaques in the AD brain, though age, gender, and ApoE ε4 carrier status may also increase the uptake of [^{11}C]PIB in the brains of healthy individuals (Klunk et al., 2004, Ikonomovic et al., 2008, Scheinin et al., 2014). Several clinical studies have shown that [^{11}C]PIB is a good tracer for in vivo Aβ imaging of the human brain (Nordberg et al., 2010, Rinne et al., 2010, Rowe and Villemagne, 2013).

[^{18}F]Flutemetamol ([^{18}F]GE-067, 3'-[^{18}F]FPIB) is a ^{18}F-fluorinated thioflavine derivative (Storey et al., 2007, Mathis et al., 2003a). In the structure of [^{18}F]flutemetamol, the ^{18}F atom is attached to the 3'-position of the aniline ring of PIB. [^{18}F]Flutemetamol is produced with nucleophilic ^{18}F-fluorination using a chlorine precursor compound with an *ortho*-nitro activating group (Mathis et al., 2003a) or nitro precursor compound (Storey et al., 2007). Studies done with [^{3}H]flutemetamol have shown that flutemetamol has a nanomolar range binding affinity towards Aβ fibrils (Juréus et al., 2010). [^{3}H]Flutemetamol binds Aβ plaques in transgenic mouse brain and human brain, but the non-specific binding is also relatively high (Juréus et al., 2010, Swahn et al., 2012). The ElogD value for flutemetamol is 3.2 (Juréus et al., 2010), which may explain the high non-specific binding. In humans, [^{18}F]flutemetamol exhibits appropriate *in vivo* behavior and is a potential tracer for diagnostic AD imaging (Rowe and Villemagne, 2013).

Benzofurane derivatives are also potential Aβ tracers. Among these, [^{18}F]AZD4694 is probably the most promising (Swahn et al., 2012). The structure of [^{18}F]AZD4694 is related to [^{18}F]flutemetamol (Figure 2.11). [^{18}F]AZD4694 is produced using nucleophilic ^{18}F-fluorination and a nitro-derived compound as a precursor (Swahn et al., 2012). The studies done with [^{3}H]AZD4694 have shown that AZD4694 has a nanomolar range binding affinity towards Aβ fibrils (Juréus et al., 2010). The ElogD value for AZD4694 is 2.8 (Juréus et al., 2010). [^{3}H]AZD4694 specifically binds Aβ plaques in the brains of transgenic tg2576 mice in vitro and ex vivo, as well as the Aβ plaques of human brain in vitro, and the non-specific binding is low (Juréus et al., 2010, Swahn et al., 2012). The

initial in vivo human studies of [^{18}F]AZD4694 have shown specific cortical retention in the AD patient brain and low non-specific binding (Cselényi et al., 2012, Rowe et al., 2013).

^{18}F-labeled stilbene derivatives have been successfully developed for Aβ imaging, being [^{18}F]florbentaben ([^{18}F]BAY 94-9172, [^{18}F]AV-1, Figure 2.11, Zhang et al., 2005) and [^{18}F]florbentapir ([^{18}F]AV-45, Figure 2.11, Choi et al., 2009) the most promising ones. [^{18}F]Florbentaben has been produced by nucleophilic ^{18}F-fluorination using mesyl derivative as the precursor (Zhang et al., 2005). The measured logP value for [^{18}F]florbentaben is 2.41. Florbentaben effectively displaces [^{125}I]IMPY and [^{3}H]PIB binding of Aβ plaques in AD brain homogenates, suggesting that all these compounds share the same Aβ plaque binding sites (Zhang et al., 2005, Ni et al., 2013). In mice, [^{18}F]florbentaben has shown appropriate in vivo kinetics and has high specific binding towards Aβ plaques in transgenic APP/PS1, tg2675, and APP-Swe mouse brains (Zhang et al., 2005, Rominger et al., 2013). In addition, studies in healthy controls and AD patients have shown that [^{18}F]florbentaben is a suitable PET tracer for imaging human Aβ in the AD patient brain (Rowe et al., 2008, Rowe and Villemagne, 2013).

[^{18}F]Florbentapir has also been produced with nucleophilic ^{18}F-fluorination using a tosylated precursor compound (Choi et al., 2009). Preclinical evaluation of this tracer using postmortem sections and homogenates of AD brain revealed that it has high specificity for Aβ plaques with low nanomolar range binding affinity (Choi et al., 2009, Lin et al., 2010). Florbentapir also effectively displaces the [^{3}H]PIB binding of plaques in AD patient brain homogenates, suggesting that all of these compounds share the same Aβ plaque binding sites (Ni et al., 2013). Studies done with mice and monkeys have shown that [^{18}F]florbentapir exhibits the appropriate in vivo kinetics and that the tracer binds specifically to Aβ plaques in the transgenic APPswe/PSEN1 mouse brain (Choi et al., 2009). In humans, [^{18}F]florbentapir has also exhibited appropriate kinetics and is a suitable PET tracer for imaging human Aβ in AD patient brains (Lin et al., 2010, Rowe and Villemagne, 2013).

Curcumin is a neuroprotective compound that inhibits the formation of Aβ oligomers and fibrils and binds Aβ plaques with high affinity (Yang et al., 2005, Garcia-Alloza et al., 2007, Begum et al., 2008). Curcumin has two tautomeric structures, the keto and enol forms, which can convert spontaneously from one to another. Structure-activity

relationship studies have shown that the enol form is the most predominant form to bind Aβ (Balasubramanian, 2006, Reinke and Gestwicki, 2007, Yanagisawa et al., 2010). Other structural features of curcumin important for Aβ binding are the planar inflexible molecule structure and conjugated optimal length linker between two terminal aromatic ring-substituted hydrogen bond-forming groups (Balasubramanian, 2006, Reinke and Gestwicki, 2007, Begum et al., 2008). Several [18F]fluoropegyl and [18F]fluoroalkyl derivatives of curcumin (Ryu et al., 2006, Cai et al., 2011, Lee et al., 2011) have been developed for PET imaging.

[18F]fluoropropoxycurcumin can be produced by nucleophilic 18F-labeling of a tosyl derivative in one-step or two-step reactions (Ruy et al., 2006). This compound has a measured logP value of 1.84. In vitro binding assays with Aβ(1-40) aggregates have shown that fluoropropoxycurcumin has high-affinity for Aβ binding (Ruy et al., 2006). Evaluation of [18F]fluoropropoxycurcumin in healthy mice revealed that uptake in the brain is fast with suitable wash-out (Ruy et al., 2006). To improve brain uptake, the hydroxyl group on the benzene ring of [18F]fluoropropoxycurcumin was replaced with a methoxy group (Figure 2.11, Lee et al., 2011). In this same study, other [18F]fluoroalkoxycurcumin derivatives were synthesized by nucleophilic 18F-fluorination of mesyl or nosyl precursor compounds (Lee et al., 2011). In vitro evaluation of the 4-fluoropropoxy-4'-methoxycurcumin derivative showed proper binding towards Aβ(1-42) aggregates in vitro, and biodistribution studies in healthy mice showed appropriate pharmacokinetics and high initial brain uptake (Lee et al., 2011); the fluoroethoxycurcumin showed a measured logP value of 2.4 and high binding affinity towards Aβ(1-42) aggregates and Aβ plaques in transgenic mouse brain sections in vitro (Lee et al., 2011).

More advanced 4-fluoropropoxy-curcumin derivatives lack one of the two keto groups in the center of the molecule but have an *N*-methylamino or *N*,*N*-dimethylamino group on the benzene ring (Figure 2.11, Cai et al., 2011). These [18F]fluoropropoxy dibenzylideneacetone derivatives were produced by nucleophilic 18F-fluorination of mesyl or tosyl derivatives (Cai et al., 2011). In vitro studies performed with Aβ(1-42) aggregates and brain sections from transgenic APP/PS1 mice have shown that modifications to the curcumin structure do not affect Aβ binding, and the Aβ affinity of [18F]fluoropropoxy dibenzylideneacetone derivatives are in the low nanomolar range (Cai

et al., 2011). The logD value of these [^{18}F]fluoropropoxy dibenzylideneacetone derivatives is roughly 3 (Cai et al., 2011). Biodistribution studies have revealed that both compounds have higher brain uptake in healthy mice than the previous [^{18}F]fluoroalkoxy curcumin derivatives (Cai et al., 2011, Lee et al., 2011, Ruy et al., 2006). As several studies have shown, [^{18}F]curcumin derivatives are potential PET tracers for Aβ imaging, but none of the developed tracers have proceeded to clinical trials.

3. AIMS OF THE STUDY

The overall aim of this thesis was to develop ^{18}F-labeling methods for novel PET imaging tracers targeting AD pathology in the brain. These tracers were evaluated using transgenic mouse models of AD.

The specific aims of each study were as follows:

1. Develop an ^{18}F-labeling method for the preparation of a S1P$_3$-receptor tracer using the ^{19}F/^{18}F isotope exchange reaction and to determine the parameters that affect yield and SA.

2. Synthesize [^{18}F]flutemetamol using aromatic nucleophilic ^{18}F-fluorination and evaluate its suitability for imaging Aβ in a mouse model of AD.

3. Develop an ^{18}F-labeling method for the preparation of a curcumin derivative using aliphatic nucleophilic ^{18}F-fluorination followed by click reaction, focusing on stabilizing the [^{18}F]curcumin derivative from oxidation and radiolysis during the purification and formulation procedures, and to evaluate the usefulness of the [^{18}F]curcumin derivative for imaging Aβ.

4. Develop a synthesis method for the preparation of functionalized [^{18}F]nanoliposomes via nucleophilic ^{18}F-fluorination followed by thin film hydration and extrusion, and to evaluate the pharmacokinetics of these functionalized [^{18}F]nanoliposomes in a mouse model of AD.

4. MATERIALS AND METHODS

4.1. Synthesis of tracers

4.1.1. Production of ^{11}C and ^{18}F

^{11}C-Carbon was produced using the $^{14}N(p,\alpha)^{11}C$ nuclear reaction (Figure 4.1, Christman et al., 1975). To generate $[^{11}C]CO_2$, nitrogen gas was irradiated in the presence of 0.2% O_2 with 17 MeV protons and a 10 µA beam current. $[^{18}F]$Fluoride was produced using the $^{18}O(p,n)^{18}F$ nuclear reaction (Figure 4.2, Solin et al., 1988). ^{18}O-Enriched water (enrichment grade 98%, 800 µl, Hyox, Rotem Industries Ltd., Israel) was irradiated with 17 MeV protons and a 10 µA beam current. Irradiations were performed with the MGC-20 cyclotron (Efremov Scientific Research Institute for Electrophysical Apparatuses (NIIEFA), St. Petersburg, Russia) at the Åbo Akademi University Accelerator Laboratory.

4.1.2. Synthesis of $[^{11}C]PIB$ (II)

$[^{11}C]$Carbon dioxide was transferred to the synthesis device and converted to $[^{11}C]$methyl triflate (Figure 4.1., Crouzel et al., 1987, Jewett, 1992). $[^{11}C]$Methyl triflate was trapped in the acetone solution of precursor 6-OH-BTA-0 (Figure 4.1.). The reaction mixture was heated for 3 min at 80°C and then purified by semipreparative HPLC. The collected HPLC fraction was evaporated to dryness using a rotary evaporator. Finally, the end product, $[^{11}C]PIB$, was formulated in propyleneglycol/ethanol/phosphate buffer (0.1 M, pH 7.4) solution at a ratio of 2/1/14 (v/v/v).
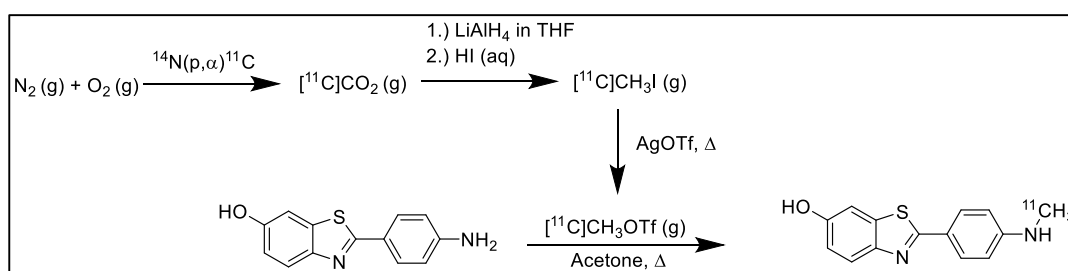
Figure 4.1. Synthesis of $[^{11}C]PIB$.

4.1.3. General ^{18}F-synthesis

^{18}F-labeling was performed using an in-house built, remote controlled device. In each synthesis, the aqueous solution of $[^{18}F]$fluoride from the cyclotron target was collected in a vessel containing a base (potassium carbonate or potassium bicarbonate) and Kryptofix

222 (Figure 4.2). Water was removed using an azeotropic distillation procedure in which acetonitrile (1 ml) was added to the solution and the liquid evaporated under a stream of helium at reduced pressure. The solution was heated at 100°C for 3 min. The distillation procedure was repeated three times, yielding a dry [^{18}F]fluoride-potassium-Kryptofix complex.
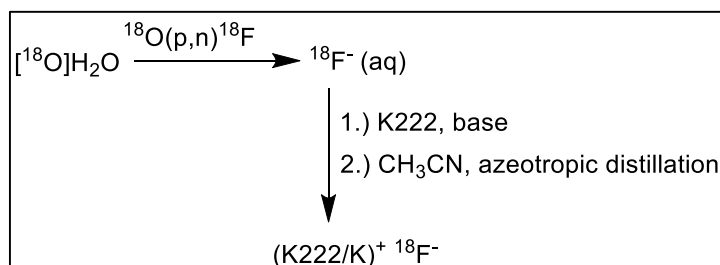
Figure 4.2. Production of [^{18}F]fluoride and the synthesis of Kryptofix 222-potassium-[^{18}F]fluoride complex.

After the ^{18}F-labeling reaction, the product was separated from the reaction mixture by semi-preparative HPLC. UV absorption and radioactivity were monitored at the outflow of the column using a UV detector and NaI(Tl) scintillation detector connected in series.

The HPLC eluent containing the end product fraction was removed by solid phase extraction. Finally, the end product was eluted from the cartridge using ethanol and formulated in a physiological solution.

4.1.4.   Synthesis of [^{18}F]flutemetamol (II)

A solution of the precursor (nitro derivative of flutemetamol) in DMSO was added to the dry residue of [^{18}F]fluoride complex (Figure 4.3.). Radiofluorination was achieved by heating the reaction mixture at 160°C for 10 min. Synthesis proceeded as described in the patent WO 2007/020400A1 (Storey et al, 2007).
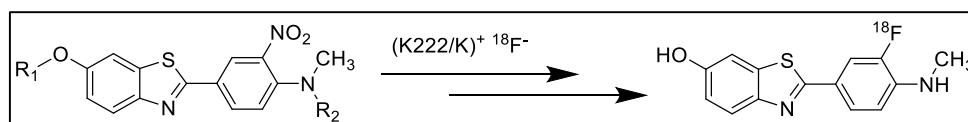
Figure 4.3. Synthesis of [^{18}F]flutemetamol.

4.1.5.   Synthesis of [^{18}F]S1P$_3$ receptor ligand (I)

[^{18}F]S1P$_3$ receptor ligand was synthesized by the ^{19}F/^{18}F isotope exchange reaction. The precursor   1-benzyl-*N*-(3,4-difluorobenzyl)-2-isopropyl-6-(2-methoxyethoxy)-1*H*-

indole-3-carboxamide was dissolved in 300 µl of DMSO. The precursor-DMSO solution was added to the dry [^{18}F]fluoride complex (Figure 4.4.). For reaction kinetics studies, the reaction mixture was heated at 170°C or 190°C with varying amounts of precursor or initial ^{18}F-activity. Aliquots were collected from the reaction mixture at intervals for up to 60 min. Starting with approximately 30 GBq of initial activity for [^{18}F]fluoride and 2 µmol of precursor, the reaction mixture was heated at 190°C for 20 min and the product purified by semipreparative HPLC.
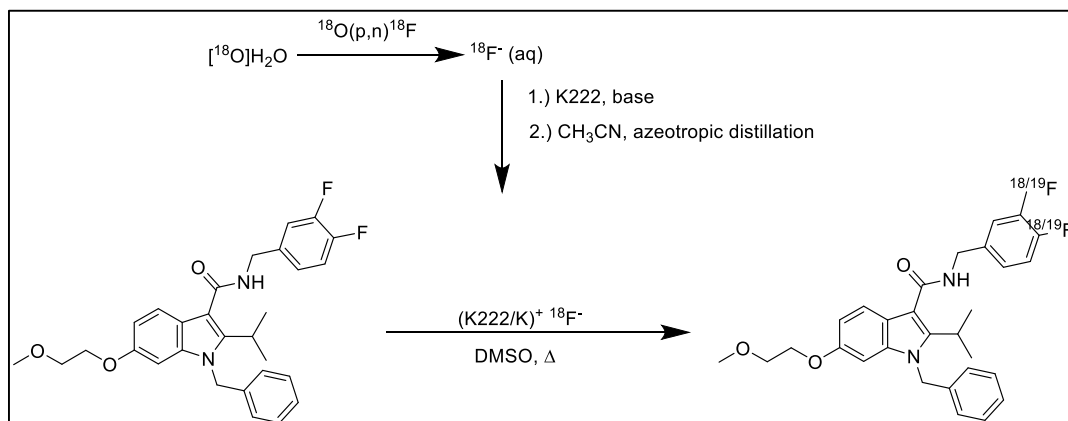
Figure 4.4. Isotope exchange reaction of [^{18}F]S1P$_3$ receptor ligand.

4.1.6. Synthesis of [^{18}F]treg-curcumin (III)

An ^{18}F-labeled curcumin derivative, [^{18}F]treg-curcumin, was synthesized using a one-pot, two-step reaction utilizing nucleophilic ^{18}F-fluorination and click chemistry (Figure 4.5.). First, 2-[2-(2-azidoethoxy)ethoxy]ethyl tosylate was dissolved in DMSO and allowed to react with the dry [^{18}F]fluoride complex. Next, 2-[2-(2-azidoethoxy)ethoxy]ethyl [^{18}F]fluoride was clicked with 2-[3,5-bis(4-hydroxy-3-methoxystyryl)-1*H*-pyrazol-1-yl]-*N*-(prop-2-yn-1-yl)acetamide in a Cu(I)-catalyzed reaction. In the purification and formulation procedures, oxidation and radiolysis of [^{18}F]treg-curcumin were inhibited by methanol-ascorbic acid or ethanol-ascorbic acid solutions.
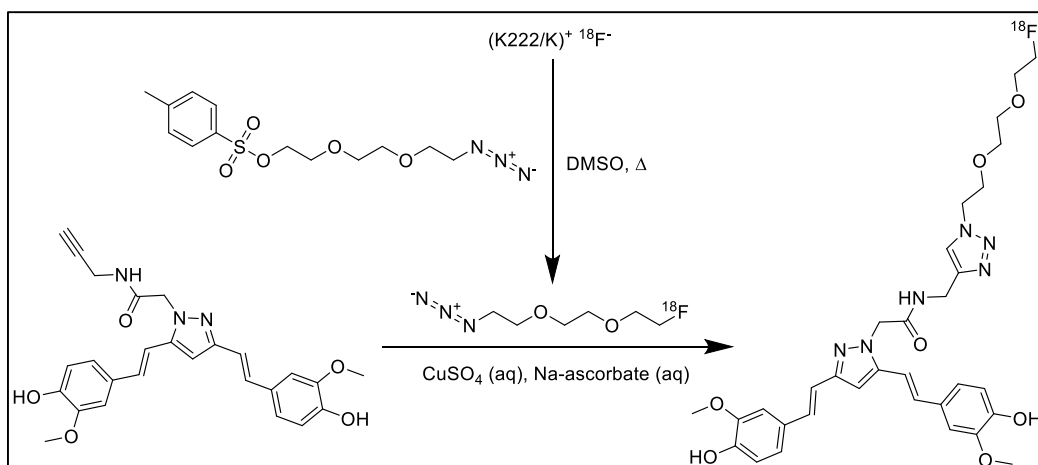
Figure 4.5. Synthesis of [^{18}F]treg-curcumin.

4.1.7. Synthesis of functionalized [^{18}F]nanoliposomes (IV)

Functionalized [^{18}F]nanoliposomes were produced by nucleophilic ^{18}F-fluorination and thin film hydration. The mesyl derivative of diacylglycerol was dissolved in DMSO and added to the dry [^{18}F]fluoride complex (Figure 4.6.). The product, [^{18}F]diacyl glycerol derivative ([^{18}F]DAG), was separated from the reaction mixture by semi-preparative HPLC.
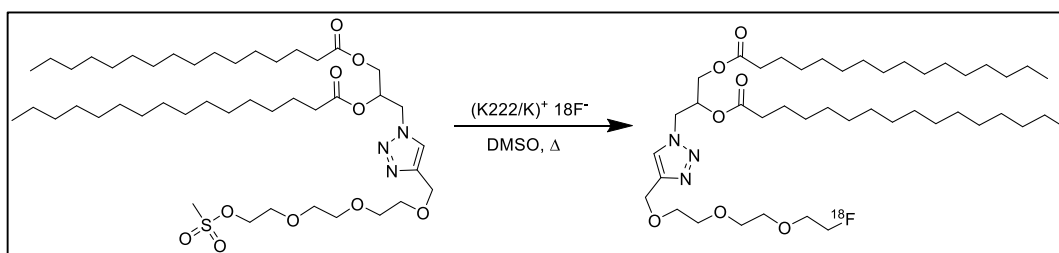
Figure 4.6. Synthesis of [^{18}F]DAG.

Monofunctionalized PA- and Curc-[^{18}F]nanoliposomes (PA- and Curc-[^{18}F]NL) were prepared using thin film hydration, by preparing a lipid solution containing cholesterol, sphingomyelin, maleimide-PEG-PE, and phosphatidic acid or curc-lipid in a molar ratio of 46.25:46.25:2.5:5, and the collected [^{18}F]DAG fraction from the preparative HPLC-column (Figure 4.7.). The particle size of the [^{18}F]liposomes was adjusted with extrusion at 55°C using a 100-nm-pore filter. Finally, these [^{18}F]nanoliposomes were purified using a PD-10 column.

In the synthesis of liposome-encapsulated [^{18}F]treg-curcumin, liposomes were produced as PA- or Curc-nanoliposomes, but without [^{18}F]DAG, and the formulation solution of

[^{18}F]treg-curcumin resulting from formulation was used as a rehydration solution (Figure 4.7.).

PA- and Curc-[^{18}F]nanoliposomes and liposomal [^{18}F]treg-curcumin were further functionalized with ApoE peptide derivative by incubating the nanoliposome solution with ApoE derivative at 37˚C for 30 min.
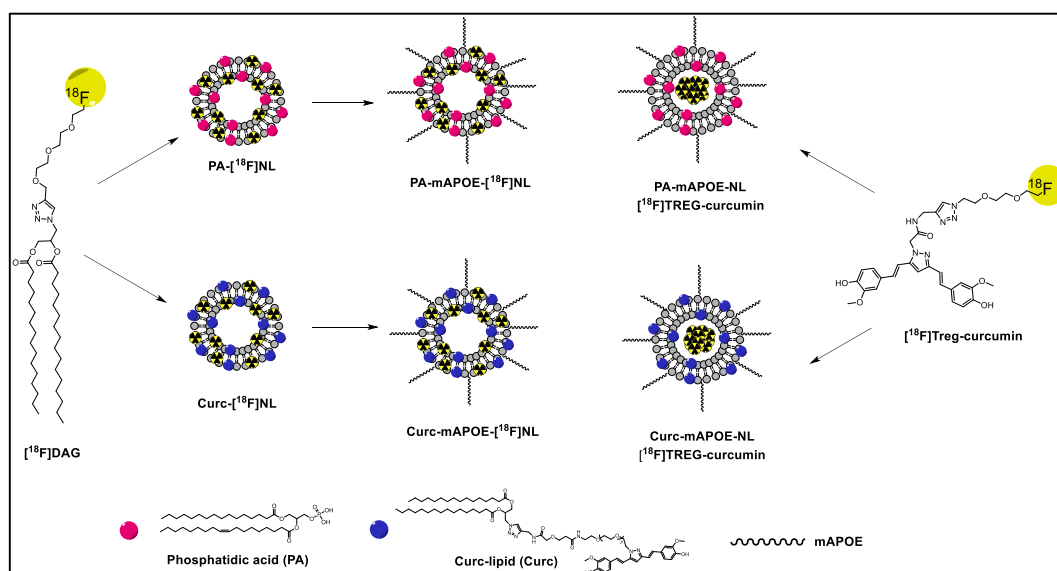
Figure 4.7. Scheme of [^{18}F]liposome syntheses. Modified from the original publication IV

4.1.8. *Analysis of PET tracers (I-IV)*

The SA, RCY, RCP, and chemical purity of the end product were analyzed using an analytical HPLC method. The concentration of the end product was analyzed by linear calibration with an authentic standard of known concentration. The HPLC fraction observed at the radioactivity detector was collected and its radioactivity measured. The cholesterol and sphingomyelin concentrations of liposome solutions were determined by an analytical HPLC method using linear calibration with an authentic standard of known concentration. The total lipid concentration of liposomes was calculated using the measured cholesterol and the molar ratio of the lipids.

RCC and RCP were also determined by a TLC method combined with digital autoradiography. TLC plates were developed using an appropriate solvent solution. Radioactivity on the plate was detected and quantified using PSL digital autoradiography.

The distribution of hydrodynamic diameters and PdI values derived using the Cumulant algorithm were measured for each liposome batch after radioactive decay. The zeta potentials and isoelectric points of the liposomes prepared in water solution were measured using the Hückel approximation and Smoluchowsky approximation, respectively. All measurements were made with a Malverin Zetasizer Nano ZS device at 25 ˚C.

4.2. Preclinical evaluation

4.2.1. Animals (II-IV)

Animal studies were performed with healthy adult male Sprague Dawley rats and healthy C57BL/6N and FVB/N mice. As animal models of AD transgenic Tg2576, APP23, and APPswe-PS1dE9 mice and corresponding wild-type (WT) control mice were also used. All animals were housed under standard conditions at the Central Animal Laboratory, University of Turku, Finland. Animal experiments were approved by the Animal Experiment Board of the Province of Southern Finland.

4.2.2. In vitro binding studies (II, III)

Binding to Aβ plaques was studied using 20-μm postmortem brain cryosections from transgenic AD and WT mice (Table 4.1.). Sections were incubated in 0.5 MBq/ml tracer in human serum albumin in phosphate buffer solution (HSA-solution) for 30 min. For heterologous competitive binding studies, non-radioactive PIB (ABX GmbH, Radeberg, Germany) was added to the incubation solution. The distribution of radioactivity in the brain sections was detected by digital autoradiography. The Aβ plaque pattern in these tissue sections was identified by thioflavin S staining.

Table 4.1. Animals and PET tracers used for preclinical in vitro evaluations in studies II and III. N = 1 for all mouse strains.

Study	Tracer	Animal strain	Age [mo]
II	[^{11}C]PIB and [^{18}F]Flutemetamol	Tg2576	16
		C57BL/6N	2
III	[^{18}F]Treg-curcumin	APP 23	18
		WT	28

4.2.3. In vivo PET imaging studies (II-IV)

The in vivo biodistribution of ^{18}F-tracers was evaluated using transgenic AD mice and WT mice (Table 4.2.). In vivo studies were performed using the Inveon Multimodality PET/ CT scanner (Siemens Medical Solutions, Knoxville, TN, USA). Animals were anesthetized and CT performed for attenuation correction and anatomical reference. Subsequently, ^{18}F-tracer was injected into a tail vein and a dynamic 60-min PET scan initiated. Data were collected in 3D list mode, divided into several time frames, and reconstructed using the 2D-filtered back-projection algorithm. Dynamic data were analyzed using the Inveon Research Workplace analysis tool v. 4 (Siemens Medical Solutions). Time-radioactivity curves were obtained for the regions of interest which were drawn after the CT image or high ^{18}F-accumulation and the results presented as percentages of the injected dose per gram of tissue (%ID/g), standard uptake values (SUVs) or as target area-to-reference area ratios.

Table 4.2. Summary of the animals used for PET experiments in studies II-IV.

Study	Tracer	Animal strain	n	Age [mo]	Injected dose [MBq]
II	[^{11}C]PIB	C57BL/6N mouse	2	2	8.5 ± 0.5
	[^{18}F]Flutemetamol	Sprague Dawley rat	4	2	32 ± 4
		C57BL/6N mouse	2	2	3.0 ± 0.5
III	[^{18}F]Treg-curcumin	APP23 mouse	2	16	3.8 ± 1.2
		WT APP23 mouse	2	25	3.8 ± 1.2
IV	[^{18}F]DAG	FVB/N mouse	1	3	4.2
	PA-[^{18}F]NL	FVB/N mouse	2	2 ; 3	5.5 ; 4.4
		APP23 mouse	2	26	5.9 ; 5.9
	Curc-[^{18}F]NL	APPswe-PS1dE9 mouse	2	6	6.8 ; 4.7
		C57 mouse	2	4	6.9 ; 4.8
	PA-mApoE-[^{18}F]NL	FVB/N mouse	2	2 ; 3	5.9 ; 5.8
		APP23 mouse	3	26	6.2 ± 0.7
	Curc-mApoE-[^{18}F]NL	APPswe-PS1dE9 mouse	1	6	4.7
		C57 mouse	2	5 ; 4	4.8 ; 6.9
	PA-mApoE-NL [^{18}F]treg-curcumin	Tg 2576 mouse	1	17	1.7
		C57 mouse	1	13	1.7
	Curc-mApoE-NL [^{18}F]treg-curcumin	APPswe-PS1dE9 mouse	1	5	7.5
		C57 mouse	1	4	7.2

4.2.4.   *Ex vivo animal studies (II-IV)*

Animals used for ex vivo biodistribution studies of tracers are listed in Table 4.3. The animals were anesthetized briefly and the tracer administered via a tail vein. Five to 60 min after tracer injection, the animals were sacrificed by CO_2 inhalation (II) and by cardiac puncture under deep isoflurane anesthesia (III, IV). The brain and other organs of interest were dissected, weighed, and evaluated for radioactivity. The measured radioactivity was corrected for decay, organ weight, and background radiation, and expressed as the percent of injected dose per gram of tissue (%ID/g) or standard uptake values (SUVs). The brains were frozen, cut into cryosections, and air dried. The distribution of radioactivity in the brain sections was detected by digital autoradiography. The Aβ plaque pattern in the brain sections was identified by thioflavin S staining. Anatomical features were detected in the brain sections by hematoxylin and eosin (HE) staining.

Table 4.3. Animals used for preclinical ex vivo evaluation of tracers in studies II-IV.

Study	Tracers	Animal strain	n	Age [mo]	Injected dose [MBq]
II	[11C]PIB	Sprague Dawley rat	19	3	32 ± 8
	[18F]Flutemetamol	Sprague Dawley rat	18	3	36 ± 7
III	[18F]Treg-curcumin	Sprague Dawley rat	1	3	34.4
		C57BL/6N mouse	1	3	9.8
IV	[18F]DAG	FVB/N mouse	2	2-3	3.3 ; 2.5
	PA-[18F]NL	FVB/N mouse	2	2-3	3.7 ; 4.6
		APP23 mouse	1	26	5.9
	Curc-[18F]NL	APPswe-PS1dE9 mouse	2	6	6.8 ; 4.7
		C57 mouse	2	4	6.9 ; 4.8
	PA-mApoE-[18F]NL	FVB/N mouse	3	2-3	4.8 ± 0.6
		APP23 mouse	2	26	5.4 ; 7.1
	Curc-mApoE-[18F]NL	APPswe-PS1dE9 mouse	1	6	4.7
		C57 mouse	2	5 ; 4	4.8; 6.9
	PA-mApoE-NL [18F]treg-curcumin	2576 mouse	1	17	1.7
		C57 mouse	1	13	1.7
	Curc-mApoE-NL [18F]treg-curcumin	APPswe-PS1dE9 mouse	1	5	7.5
		C57 mouse	1	4	7.2

4.3. Statistical analyses (I-IV)

Mean values were calculated from the individual measurements and expressed at a precision of one standard deviation (mean ± SD). Saturation binding analyses were performed using GraphPad Prism, version 2.01 (GraphPad Software, San Diego, CA, USA).

5. RESULTS

5.1. Tracer synthesis

5.1.1. Synthesis of [^{18}F]S1P$_3$-receptor ligand (I)

The [^{18}F]S1P$_3$ receptor ligand was synthesized using the ^{19}F/^{18}F isotope exchange reaction. A high temperature was needed to start the reaction. A long reaction time at a high temperature increased the RCC (as well as the RCY) and SA until precursor degradation, which limited this increase. Increasing the amount of precursor also increased the RCC but simultaneously decreased the SA (Figure 5.1A and 5.1C.). The initial ^{18}F-activity had only a minor impact on the SA (Figure 5.1D.). The best RCY was achieved with moderately low initial ^{18}F-activity (Figure 5.1B.). Starting with 2 µmol of precursor and 30 GBq of initial ^{18}F-activity, the [^{18}F]S1P$_3$ tracer was purified from the reaction mixture after heating at 190˚C for 20 min. The average RCY for the [^{18}F]S1P$_3$ tracer was $1.0 \pm 0.5\%$, the SA was 0.36 ± 0.19 GBq/µmol, and the RCP exceeded 98% (EOB, n = 16).
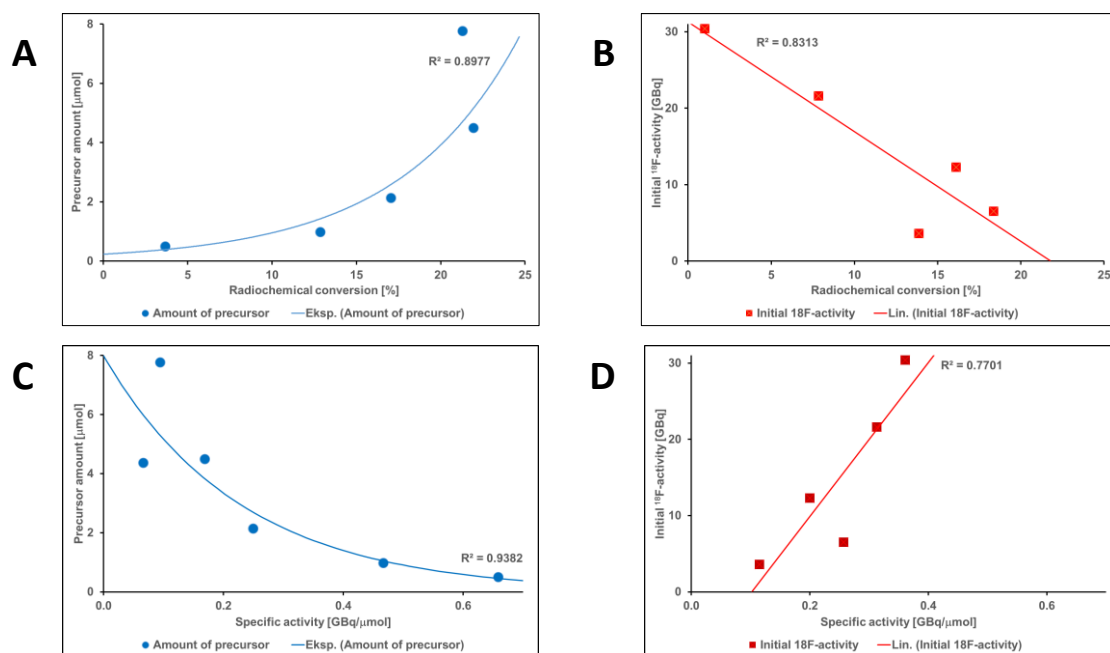
Figure 5.1. The amount of precursor is presented as a function of radiochemical conversion (A) and specific activity (C) using a reaction time of 15 min. Initial ^{18}F-activity as a function of radiochemical yield (B) and specific activity (D) using a reaction time of 20 min. All syntheses were performed at 190˚C. Values at 30 GBq are average values (n=16) from the production of [^{18}F]S1P$_3$ receptor ligand. Modified from the original publication I.

5.1.2. Synthesis of [¹¹C]PIB and [¹⁸F]flutemetamol (II)

[¹¹C]PIB was synthesized using [¹¹C]methyl triflate produced from [¹¹C]carbon dioxide. The SA of [¹¹C]PIB was 50 ± 11 GBq/µmol and the RCP more than 95% (EOS, n=13). [¹⁸F]Flutemetamol was produced using nucleophilic ¹⁸F-fluorination. The average SA of [¹⁸F]flutemetamol was more than 1 TBq/µmol and the RCP exceeded 98% (EOS, n=10).

5.1.3. [¹⁸F]Treg-curcumin (III)

[¹⁸F]Treg-curcumin was synthesized using a one-pot, two-step synthesis. After radiofluorination of the tosyl precursor, the RCY of 2-[2-(2-azidoethoxy)ethoxy]ethyl [¹⁸F]fluoride was $77 \pm 10\%$ (EOB, n = 9). Without intermediate purification, a click-reaction was performed using *in situ* prepared Cu(I) as the catalyst for the reaction. The non-optimized RCY of [¹⁸F]treg-curcumin was $21 \pm 11\%$ (EOS), the RCP was more than 99.3%, and the SA higher than 1 TBq/µmol (EOS, n = 9).

5.1.4. Synthesis of [¹⁸F]nanoliposomes (IV)

[¹⁸F]DAG was produced using nucleophilic ¹⁸F-fluorination of the mesyl precursor. Synthesis time was approximately 45 min. The RCY of [¹⁸F]DAG was $18 \pm 9\%$ (EOB), the SA more than 1 TBq/µmol, and the RCP exceeded 95% (EOS, n = 18).

Functionalized [¹⁸F]nanoliposomes (Table 5.1.) were produced using thin film hydration, extrusion, and purification. ¹⁸F-fluorine was introduced into the liposomes using [¹⁸F]DAG or [¹⁸F]treg-curcumin. [¹⁸F]Nanoliposomes were further functionalized with mApoE. The functionalization had no effect on the RCP. No other analysis was performed after mApoE functionalization.

Table 5.1. The radioactivity concentration (RAC), radiochemical purity (RCP), lipid concentration, hydrodynamic diameter (dH), polydispersity index (PdI), zeta (ζ) potential, and isoelectric point (pHIEP) of liposomes. The ζ potential and isoelectric point were measured for liposomes prepared in water solution. All measurements were made at 25°C. Modified from the original publication IV.

Liposome	n	RAC [MBq/ml]	RCP [%]	c(lipids) [μmol/l]	dH [nm]	PdI	ζ-potential [mV]	pHIEP
PA-[^{18}F]NL	10	160 ± 110	> 95	11 ± 6	133 ± 22	0.12	-75.2 ± 1.4	2.0
PA-NL [^{18}F]treg-curcumin	1	10.3	> 99	30	263	0.32		
Curc-[^{18}F]NL	3	130 ± 120	> 96	18 ± 3	237 ± 3	0.39	-73.4 ± 1.7	2.5
Curc-NL [^{18}F]treg-curcumin	1	56	>98	8	390	0.40		

5.2. Preclinical evaluation of Aβ tracers (I, III)

5.2.1. *In vitro binding studies (II, III)*

In vitro binding studies were performed using postmortem brain cryosections from transgenic AD and WT mice to evaluate the binding of tracer to fibrillar Aβ. The binding of [^{18}F]treg-curcumin in APP23 mouse brain sections and histochemical staining indicated that the Aβ plaque patterns were compatible with [^{18}F]treg-curcumin binding. With [^{11}C]PIB and [^{18}F]flutemetamol, the binding of tracers in Tg2576 mouse brain sections was comparable to the histochemical staining of Aβ plaques. In all cases, tracers binding Aβ in AD mouse brain sections were displaced by adding non-radioactive PIB to the incubation solution. Displacement with PIB was successful and did not change the binding of these tracers in the white matter. The high IC$_{50}$ (100 μM) of PIB determined for fibrillar Aβ using [^{18}F]treg-curcumin suggests that the binding site of [^{18}F]treg-curcumin is not strictly associated with the high-affinity binding site of PIB. The non-specific uptake in the AD mouse brain was low with [^{11}C]PIB and [^{18}F]treg-curcumin but relatively high with [^{18}F]flutemetamol.

5.2.2.   *Biodistribution studies (II, III)*

The biodistribution of tracers in rats and mice was studied using in vivo and ex vivo methods. The in vivo studies showed that [^{11}C]PIB and [^{18}F]flutemetamol rapidly entered the rodent brain, whereas only minor brain uptake was seen with [^{18}F]treg-curcumin, even in APP23 mice. Ex vivo digital autoradiography of Tg2576 mice revealed that [^{11}C]PIB and [^{18}F]flutemetamol bind to Aβ plaques in the brain. Non-specific binding to the white matter was relatively high with [^{18}F]flutemetamol but low with [^{11}C]PIB. With [^{18}F]treg-curcumin, accumulation in the rodent brain was observed only in the ventricles.

The peripheral biodistribution of [^{18}F]treg-curcumin and [^{18}F]flutemetamol had a similar profile in rodents. Both tracers rapidly cleared from the blood and exhibited immediate uptake into the liver. At a later phase, high and persistent accumulation of the tracers was observed in the intestine.

5.3.   Preclinical evaluation of [^{18}F]nanoliposomes (IV)

The in vivo and ex vivo biodistribution of liposomal [^{18}F]treg-curcumin revealed that these liposomal formulations were not successful in vivo, and the biodistribution results were similar to those of [^{18}F]treg-curcumin in study III.

The in vivo and ex vivo biodistribution of [^{18}F]DAG-labeled liposomes in mice varied between individuals, but no difference was seen between transgenic AD mice and control WT mice. Functionalization affected the liposome biodistribution. In blood, high amounts of PA- and Curc-[^{18}F]NLs were found 60 min after injection. The lung uptake of PA-mApoE- and Curc-mApoE-[^{18}F]NLs was high compared to the uptake of PA- and Curc-[^{18}F]NLs or [^{18}F]DAG. Liver uptake was highest with PA-mApoE- and Curc-mApoE-[^{18}F]NLs. With all [^{18}F]liposomes, the total radioactivity in the mouse brain was low.

With all [^{18}F]DAG-labeled liposomes, radioactive "hot spots" were observed in the ex vivo autoradiography images of mouse brain sections. The radioactive distribution did not match the thioflavine-positive Aβ plaque pattern in the AD mouse brain, indicating that when these liposomes pass the BBB, 60 min is too short a time for these liposomes to reach the Aβ plaques in the brain. HE staining of adjacent brain sections revealed normal brain morphology indicating that these liposomes do not cause acute neurotoxicity in the mouse brain.

6. DISCUSSION

6.1. Synthesis of PET tracers

Nucleophilic ^{18}F-fluorination is a widely used method to introduce ^{18}F-fluorine into PET precursor molecules. In this thesis, ^{18}F-labeling was achieved using nucleophilic ^{18}F-fluorination with different synthetic approaches and leaving groups. The ^{18}F-fluorination strategy affected the RCY and SA of the tracers.

6.1.1. Aromatic nucleophilic ^{18}F-fluorination synthesis (I and II)

In aromatic ^{18}F-fluorination reactions, ^{18}F-fluoride substituted a nitro group on the aryl ring (study II) or ^{19}F/^{18}F isotope exchange was used (study I). Previous studies have demonstrated that the structure of the precursor compound and substituents in the benzene ring can accelerate the reaction kinetics, though they more often reduce the reaction rate (Cacace et al., 1982, Attina et al., 1983, Cai et al., 2008, Blom et al., 2009, Shen et al., 2009, Malik et al., 2011). To some extent the substituent-induced reaction rate decline can be compensated by elevating the reaction temperature in order to increase the reaction yield as several studies have shown (Babich et al., 1996, Ryzhikov et al., 2004, Al-Labadi et al., 2006, Blom et al., 2009, Wagner et al., 2009). Thus, ^{18}F-fluorination reactions of [^{18}F]flutemetamol (study II) and [^{18}F]S1P$_3$ receptor ligand (study I) were performed under harsh conditions with elevated temperature.

In study I, the increase in reaction temperature could not fully compensate for the reduction in reactivity caused by the complicated structure of the [^{18}F]S1P$_3$ precursor, particularly the large substituent at the *para* position of the 1,2-difluorobenzene ring; thus, the RCY remained low in this synthesis. Earlier studies showed that direct ^{19}F/^{18}F isotope exchange in large aromatic compounds is challenging and, therefore, ^{19}F/^{18}F isotope exchange reactions are usually used for ^{18}F-fluorination of aromatic small molecules that have only a few substituents in the aromatic ring (Langer et al., 2003a, Langer et al., 2003b, Ryzhikov et al., 2004, Al-Labadi et al., 2006, Wagner et al., 2009, Blom et al., 2009).

An extended reaction time increased the RCC of [^{18}F]S1P$_3$ receptor ligand, but the high reaction temperature caused heat-induced degradation of the precursor and [^{18}F]S1P$_3$ tracer; eventually, this degradation limits the increase in RCY. Surprisingly, high initial

^{18}F-activity also decreased the RCC of the [^{18}F]S1P$_3$ receptor ligand. A high reaction temperature and radioactivity concentration of the reaction solution caused radiolysis and poor RCC for the [^{18}F]S1P$_3$ receptor ligand.

In the ^{19}F/^{18}F isotope exchange reaction of [^{18}F]S1P$_3$ receptor ligand, the amount of precursor affected the RCC. High RCC was achieved using high amounts of precursor, whereas low amounts of precursor yielded small amounts of [^{18}F]S1P$_3$ receptor ligand. The effect of the amount of precursor on RCY has been reported in several ^{19}F/^{18}F isotope exchange reaction studies (Cacace et al., 1982, Al-Labdi et al., 2006, Blom et al., 2009, Malik et al., 2011).

Of note, as expected from isotopic exchange reactions, the SA of the resulting labeled species remained low, due to the fact that the precursor and the labeled compound are the same chemical entity. These values are, however, in the range of those obtained for other [^{18}F]tracers produced by ^{19}F/^{18}F isotope exchange (Table 2.2, Babich et al., 1996, Langer et al., 2003a, Langer et al., 2003b, Blom et al., 2009). Interestingly, in our reaction the initial ^{18}F-activity had only a slight impact on the SA of the [^{18}F]S1P$_3$ receptor ligand.

[^{18}F]Flutemetamol (study II) was produced using aromatic nucleophilic ^{18}F-fluorination. The initial ^{18}F-activity was produced with high SA (Solin et al., 1989), and the reaction mixture did not contain a source of ^{19}F-fluoride. Thus, the SA of the synthesized [^{18}F]flutemetamol was also high.

6.1.2.   *Aliphatic nucleophilic ^{18}F-fluorination synthesis (III and IV)*

In aliphatic ^{18}F-fluorination of [^{18}F]treg-curcumin (study III) and [^{18}F]DAG tosyl (study IV), ^{18}F-fluorine was attached to the end of the ethylene oxide chain. Tosyl and mesyl groups are good leaving groups and easy to substitute with ^{18}F-fluoride; therefore, a moderate reaction temperature and short reaction time were sufficient to achieve good RCY and high SA of the ^{18}F-labeled product.

[^{18}F]Treg-curcumin was synthesized using a one-pot synthesis with nucleophilic ^{18}F-fluorination and copper(I)-catalyzed click chemistry. In this reaction, only a small amount of copper was used and the reaction mixture was subsequently purified by preparative HPLC. Thus, the cytotoxicity of copper was not anticipated to be a major problem. The click-reaction was performed at room temperature to preserve [^{18}F]treg-curcumin from

degradation. During synthesis, the combination of alcohol and ascorbic acid stabilized and decreased the oxidative decomposition and radiolysis of [^{18}F]treg-curcumin. Thus, [^{18}F]treg-curcumin was synthesized with high RCP and RCY. The high RCP of [^{18}F]treg-curcumin was maintained for up to 6 hours when it was kept in the formulation solution. However, the chemical purity of [^{18}F]treg-curcumin was poor due to closely eluting non-radioactive curcumin derivatives in preparative HPLC, which could not be properly separated from the desired labeled species. High SA values were achieved.

6.1.3. *Synthesis of ^{18}F-labeled nanoliposomes (IV)*

[^{18}F]Nanoliposomes were produced using two different labeling methods. In the first approach, [^{18}F]DAG was incorporated in the core lipid of the liposome; in the second approach, [^{18}F]treg-curcumin was encapsulated inside the liposome. In both approaches, ^{18}F-labeling was done before liposome synthesis and, therefore, high RCY of the ^{18}F-labeling process were required.

Incorporation of ^{18}F-activity into the liposomes using [^{18}F]DAG was straightforward, as [^{18}F]DAG mixed well with the other lipids. The spontaneously formed liposomes incorporated [^{18}F]DAG relatively well as measured by the total radioactivity of the liposomes. Good ^{18}F incorporation has also been reported in other studies that used a similar labeling approaches (Malik et al., 2007, Emmetiere et al., 2013). The RCY was higher when [^{18}F]DAG was used as the ^{18}F-fluorination compound for liposomes than when [^{18}F]treg-curcumin was encapsulated inside the liposomes. Spontaneously formed liposomes can encapsulate only a small fraction of the [^{18}F]treg-curcumin present in the rehydration solution. With [^{18}F]treg-curcumin, liposomal incorporation also depends on the lipid content and size of the liposomes. Encapsulation of [^{18}F]treg-curcumin was more effective with Curc-NLs than with PA-NLs. This difference may originate from repulsion or attraction between [^{18}F]treg-curcumin and lipids or size of liposomes. A low encapsulating efficiency was reported in other studies in which a PET tracer was encapsulated inside liposomes (Hatakana et al., 2010, Medina et al., 2011, Benezra et al., 2012).

Thin film hydration is a simple and robust method for producing liposomes and easy to adapt for different methodologies because the technique has only two steps: evaporation and hydration. Thin film hydration was used in study IV to produce [^{18}F]nanoliposomes

for preliminary animal studies. Of note, a more refined method would be required for large-scale liposome synthesis. Reproducibility of the thin film hydration method was not good, as seen in the varying lipid and radioactivity concentrations, especially in [^{18}F]treg-curcumin encapsulation. More refined methods (Buboltz and Feigenson, 1999, Otake et al., 2001, Pons et al., 1993, Zhigaltsev et al., 2012) may lead to more controlled and reproducible liposome sizes. Such refined methods require more advanced equipment and automation, not available in our lab during execution of the experiments.

[^{18}F]Liposome analysis revealed that liposomes stabilized the radioactive compounds, and no radiolysis of [^{18}F]DAG or [^{18}F]treg-curcumin was observed. Radioactivity did not cause liposome destruction, as observed in the particle size analysis. All of the prepared liposomes were anionic with high ζ potential, indicating that these liposomes should be relatively stable in water solutions. [^{18}F]Treg-curcumin encapsulation increases the hydrodynamic size of the liposomes, which may be the result of the large size of [^{18}F]treg-curcumin. Although mApoE may change the surface properties, previous studies have shown that mApoE on the surface of liposomes does not significantly affect the size or ζ potential of liposomes (Re et al., 2011, Taylor et al., 2011). The hydrodynamic diameter or ζ potential of mApoE-functionalized liposomes was not measured.

6.2. Preclinical evaluation of tracers (II-IV)

6.2.1. Preclinical evaluation of [^{18}F]flutemetamol and [^{18}F]treg-curcumin (II, III)

Several tracers have been developed for Aβ imaging in AD research and diagnostics (Rowe and Villemagne, 2013). In this thesis, two potential ^{18}F-labeled tracers are presented for Aβ plaque imaging, [^{18}F]flutemetamol (study II) and [^{18}F]treg-curcumin (study III). Both of these ^{18}F-labeled tracers were evaluated in healthy rodents and transgenic mouse models of AD.

The structures of [^{18}F]flutemetamol and the curcumin-like moiety of [^{18}F]treg-curcumin match the properties important for BBB penetration and Aβ plaque binding (Balasubramanian, 2006, Reinke and Gestwicki, 2007, Wu et al., 2008, Begum et al., 2008, Reinke and Gestwicki, 2011). Both of these tracers have a planar structure with double bond conjugations through the center of the compound that bridge two aromatic rings. Similar conjugation through the center of the molecule is also observed in other Aβ tracers, such as [^{11}C]PIB, [^{18}F]AZD4694, [^{18}F]florbetaben, and [^{18}F]florbetapir. In

[^{18}F]treg-curcumin, the distance between the two phenyl rings is longer than in [^{18}F]flutemetamol and other potential Aβ tracers, but this longer linker should also be more favorable for Aβ plaque binding (Balasubramanian, 2006, Reinke and Gestwicki, 2007, Begum et al., 2008). To further enhance the Aβ binding properties of [^{18}F]treg-curcumin, the pyrazole ring has been used to create an enol form arrangement, which is the predominant configuration of curcumin in Aβ binding (Balasubramanian, 2006, Reinke and Gestwicki, 2007, Yanagisawa et al., 2010). In [^{18}F]flutemetamol, the *N*-methyl group of aniline forms hydrogen bonds with the hydrophobic pocket of Aβ, enhancing binding capacity (Lockhart et al., 2005, Wu et al., 2008).

[^{18}F]Flutemetamol and [^{18}F]treg-curcumin both bind strongly to the Aβ plaques of transgenic mouse brain in vitro. The non-specific binding of [^{18}F]flutemetamol is relatively high due to its lipophilicity, whereas the non-specific binding of [^{18}F]treg-curcumin was surprisingly low, as the calculated logP (ClogP 3.0) of [^{18}F]treg-curcumin suggests high lipophilicity. Both [^{18}F]flutemetamol and [^{18}F]treg-curcumin were displaced when an excess of PIB was added to the incubation solution. The results of the displacement study of [^{18}F]treg-curcumin suggest that the binding sites of [^{18}F]treg-curcumin and PIB are not exactly the same. Structure-activity relationship studies also confirmed that PIB and curcumin share one Aβ binding site, but both of these compounds have at least one binding site of their own (Reinke and Gestwicki, 2007). The conclusion of the in vitro studies is that both [^{18}F]flutemetamol and [^{18}F]treg-curcumin have suitable binding behavior in vitro for preclinical Aβ imaging.

In vivo and ex vivo studies showed that [^{18}F]flutemetamol has suitable kinetics for preclinical PET imaging; it penetrates the BBB fast and washes out from the rodent brain relatively quickly. The addition of fluorine to the thioflavine-based structure increased the lipophilicity, as shown in ex vivo rat brain sections in study II. The ElogD for flutemetamol is 3.2, which is much higher than the measured logP of 1.2 for [^{11}C]PIB (Mathis et al., 2003b, Juréus et al., 2010). A high non-specific binding of [^{18}F]flutemetamol has been observed in preclinical in vivo studies; this leads to a decreased sensitivity, hampering potential utilization for Aβ imaging (Snellman et al., 2014).

[^{18}F]flutemetamol showed higher accumulation in transgenic AD mouse brain than in age-matched wild-type mouse brain. [^{18}F]flutemetamol binding in transgenic AD mouse brain was dependent on the animal model (Snellman et al., 2014). Similar observations have been made with [^{11}C]PIB (Klunk et al., 2005, Toyama et al., 2005, Maeda et al., 2007, Snellman et al., 2013).

In vivo and ex vivo studies of [^{18}F]treg-curcumin revealed low penetration of the BBB in rodents. The small amount of ^{18}F-activity observed in vivo in PET imaging of mouse brains after [^{18}F]treg-curcumin administration was localized in the ventricles. The low brain uptake is surprising, because The ClogP of [^{18}F]treg-curcumin (ClogP 3.0) is within the optimal range for BBB penetration (Levin, 1980, Pardridge, 2012). Similar logP values have been measured for other Aβ-[^{18}F]tracers (Agdeppa et al., 2001, Zhang et al., 2005, Juréus et al., 2010, Cai et al., 2011, Lee et al., 2011). Of note, the curcumin-like moiety of [^{18}F]treg-curcumin is similar to the curcumin derivative CBN-001. Both of these compounds have a pyrazole ring that replaces the dicarbonyl structure of curcumin, but CBN-001 has a phenyl ring as a substituent in the pyrazole ring. CBN-001 can pass the BBB in rodents (Maher at al., 2010), suggesting that the substituted pyrazole structure does not inhibit BBB penetration. A fluoropegylated tail can be found in several compounds, such as the fluoropegylated curcumin derivatives and stilbene analogs [^{18}F]florbetaben and [^{18}F]florbetapir, and all these compounds penetrate the BBB in rodents (Zhang et al., 2005, Ruy et al., 2006, Lee et al., 2011, Swahn et al., 2012, Rominger et al., 2013). The molecular weight of [^{18}F]treg-curcumin is higher than that of related compounds (Zhang et al., 2005, Ruy et al., 2006, Lee et al., 2011, Swahn et al., 2012, Rominger et al., 2013), and it is in the range considered to limit passage across the BBB (Levin, 1980, Pardridge, 2012). In conclusion, observations of the molecular structure suggest an inability of [^{18}F]treg-curcumin to penetrate the BBB due to high molecular weight and the large non-aromatic group attached to the pyrazole ring.

6.2.2. Preclinical evaluation of [^{18}F]nanoliposomes (IV)

Some variation in [^{18}F]nanoliposome biodistribution was observed between individual mice. In biodistribution studies, the same radioactive dose was injected into the mice; therefore, injected liposome volumes and masses were different. High liposome masses induce RES easier leading to fast clearance from the blood (Moghimi et al., 2001).

The preclinical evaluation of liposomes encapsulating [^{18}F]treg-curcumin showed that these liposomes were not useful in mice. The [^{18}F]treg-curcumin solution inside the liposome contained approximately 10 % ethanol, which may degrade the liposome core or cause liposomal leakage. The position of [^{18}F]treg-curcumin on the liposome was not thoroughly characterized, and [^{18}F]treg-curcumin may not have been encapsulated completely inside the liposome; rather, it may have been bound to the surface of the liposomes by electrostatic interaction or hydrogen bonding. These interactions may be strong enough to hold [^{18}F]treg-curcumin on the surface of the liposome during the purification protocol, but after administration into the body [^{18}F]treg-curcumin may detach from the liposomes.

In mice, the biodistribution of [^{18}F]DAG was different from [^{18}F]DAG-labeled liposomes. The functional groups of [^{18}F]liposomes affect the biodistribution. High ^{18}F-activity was observed in the blood one hour after the injection of PA- and Curc-[^{18}F]NLs, indicating that these liposomes are relatively stable in vivo. The mApoE-functionalized [^{18}F]liposomes accumulated mainly in the lungs. In addition to the BBB, the lungs also express LDL receptors (Yao et al., 2012), which may explain the high retention of mApoE-functionalized [^{18}F]liposomes in the lungs. These mApoE-functionalized [^{18}F]liposomes also had higher uptake in the liver than PA- and Curc-[^{18}F]NLs, whereas low ^{18}F-activity was observed in the blood. Although previous studies reported that mApoE functionalization did not notably increase the hydrodynamic diameter or ζ potential of mApoE-functionalized liposomes (Re et al., 2011, Taylor et al., 2011), the biodistribution results suggest that PA- and Curc-mApoE-[^{18}F]NLs may be larger or form agglomerates which induce RES activation (Allen and Chonn, 1987, Levchenko et al., 2002, Li and Huang, 2008). High accumulation in the liver, spleen, lungs, and kidneys has also been observed with other PET-liposomes (Marik et al., 2007, Urakami et al., 2007, Devaraj et al., 2009).

Biodistribution studies and ex vivo mouse brain autoradiography studies have shown that only a small fraction of the total radioactivity accumulates in the brain one hour after [^{18}F]liposome injection. The mApoE functionalization increased [^{18}F]liposome brain-to-blood ratios but the fast metabolism of these [^{18}F]liposomes limited the [^{18}F]liposome accumulation in the brain. In the AD mouse brain, the distribution of ^{18}F-radioactivity did not match the Aβ plaques seen in the thioflavine-stained sections. In a previous study with

the 200-nm liposomes it was shown that liposomes distribute slowly in the rat brain (MacKay et al., 2005) which suggests that also [^{18}F]liposomes need more than one hour to reach their targets.

6.3. Utility of tracers

In studies I-IV, new ^{18}F-labeled PET tracers [^{18}F]flutemetamol, [^{18}F]S1P$_3$ receptor ligand, and [^{18}F]curcumin derivative, as well as four functionalized [^{18}F]nanoliposomes, were introduced for preclinical studies of AD. All of these compounds might be used to study the pathology and treatment of AD and other diseases. Collected information can benefit the pharmaceutical industry and clinics in the development of new drugs and more accurate diagnostic methods.

In study I, a [^{18}F]S1P$_3$ receptor ligand was synthesized for S1P$_3$ receptor studies. This labeling method was used for preclinical applications starting with approximately 10 GBq of initial ^{18}F-activity and 2 μmol of precursor. The preclinical evaluation of the [^{18}F]S1P$_3$ receptor ligand reveals the suitability of the [^{18}F]S1P$_3$ receptor ligand for S1P$_3$ receptor imaging if the low SA of [^{18}F]S1P$_3$ tracer enables the use of this tracer. For further studies, the development of an alternative ^{18}F-synthesis route will be beneficial because it could increase the SA of this [^{18}F]S1P$_3$ receptor ligand. If preclinical evaluation proves that the [^{18}F]S1P$_3$ receptor ligand has a specific affinity towards the S1P$_3$ receptor, it will allow the study of the involvement of S1P$_3$ receptor in the formation and progression of AD and other CNS disorders, as well as cardiovascular diseases in which S1PRs are involved.

[^{18}F]Flutemetamol had promising properties as a preclinical PET tracer (study II), and since then [^{18}F]flutemetamol has been studied for preclinical imaging in several AD mouse models (Snellman et al., 2014). [^{18}F]Flutemetamol is an ^{18}F-fluorine derivative of PIB that shares the same drawbacks as PIB. Both of these tracers can only be used for animal imaging studies in certain transgenic AD mouse models (Klunk et al., 2005, Toyama et al., 2005, Maeda et al., 2007, Snellman et al., 2013, Snellman et al., 2014). [^{18}F]Flutemetamol has also had promising results in clinical studies and is one of the potential new ^{18}F-tracers for Aβ PET imaging in humans (Rowe and Villemagne, 2013).

The importance of the reaction conditions and reagents used for synthesis was observed during the synthesis of [^{18}F]treg-curcumin (study III). By carefully choosing the reaction, purification, and formulation conditions, the chemical and radiolytic decomposition of

[^{18}F]treg-curcumin was inhibited. These observations can be utilized when new curcumin derivatives are synthesized. In vitro studies of [^{18}F]treg-curcumin revealed that [^{18}F]treg-curcumin has very high and specific binding towards Aβ plaques. Thus, curcumin derivatives should be studied further as potential tracers for Aβ imaging. Good pharmacokinetic properties of [^{18}F]treg-curcumin combined with high Aβ binding show that this tracer and its derivatives could be appropriate probes for peripheral plaque imaging.

Nanoliposomes are the focus of drug delivery studies and imaging agent research studies (Lammers et al., 2010, Liu and Welch, 2012, Allen and Cullis, 2013, Lai et al., 2013, Qin et al., 2013). In this thesis, two different approaches are presented that can be utilized for pharmacokinetic studies of functionalized nanoliposomes. Although the functional groups targeted Aβ and aimed to enhance BBB penetration, the developed synthesis approaches allow the functional group to be changed easily. These approaches can be utilized to study the effects of the functional group on the pharmacokinetics of the liposome. With the second approach, the encapsulation efficiency of the functionalized liposomes can be studied, as well as the in vivo stability of the encapsulated liposomes. Both of these synthetic approaches can be used in studies of various liposome applications.

6.4. Future aspects

AD is one of the leading disease among elderly people in Western countries. Currently, no curative treatment is available for AD. Thus, as the number of elderly people increases, WHO predicts that there will be approximately 115 million AD patient in the world by the year 2050 which means that the number of AD patient will increase 225% in next 40 years (Duthey, 2013).

The Aβ cascade is one of the leading AD pathophysiology hypotheses. Several PET tracers have been developed for Aβ imaging in AD (Nordberg et al., 2010, Rowe and Villemagne, 2013). With the help of new imaging tracers, such as [^{18}F]flutemetamol, new information on the progression of AD and distribution of Aβ can be obtained. However, the ultimate question has not been answered – what triggers the Aβ cascade?

To answer this question, more information is needed from the earlier stages of the Aβ cascade. To gather this information, new PET tracers with specific binding towards Aβ

oligomers are needed. As seen in study III and other studies (Ruy et al., 2006, Cai et al., 2011, Lee et al., 2011), the curcumin derivatives have high Aβ plaque binding. Curcumin has also been shown to bind Aβ peptides and oligomers (Yang et al., 2005, Begum et al., 2008). The next step may be to develop a tracer that binds Aβ before plaques are formed. Curcumin derivatives may be good candidates for this purpose. By gathering knowledge on the early stages of the Aβ cascade, new potential drug targets can be found that may prevent the progression of AD.

Yet, AD is not all about Aβ. As Dr. Alzheimer discovered in 1906, neurofibrillary tangles are also among the Aβ plaques in the AD brain. These neurofibrillary tangles are formed by phosphorylation of tau protein, and the events related to this phenomenon are called the tau cascade. Currently, [^{18}F]FDDNP is a tracer used for neurofibrillary tangle imaging (Kepe et al., 2013). In addition, new PET tracers are in the development phase for imaging studies of the tau cascade (Shao et al., 2012, Harada et al., 2013, Hashimoto et al., 2014, Villemagna et al., 2014). The tau and Aβ cascades have been speculated to be linked together (Karran et al., 2011), so studying both of these cascades is important to find the factors that ultimately trigger AD.

In addition to the Aβ and tau cascades, several other pathogenetic mechanisms have been related to AD (Nordberg et al., 2010, Serrano-Pozo et al., 2011). Various studies have been performed to study AD-related neuroinflammation (March, 2014, Villemagne and Okamura, 2014, Zimmer et al., 2014). Most of these PET studies aimed at imaging the translocator protein (TSPO), but tracers for new inflammation targets are also currently under development (March, 2014, Villemagne and Okamura, 2014, Zimmer et al., 2014). The S1P$_3$ receptor has also been associated with the inflammation processes. By studying the involvement of the S1P$_3$ receptor in the inflammation processes, new AD drug targets may be discovered.

In recent years, multimodality imaging has been of interest to researchers. PET/CT and PET/MR scanners are currently in use, but no multimodality imaging agents are available. Nanoparticles have a large surface-to-volume ratio and can be used as a platform for multimodality agents by functionalizing these particles with several different functional groups. A few attempts have already been made to create nanoparticle-based multimodality agents (Devaraj et al., 2009, Abou et al., 2013, Li et al., 2012) and the research around this subject is ongoing. Because liposomes are biocompatible and easy

to prepare, modify, and functionalize they are suitable platform for multimodality imaging agents and thus the liposome research has also expand from the medicinal sector to the imaging sector.

7. CONCLUSIONS

The major conclusions of the work presented in this thesis are:

1. $[^{18}F]S1P_3$ receptor ligand can be synthesized through the $^{19}F/^{18}F$ isotope exchange reaction. During synthesis development, the yield of the $[^{18}F]S1P_3$ receptor ligand was observed to be in proportion to the amount of precursor and inversely proportional to the initial ^{18}F-activity. The SA of $[^{18}F]S1P_3$ receptor ligand decreases in proportion to the amount of precursor, whereas the initial ^{18}F-activity had only a slight effect on the SA of the radiotracer.

2. $[^{18}F]$Flutemetamol can be produced using the aromatic ^{18}F-fluorination reaction with high SA. Preclinical evaluation in experimental animals showed that $[^{18}F]$flutemetamol binds to the Aβ plaques in transgenic AD mice in vitro and is a suitable Aβ tracer for preclinical imaging.

3. $[^{18}F]$Treg-curcumin can be synthesized in a two-step reaction using aliphatic nucleophilic ^{18}F-fluorination and a click reaction. The reaction and purification conditions impact the yield and RCP. Therefore, moderate heat over a short period of time was used for nucleophilic ^{18}F-fluorination, and the click reaction was performed at room temperature. Radiolysis and oxidation of $[^{18}F]$treg-curcumin can be inhibited by alcohol and ascorbic acid in the purification and formulation solutions. $[^{18}F]$Treg-curcumin, which was produced with good RCY, high SA, and high RCP, binds Aβ in the transgenic AD mouse brain in vitro but has low penetration of the BBB in mice and rats.

4. Functionalized $[^{18}F]$nanoliposomes can be produced using two different ^{18}F-fluorination approaches, thin film hydration, and extrusion. In the first ^{18}F-fluorination approach, $[^{18}F]$DAG, the core lipid of nanoliposomes was synthesized using nucleophilic ^{18}F-fluorination. In the second approach, $[^{18}F]$treg-curcumin was encapsulated inside the nanoliposome. Preclinical evaluation of functionalized $[^{18}F]$nanoliposomes in experimental animals showed that the functional group affected the biodistribution of the nanoliposome. Monofunctionalized $[^{18}F]$nanoliposomes were found in the blood 60 min after injection, but mApoE-$[^{18}F]$nanoliposomes accumulated in the lungs. The total

brain uptake of all [^{18}F]nanoliposomes was low. The in vivo stability of [^{18}F]treg-curcumin liposomes was low.

8. ACKNOWLEDGEMENTS

to work with you. Thank you also for the great memories from the several journeys we have shared. I also want to thank Francisco Lopez-Picon for his constructive comments and suggestions, and Aake Honkaniemi, Elisa Riuttala, and Marko Vehmanen for their assistance in the preclinical work.

I thank the leaders of the Radiopharmaceutical chemistry laboratory, Jörgen Bergman and Sarita Forsback, as well as Olli Eskola, Eveliina Arponen, Miika Lehtinen, and Semi Helin for giving me the opportunity to be involved in routine radiotracer production; all of you have taught me numerous things related to tracer production for patients and I am thankful for the time you have given me. Riikka Kivelä, Anna Kirjavainen, Paula Lehtiniemi, Nina Sarja, Pertti Lehikoinen, Tapio Viljanen, Cheng-Bin Yim, Hanna-Maarit Seikkula, Juha Seikkula, Piritta Saipa, Enni Saksa, Riikka Purtanen, Jani Uotinen, Laura Auranen, I thank you for all the practical advices and helpful suggestions. I would also like to thank all of you, the personnel of radiochemistry, for the joyful moments that we have shared outside the laboratory.

I thank Sven-Johan Heselius, Stefan Johansson, Per-Olof Eriksson, Erkki Stenvall, and Johan Rajander, the personnel at the Accelerator Laboratory of Åbo Akademi University, for faultless radionuclide production. I also thank Esa Kokkomäki Simo Vauhkala, and Timo Saarinen for their development of devices, automatization, and maintenance. Without MacGyvers like you this research could not have been done. Nina Lauren and Margit Åhman-Kantola are acknowledged for their help with ordering and disposal of chemicals. I also thank Marja-Liisa Pakkanen for cleaning up my messes, as well as many laughs during coffee breaks. I also wish to thank Tarja Marttila and Mirja Jyrkinen for looking after my service agreements.

My greatest gratitude I owe to my family, to my farther Jarmo and my brother Jaakko, as well as my true-life idols, Grandmothers Raila and Marjatta. Thank you for all your love, care, and support. Together, you were my rock, by believing in me, even when I did not believe in myself. I am also grateful to all my dear friends for the love, tenderness, consolation, and marvelous happyhappyfunfun times.

Turku, January 2015

Johanna Pokka

9. REFERENCES

Abou D, Thorek D, Ramos N, Pinkse M, Wolterbeek H, Carlin S, Beattie B, Lewis J. [89]Zr-Labeled paramagnetic octreotide-liposomes for PET-MR imaging of cancer. Pharm Res 2013;30:878–888.

Agdeppa ED, Kepe V, Liu J, Flores-Torres S, Satyamurthy N, Petric A, Cole GM, Small GW, Huang SC, Barrio JR. Binding characteristic of radiofluorinated 6-dialkylamino-2-naphthylethylidene derivatives as positron emission tomography imaging probes for β-amyloid plaques in Alzheimer's disease. J. Neurosci. 2001;21:RC189(1-5).

Agdeppa ED, Kepe V, Satyamurthy P, Liu J, Huang SC, Small G, Cole G, Barrio J. In vitro detection of (S)-naproxen and ibuprofen binding to plaques in the Alzheimer's brain using the positron emission tomography molecular imaging probe 2-(1-{6-[(2-[^{18}F]fluoroethyl)(methyl)amino]-2-naphthyl}ethylidene)malononitrile. Neuroscience 2003;117:723–730.

Al-Labadi A. Zeller KP, Machulla HJ. Synthesis of 6 - [^{18}F]fluoroveratraldehyde by nucleophilic halogen exchange at electron -rich precursors. J. Radioanal. Nucl. Chem. 2006; 270:313-318.

Allen TM , Chonn A. Large unilamellar liposomes with low uptake into the reticuloendothelial system. FEBS Lett. 1987;223:42-46.

Allen TM, Cullis PR. Liposomal drug delivery system: From concept to clinical applications. Adv. Drug Deliv. Rev. 2013;65:36–48.

Alzheimer's Assosiation: Fargo K, Bleiler L: Alzheimer's association report, 2014 Alzheimer's disease facts and figures. Alzheimers Dement 2014; 10:e47-e92.

Attina M, Cacace F, Wolf A. Displacement of a nitro-group by [^{18}F]fluoride ion. A new route to aryl fluorides of high specific activity. J. Chem. Soc., Chem. Commun. 1983;3:108-109.

Aubin-Tam ME, Hamad-Schifferli K. Structure and function of nanoparticle-conjugates. Biomed. Mater. 2008;3:1–17.

Babich JW, Rubin RH, Graham WA, Wilkinson RA, Vincent J, Fischman AJ. [^{18}F]-Labeling and biodistribution of the novel fluoro-quinolone antimicrobial agent, trovafloxacin (CP 99,219). Nucl Med Biol 1996;23:995-998.

Balasubramanian K. Molecular orbital basis for yellow curry spice curcumin's prevention of Alzheimer's disease. J. Agric. Food Chem. 2006;54:3512-3520.

Bana L, Minniti S, Salvati E, Sesana S, Zambelli V, Cagnotto A, Orlando A, Cazzaniga E, Zwart R, Scheper W, Masserini M, Re F. Liposome bi-functionalized with phosphatidic acid and an ApoE-derived peptide affect Aβ aggregation features and cross blood-brain-barrier: Implications for therapy of Alzheimer disease. Nanomedicine: NBM 2013 http://dx.doi.org/10.1016/j.nano.2013.12.001.

Bangham A, Standish M, Watkins J. Diffusion of univalent ions across the lamellae of swollen phospholipids. J. Mol. Biol. 1965;13:238-252.

Baskin J, Prescher J, Laughlin S, Agard N, Chang P, Miller I, Lo A, Codelli J, Bertozz C. Copper-free click chemistry for dynamic in vivo imaging. Proc Natl Acad Sci USA 2007;14:16793-16797.

Beard RL, Yuan H, Donello JE, Liu X, Duong T. 6-Substituted indole-3-carboxylic acid amide compounds having sphingosine-1-phosphate (S1P) receptor antagonist biological activity. US Patent Application Publication US 2008/0171772 A1 17.7.2008.

Begum AN, Jones MR, Lim GP, Morihara T, Kim P, Heath DD, Rock CL, Pruitt MA, Yang F, Hydspeth B, Hu S, Faull KF, Teter B, Cole GM, Frautschy SA. Curcumin structure-function, bioavailability, and efficacy in models of neuroinflammation and Alzheimer's disease. J. Pharm. Exp. Ther. 2008;326:196-208.

Benezra M, Hambardzumyan D, Penate-Medina O, Veach DR, Pillarsetty N, Smith-Jones P, Phillips E, Ozawa T, Zanzonico PB, Longo V, Holland EC, Larson SM, Bradbury MS. Fluorine-labeled dasatinib nanoformulations as targeted molecular imaging probes in a PDGFB-driven murine glioblastoma model. Neoplasia. 2012;14:1132-1143.

Berridge M, Tewson T, Welch M. Synthesis of 18F-labeled 6-and 7-fluoropalmitic acids. Int J Appl Radiat Isot 1983;34:727-730.

Blackman M, Royzen M, Fox J. The tetrazine ligation: fast bioconjugation based on inverse- electron-demand Diels-Alder reactivity. J Am Chem Soc 2008;130:13518-13519.

Blom E, Karimi F, Långström B. [^{18}F]/[^{19}F] exchange in fluorine containing compounds for potential use in

[18]F-labelling strategies. J Label Compd Radiopharm 2009;52:504–511.

Braak H, Braak E. Frequency of stages of Alzheimer-related lesions in different age categories. Neurobiol Aging 1997;18:351-357.

Bubolzt W, Feigenson J. A novel strategy for the preparation of liposomes: rapid solvent exchange. Biochim. Biophys. Acta 1999;1417:232-245.

Cacace F, Speranza M, Wolf AP, Fowler JS. Labelling of fluorinated aromatics by isotopic exchange with [18F]fluoride. J Label Compd Radiopharm 1981; 27:1721–1730.

Cacace F, Speranza M, Wolf AP, Macgregor RR. Nucleophilic aromatic substitution; kinetics of fluorine-18 substitution reactions in polyfluorobenzenes. Isotopic exchange between $^{18}F^-$ and polyfluorobenzenes in dimethylsulfoxide. A kinetic study. J Fluor Chem 1982; 21:145–158.

Cai L, Lu S, Pike W. Chemistry with [18F]fluoride ion. Eur. J. Org. Chem. 2008:2853–2873.

Cai M, Ono M, Kimura H, Liu B, Saji H. Synthesis and structure-affinity relationships of novel dibenzylideneacetone derivates as probes for β-amyloid plaques. J Med Chem 2011;54:2225-2240.

Campbell-Verduyn L, Mirfeizi L, Schoonen A, Dierckx R, Elsinga P, Feringa B. Strain-promoted copper-free "click" chemistry for ^{18}F radiolabeling of Bombesin. Angew. Chem. Int. Ed. 2011;50:11117–11120.

Carpenter R, Hausner S, Sutcliffe J. Copper-Free Click for PET: Rapid 1,3-Dipolar Cycloadditions with a Fluorine-18 Cyclooctyne. ACS Med. Chem. Lett. 2011;2:885−889.

Choi SR, Golding G, Zhuang Z, Zhang W, Lim N, Hefti F, Benedum TE, Klibourn MR, Skovronsky D, Kung HF. Preclinical properties of 18F-AV-45: A PET agent for Aβ plaques in the brain. J Nucl Med 2009;50:1887-1894.

Chrishti MA, Yang DS, Janus C, Phinney AL; Horne P, Pearson J, Strome R, Zuker N, Loukides J, French J, Turner S, Lozza G, Grilli M, Kunicki S, Morissette C, Paquette J, Gervais F, Bergeron C, Fraser PE, Carlson GA, St. George-Hyslop P, Westaway D. Early-onset amyloid deposition and cognitive deficient in transgenic mice expressing a duuple mutant form of amyloid precursor protein 695. J. Biol. Chem. 2001;276:21562-21570.

Christman DR, Finn RD, Karlstrom KI, Wolf AP. The production of ultra high activity ^{11}C-labeled hydrogen cyanide, carbon dioxide, carbon monoxide and methane via the $^{14}N(p,\alpha)^{11}C$ reaction (XV). Int J Appl Radiat Isot 1975;26:435–442.

Couttas T, Kain N, Daniels B, Lim XY, Shepherd C, Kril J, Pickford R, Li H, Garner B, Don AS. Loss of the neuroprotective factor Sphingosine 1-phosphate early in Alzheimer's disease pathogenesis. Acta Neuropathol Commun. 2014;2:9.

Crouzel C, Långström B, Pike V. Recommendations for a practical production of [11C]methyl iodide. Appl Radiat Isot 1987;38:601-603.

Cselényi Z, Jönhagen ME, Forsberg A, Halldin C, Julin P, Schou M, Johnström P, Varnäs K, Svensson S, Farde L. Clinical validation of 18F-AZD4694, an amyloid-β-specific PET radioligand. J Nucl Med 2012;53:415-424

Cui Z, Lockman PR, Atwood CS, Hsu CH, Gupte A, Allen DD, Mumper RJ. Novel D-penicillamine carrying nanoparticles for metal chelation therapy in Alzheimer's and other CNS diseases. Eur J Pharm Biopharm. 2005;59:263-272.

Culbert PA, Adam MJ, Hurtado ET, Huser JMA, Jivan S, Lu J, Ruth TJ, Zeisler SK. Automater synthesis of [18F]FDG using tetrabutylammonium bicarbonate. Appl Radiat Isot 1995;46:887-891.

Davis M, Clemens J, Macdonald T, Lynch K. Sphingosine 1-phosphate analogs as receptor antagonists. J Biol Chem 2005;280:9833-9841.

Deamer D, Bangham A. Large volume liposomes by an ether vaporization method. Biochim. Biophys. Acta 1976;443:629-634

Devaraj N, Keliher E, Thurber G, Nahrendorf M, Weissieder R. ^{18}F labeled nanoparticles for in vivo PET-CT imaging. Bioconjug Chem 2009;20:397-401.

Devaraj N, Thurber G, Keliher E, Marinelli B, Weissleder R. Reactive polymer enables efficient in vivo bioorthogonal chemistry. Proc Natl Acad Sci USA 2012;109:4762–4767.

Doane T, Chuang CH, Hill R, Budra C. Nanoparticle ζ –Potentials. Acc. Chem. Res 2012;45:317–326.

Duthey B. Background paper 6.11 Alzheimer Disease and other dementias. Update on 2004 background paper. WHO website. http://www.who.int/medicines/areas/priority_medicines/BP6_11Alzheimer.pdf. Published 23.2.2013. Accessed 5.10.2014.

Edwards K, Bauemner A. Analysis of liposomes. Talanta 2006;68:1432-1441.

Emmetiere F, Irwin C, Viola-Villegas NT, Longo V, Cheal SM, Zanzonico P, Pillarsetty N, Weber WA, Lewis JS, Reiner T. ^{18}F-Labeled-bioorthogonal liposomes for in vivo targeting. Bioconjugate Chem 2013;24:1784−1789.

Garcia-Alloza M, Borrelli LA, Razkalne A, Hyman BT, Bacskai BJ. Curcumin labels amyloid pathology in vivo, disrupts exiting plaques, and partially restores distorted neutrites in an Alzheimer mouse model. J. Neurochem. 2007;102:1095-1104.

Gatley SJ, Shaughnessy WJ. Synthesis of ^{18}F-3-deoxy-3-fluoro-D-glucose wit reactor-produced ^{18}F. Int J Appl Radiat Isot 1980;31:339-341.

Glaser M, Årstad E. "Click labeling" with 2-[^{18}F]fluoroethylazide for positron emission tomography. Bioconjugate Chem. 2007;18:989-993.

Gobbi M, Re F, Canovi M, Beeg M, Gragori M, Sesana S, Sonnino S, Brogioli D, Musicanti C, Gasco P, Salmona M, Masserini ME. Lipid-based nanoparticles with high binding affinity for amyloid-β_{1-42} peptide. Biomaterials 2010;31:6519-6529.

Grierson JR, Shields AE. Radiosynthesis of 3'-deoxy-3'-[^{18}F]fluorothymidine: [^{18}F]FLT for imaging of cellular proliferation in vivo. Nucl Med Biol 2000;27:143-156.

Haaparanta M, Grönroos T, Eskola O, Bergman J, Solin O. Planar chromatographic analysis and quantification of short-lived radioactive metabolites from microdialysis fractions. J. Chromatogr. A 2006;1108:136-139.

Hamacher K, Coenen H, Stocklin G. Efficient stereospecific synthesis of no-carrier-added 2-[^{18}F]-fluoro-2-deoxy-D-glucose using aminopolyether supported nucleophilic substitution. J Nucl Med 1986;27:235-238.

Hanaor D, Michelazzi M, Leonelli C, Sorrella C. The effects of carboxylic acids on the aqueous dispersion and electrophoretic deposition of ZrO2. J Eur Ceram Soc 2012;32:235–244.

Hao ZF, Cui YX, Li MH, Du D, Liu MF, Tao HQ, Li S, Cao FY, Chen YL, Lei XH, Wang L, Zhu DL, Peng HS, Jiang CL. Liposomes modified with P-aminophenyl-α-D-mannopyranoside: A carrier for targeting cerebral functional regions in mice. Eur. J. Pharm. Biopharm 2013;84:505-516.

Harada R, Okamura N, Furumoto S, Tago T, Maruyama M, Higuchi M, Yoshikawa T, Arai H, Iwata R, Kudo Y, Yanai K. Comparison of the binding characteristics of [^{18}F]THK-523 and other amyloid imaging tracers to Alzheimer's disease pathology. Eur J Nucl Med Mol Imaging 2013;40:125-132.

Hardy J, Selkoe DJ. The amyloid hypothesis of Alzheimer's disease: Progress and problems on the road to therapeutics. Science 2002;297:353-356.

Hashimoto H, Kawamura K, Igarashi N, Takei M, Fujishiro T, Aihara Y, Shiomi S, Muto M, Ito T, Furutsuka K, Yamasaki T, Yui J, Xie L, Ono M, Hatori A, Nemoto K, Suhara T, Higuchi M, Zhang MR. Radiosynthesis, photoisomerization, biodistribution, and metabolite analysis of 11C-PBB3 as a clinically useful PET probe for imaging of Tau pathology. J Nucl Med 2014 pii: jnumed.114.139550.

Hashizume K, Tamakawa H, Hashimoto N, Miyake Y. Single-step synthesis of [18F]haloperidol from the chloro-precursor and its applications in PET imaging of a cat's brain. Appl Radiat lsot 1997;48:1179-1185.

Hatakana K, Asai T, Koide H, Kenjo E, Tsuzuku T, Harada N, Tsukada H, Oku N. Development of double-stranded siRNA labeling method using positron emitter and its in vivo trafficking analyzed by positron emission tomography. Bioconjugate Chem. 2010;21:756–763.

Hla T, Brinkmann V. Sphingosine 1-phosphate (S1P) Physiology and effects of S1P receptor modulation. Neurology 2011;76(Suppl 3):S3-S8.

Hoyte RM, Zhang JX, Lerum R, Oluyemi A, Persaud P, O'Connor C, Labaree DC, Hochberg RB. Synthesis of halogen-substituted pyridyl and pyrimidyl derivatives of [3,2-c]pyrazolo corticosteroids: strategies for the development of glucocorticoid receptor mediated imaging agents. J Med Chem 2002;45:5397-5405.

Hsiao K, Chapman P, Nilsen S, Eckman C, Harigaya Y, Younkin S, Yang F, Cole G. Correlative memory deficits, Abeta elevation, and amyloid plaques in transgenic mice.Science 1996;274:99-102.

Huang FY, Chen WJ, Lee WY, Lo ST, Lee TW, Lo JM. In vitro and in vivo evaluation of lactoferrin-conjugated liposomes as a novel carrier to improve the brain delivery. Int. J. Mol. Sci. 2013;14:2862-2874.

Huisgen R. 1,3-Dipolar Cycloadditions. Past and Future. Angew. Chem. Intern. Edit. 1963;2:565-598.

Huwiler A, Pfeilschifter J. New players on the center stage: sphingosine 1-phosphate and its receptors as

drug targets. Biochem Pharmacol. 2008;75:1893-900.

Ikonomovic MD, Klunk WE, Abrahamson EE, Mathis CA, Price JC, Tsopelas ND, Lopresti BJ, Ziolko S, Bi W, Paljug WR, Debnath ML, Hope CE, Isanski BA, Hamilton RL, DeKosky ST. Post-mortem correlates of in vivo PiB-PET amyloid imaging in a typical case of Alzheimer's disease. Brain 2008;131:1630-1645.

Immordino ML, Dosio F, Cattel L. Stealth liposomes: review of the basic science, rationale, and clinical applications, existing and potential. Int J Nanomedicine 2006;1:297–315.

Jankowsky JL, Slunt HH, Gonzales V, Jenkins NA, Copeland NG, Borchelt DR APP processing and amyloid deposition in mice haplo-insufficient for presenilin 1. Neurobiol Aging. 2004;25:885-892.

Jaruszewski KM, Curran GL, Swaminathan SK, Rosenberg JT, Grant SC, Ramakrishnan S, Lowe VJ, Poduslo JF, Kandimalla KK. Multimodal nanoprobes to target cerebrovascular amyloid in Alzheimer's disease brain. Biomaterials 2014;35:1967-1976.

Jensen AT, Binderup T, Andresen T, Kjær A, Rasmussen P. PET imaging of liposomes labeled with an [18F]-fluorocholesteryl ether probe prepared by automated radiosynthesis. J Liposome Res 2012;22:295-305.

Jesorka A and Orwar O. Liposomes: Technologies and analytical applications. Annu. Rev. Anal. Chem. 2008;1:801–832.

Jewett DM. A simple synthesis of [^{11}C]methyl triflate. Int J Rad Appl Instrum A. 1992;43:1383-1385.

Juréus A, Swahn BM, Sandell J, Jeppson F, Johnson AE, Johnström P, Neelissen JAM, Sunnemark D, Farde L, Svensson SPS. Characterization of AZD4694, a novel fluorinated Aβ plaque neuroimaging PET radioligand. J. Neurochem. 2010;114:784-794.

Kahn MG, Konde E, Dossou F, Labaree DC, Hochberg RB, Hoyte RM. Microwave-enhanced nucleophilic fluorination in the synthesis of fluoropyridyl derivatives of [3,2-c]pyrazolo-corticosteroids, potential glucocorticoid receptor-mediated imaging agents. Bioorg Med Chem Lett 2006;16:3454-3458.

Kang SH, Oh SJ, Yoon MK, Ryu JS, Lee WK, Choi SJ, Park KP, Moon DH. Simple and high radiochemical yield synthesis of 2'-deoxy-2'-[^{18}F]fluorouridine via a new nosylate precursor. J Label Compd Radiopharm 2006;49:1237–1246.

Kang CM, Koo H-J, Lee S, Lee KC, Oh Y-K, Choe YS. ^{64}Cu-Labelled tetraiodothyroacetic acid-conjugated liposomes for PET imaging of tumor angiogenesis. Nucl Med Biol 2013;40:1018-1024.

Karran E, Mercken M, De Strooper B. The amyloid cascade hypothesis for Alzheimer's disease: an appraisal for the development of therapeutics. Nat Rev Drug Discov 2011;10:698-712.

Kepe V, Bordelon Y, Boxer A, Huang SC, Liu J, Thiede FC, Mazziotta JC, Mendez MF, Donoghue N, Small GW, Barrio JR. PET imaging of neuropathology in tauopathies: progressive supranuclear palsy. J Alzheimers Dis. 2013;36:145-153.

Kikuchi H, Yamauchi H, Hirota S. A spray-drying method for mass production of liposomes. Chem. Pharm. Bull. 1991;39:1522-1527.

Kilbourn MR, Subramanian R. Synthesis of fluorine-18 labeled 1,1,-difluoro-2,2-dichloroethyl aryl ethers by ^{18}F-for-^{19}F exchange. J Label Compd Radiopharm 1990; 28:1355–1361.

Kirjavainen A, Forsback S, Grönroos T, Haavisto L, Haaparanta M, Solin O. Electrophilic addition of chlorine monofluoride for PET tracers. Mol Imaging Biol 2013;15:131-135.

Klibanov AL, Maruyama k, Torchilin VP, Huang L. Amphipatic polyethyleneglycols effectively prolong the circulation time of liposomes. FEBS Lett. 1990; 268:235–238.

Klunk WE, Bacskai BJ, Mathis CA, Kajdasz ST, McLellan ME, Frosch MP, Debnath ML, Holt DP, Wang Y, Hyman BT. Imaging Abeta plaques in living transgenic mice with multiphoton microscopy and methoxy-X04, a systemically administered Congo red derivative. J Neuropathol Exp Neurol. 2002;61:797-805.

Klunk WE, Engler H, Nordberg A, Wang Y, Blomqvist G, Holt DP, Bergström M, Savitcheva I, Huang G-f, Estrada S, Ausén B, Debnath ML, Barletta J, Price JC, Sandell J, Lopresti BJ, Wall A, Koivisto P, Antoni G, Mathis CA, Långström B. Imaging brain amyloid in Alzheimer's disease with Pittsburh compound-B. Ann Neurol 2004;55:306-319.

Klunk WE, Lopresti BJ, Ikonomovic MD, Lefterov IM, Koldamova RP, Abrahamson EE, Debnath ML, Holt DP, Huang G-f, Shao L, DeKosky ST, Price JC, Mathis CA. Binding of the positron emission tomography tracer Pittsburgh compound-B reflects the amount of amyloid-β in Alzheimer's disease brain but not in transgenic mouse brain. J. Neurosci. 2005;25:10598-10606.

Knight J, Cornelissen B. Bioorthogonal chemistry: implications for pretargeted nuclear (PET/SPECT) imaging and therapy. Am J Nucl Med Mol Imaging 2014;4:96-113.

Kulkarni P, Roney C, Antich P, Bonte F, Raghu A, Aminabhavi T. Quinoline-n-butylcyanoacrylate-based nanoparticles for brain targeting for the diagnosis of Alzheimer's disease. WIREs Nanomed Nanobiotechnol 2009;2:35-47.

Kämäräinen EL. Haaparanta M, Siitari-Kauppi M, Koivula T, Lipponen T, Solin O. Analysis of ^{18}F-labelled synthesis products on TLC plates: Comparison of radioactivity scanning, film autoradiography, and a phosphoimaging technique. Appl Radiat Isot 2006;64:1043-1047.

Lai F, Fadda AM, Sinico C. Liposomes for brain delivery. Expert Opin. Drug Deliv. 2013;10:1003-1022.

Lammers T, Kiessling F, Hennik W, Storm G. Nanotheranostics and image-guided drug delivery: Current concepts and future directions. Mol Pharm 2010;7:1899-1912.

Langer O, Mitterhauser M, Brunner M, Zeitlinger M, Wadsak W, Mayer BX, Kletter K, Müller M. Synthesis of fluorine-18-labeled ciprofloxacin for PET studies in humans. Nucl Med Biol 2003a;30:285-291.

Langer O, Mitterhauser M, Wadsak W, Brunner M, Müller U, Kletter K, Müller M. A general method for the fluorine-18 labelling of fluoroquinolone antibiotics. J Label Compd Radiopharm 2003b;46:715-727.

Lazar A, Mourtas S, Youssef I, Paizot C, Dauphin A, Delatour B, Antimisiaris S, Duyckaerts C. Curcumin-conjugated nanoliposomes with high affinity for Aβ deposits: Possible application to Alzheimer disease. Nanomedicine NBM 2013;9:712-721.

Lee I, Yang J, Lee JH, Choe YS. Synthesis and evaluation of 1-(4-[^{18}F]fluoroethyl)-7-(4´-methyl)curcumin with improved brain permeability for β-amyloid plaque imaging. Bioorg. Med. Chem. Lett. 2011;21:5765-5769.

Lehn JM, Sauvage JP. Cation and cavity selectivities of alkali and alkaline-earth "cryptates". Chem. Comm. 1971;9:440-441.

Levchenko T, Rammohan R, Lukyanov A, Whiteman K, Torchilin V. Liposome clearance in mice: the effect of a separate and combined presence of surface charge and polymer coating. Int. J. Pharm. 2002;240:95–102.

Levin VA. Relantionship of octanol/water partition coefficient and molecular weight to rat brain capillary permeability. J Med Chem 1980;23:682-684.

Levy S, Elmaleh DR, Livni E. A new method using anhydrous [^{18}F]fluorine to radiolabel 2-[^{18}F]fluoro-2-deoxy-D-glucose. J Nucl Med 1982;23:918-922.

Li SD, Huang L. Pharmacokinetics and biodistribution of nanoparticles. Mol. Pharm. 2008;5:496-504.

Li S, Goins B, Zhang L, Bao A. Novel multifunctional theranostic liposome drug delivery system: construction, characterization, and multimodality MR, near-infrared fluorescent and nuclear imaging. Bioconjug Chem 2012;23:1322-32.

Lin KJ, Hsu WC, Hsiao IT, Wey SP, Jin LW, Skovronsky D, Wai YY, Chang HP, Lo CW, Yao CH, Yen TC, Kung MP. Whole-body biodistribution and brain PET imaging with [18F]AV-45, a novel amyloid imaging agent – a pilot study. J Nucl Med 2010;37:497-508.

Liu Y, Welch MJ. Nanoparticles labeled with positron emitting nuclides: Advantages, methods, and applications. Bioconjug. Chem 2012;23:671-682.

Locke L, Mayo M, Yoo A, Williams M, Berr S. PET imaging of tumor associated macrophages using mannose coated ^{64}Cu liposomes. Biomaterials 2012;33:7785-7793.

Lockhart A, Ye L, Judd DB, Merritt AT, Lowe PN, Morgenstern JL, Hong G, Gee AD, Brown J. Evidence for the presence of three distinct binding sites for the thioflavin T class of Alzheimer's disease PET imaging agents on beta-amyloid peptide fibrils. J Biol Chem 2005;280:7677-84.

Maceyka M, Harikumar KB, Milstien S, Spiegel S. Sphingosine-1-phosphate signaling and its role in disease. Trends Cell Biol 2012;22:50–60.

MacKay JA, Deen D, Szoka Jr F. Distribution in brain of liposomes after convection enhanced delivery; modulation by particle charge, particle diameter, and presence of steric coating. Brain Res. 2005;1035:139-153.

Maeda J, Ji B, Irie T, Tomiyama T, Maruyama M, Okauchi T, Staufenbiel M, Iwata N, Ono M, Saido TC, Suzuki K, Mori H, Higuchi M, Suhara T. Lognitudinal, quantitative assessment of amyloid, neuroinflammation, and anti-amyloid treatment in a living mouse model of Alzheimer's disease enabled

by positron emission tomography. J. Neurosci. 2007;27:10957-10968.

Malik N, Voelter W, Machulla H-J, Solbach C. Radopfluorination of 2-fluoropyridines by isotopic exchange with [^{18}F]fluoride. J Radioanal Nucl Chem 2011;287:287–292.

Mandala S, Hajdu R, Bergstrom J, Quackenbush E, Xie J, Milligan J, Thornton R, Shei GJ, Card D, Keohane C, Rosenbach M, Hale J, Lynch CL, Rupprecht K, Parsons W, Rosen H. Alteration of lymphocyte trafficking by sphingosine-1-phosphate receptor agonists. Science 2002;296:346-349.

March RH. New Targets for the development of PET tracers for imaging neurodegeneration in Alzheimer disease. J Nucl Med 2014 Doi: 10.2967/jnumed.114.127811.

Marik J, Hausner SH, Fix LA, Gagnon MK, Sutcliffe JL. Solid-phase synthesis of 2-[18F]fluoropropionyl peptides. Bioconjug Chem. 2006;17:1017-1021.

Marik J, Tartis MS, Zhang JL, Fung JY. Long-circulating liposomes radiolabeled with [^{18}F]fluoropalmitin ([^{18}F]FDP). Nucl Med Biol 2007;34:165-171.

Markoutsa E, Pampalakis G, Niarakis A, Romero I, Weksler B, Couraud P-O, Antimisiaris S. Uptake and permeability of studies of BBB-targeting immunoliposomes using the hCMEC/D3 cell line. Eur J Pharm Biopharm 2011;77:265-274.

Markoutsa E, Papadia K, Giannou AD, Spella M, Cagnotto A, Salmona M, Stathopoulos GT, Antimisiaris SG. Mono and dually decorated nanoliposomes for brain targeting, in vitro and in vivo studies. Pharm Res. 2014;31:1275-1289.

Marsolais D, Rosen H. Chemical modulators of sphingosine-1-phosphate receptors as barrier-oriented therapeutic molecules. Nat Rev Drug Discov 2009;8:297-307.

Mathew A, Fukuda T, Nagaoka Y, Hasumura T, Morimoto H, Yoshida Y, Maekawa T, Venugopal K, Kumar DS. Curcumin loaded-PLGA nanoparticles conjugated with Tet-1 peptide for potential use in Alzheimer's disease. Plos One 2012;7:e32616

Mathis CA, Holt YW, Huang GF, Shao L, Debnath ML, Klunk WE. Development of ^{18}F-labelled thioflavin-T analogues as amyloid plaque imaging agents. J Label Compd Radiopharm 2003a;46:S62.

Mathis CA, Wang Y, Holt DP, Huang GF, Debnath ML, Klunk WE. Synthesis and evaluation of ^{11}C-labeled

6-substituted 2-arylbenzothiazoles as amyloid imaging agents. J Med Chem 2003b;46:2740-2754.

Mauer K, Volk S, Gerbaldo H. Auguste D and Alzheimer's disease. Lancet 1997;349:1546-49.

Medina O, Pillarsetty N, Glekas A, Punzalan B, Longo V, Gönen M, Zanzonico P, Smith-Jones P, Larson S. Optimizing tumor targeting of the lipophilic EGFR-binding radiotracer SKI 243 using a liposomal nanoparticle delivery system J Control Release 2011;149:292-298.

Mitchell N, Kalber TL, Cooper MS, Sunassee K, Chalker SL, Shaw KP, Ordidge KL, Badar A, Janes SM, Blower PJ, Lythgoe MF, Hailes HC, Tabor AB. Incorporation of paramagnetic, fluorescent and PET/SPECT contrast agents into liposomes for multimodal imaging. Biomaterials 2013;34:1179-1192.

Moghimi SM, Hunter C, Murray JC. Long-circulation and target-specific nanoparticles: theory to practice. Pharmacol. Rev. 2001; 53:283–318.

Mourtas S, Canovi M, Zona C, Aurilia D, La Ferla B, Salmona M, Nicotra F, Gobbi M, Antimisiaris SG. Curcumin-decorated nanoliposomes with very high affinity for amyloid-β1-42 peptide. Biomaterials 2011;32:1635-1645.

Mu L, Fischer C, Holland J, Becaud J, Schubiger P, Schibli R, Ametamey S, Graham K, Stellfeld T, Dinkelborg L, Lehmann L. ^{18}F-Radiolabeling of aromatic compounds using triarylsulfonium salts. Eur. J. Org. Chem. 2012:889–892

Mufamadi MS, Choonara YE, Kumar P, Modi G, Naidoo D, Ndesendo VM, du Toit LC, Iyuke SE, Pillay V. Surface-engineered nanoliposomes by chelating ligands for modulating the neurotoxicity associated with β-amyloid aggregates of Alzheimer's disease. Pharm Res. 2012;29:3075-3089.

Murakami A1, Takasugi H, Ohnuma S, Koide Y, Sakurai A, Takeda S, Hasegawa T, Sasamori J, Konno T, Hayashi K, Watanabe Y, Mori K, Sato Y, Takahashi A, Mochizuki N, Takakura N. Sphingosine 1-phosphate (S1P) regulates vascular contraction via S1P3 receptor: investigation based on a new S1P3 receptor antagonist. Mol Pharmacol. 2010;77:704-713.

Nakamura T, Asano M, Sekiguchi Y, Mizuno Y, Tamaki K, Nara F, Kawase Y, Yabe Y, Nakai D, Kamiyama E, Urasaki-Kaneno Y, Shimozato T, Doi-Komuro H, Kagari T, Tomisato W, Inoue R, Nagasaki M, Yuita H, Oguchi-Oshima K, Kaneko R, Nishi T. Synthesis and evaluation of CS-2100, a

potent, orally active and S1P(3)- sparing S1P(1) agonist. Eur J Med Chem. 2012;51:92-98.

Ni R, Gillberg PG, Bergfors A, Marutle A, Nordberg A. Amyloid tracers detect multiple binding sites in Alzheimer's disease brain tissue. Brain 2013;136:2217-2227.

Nickles RJ, de Jesus OT, Solin O, Haaparanta-Solin M. A flo-through detector for nano-curie activities encountered in HPLC analysis of PET radiopharmaceutical metabolites. IEEE Trans Nucl Sci 1992;39:2316-2321.

Nordberg A, Rinne JO, Långström B. The use of PET in Alzheimer disease. Nat. Rev. Neurol. 2010;6:78–87.

Oh SJ, Mosdzianowski C, Chi DY, Kim JY, Kang SH, Ryu JS, Yeo JS, Moon DH. Fully automated synthesis system of 3'-deoxy-3'-[^{18}F]fluorothymidine. Nucl Med Biol 2004;31:803-809.

Oku N, Yamashita M, Katayama Y, Urakami T, Hatanaka K, Shimizu K, Asai T, Tsukada H, Akai S, Kanazawa H. PET imaging of brain cancer with positron emitter-labeled liposomes Int J Pharm. 2011;403:170-177.

Olson F, Hunt CA, Szoka FC, Vail WJ, Papahadjopoulos D. Preparation of liposomes of defined size distribution by extrusion through polycarbonate. Biochim. Biophys. Acta 1979;557:9-23.

Otake K, Imura T, Sakai H, Abe M. Development of a new preparation method of liposomes using supercritical carbon dioxide. Langmuir 2001;17:3898-3901.

Pascali C, Luthra SK, Pike VW, Price GW, Aher RG, Hume SP, Myers R, Manjil L, Cremer JE. The radiosynthesis of [^{18}F]PK 14105 as an alternative radioligand for peripheral type benzodiazepin binding sites. Appl Radiat Isot 1990;41:477-482.

Pardridge WM. Drug transport across the blood-brain barrier. J. Cereb. Blood Flow Metab. 2012;32:1959-1972.

Petersen AL, Binderup T, Rasmussen P, Henriksen JR, Elema DR, Kjær A, Andresen TL. ^{64}Cu loaded liposomes as positron emission tomography imaging agents. Biomaterials. 2011;32:2334-2341.

Petersen AL, Binderup T, Jølck RI, Rasmussen P, Henriksen JR, Pfeifer AK, Kjær A, Andresen TL. Positron emission tomography evaluation of somatostatin receptor targeted ^{64}Cu-TATE-

liposomes in a human neuroendocrine carcinoma mouse model. J Control Release 2012;160:254-63.

Phelps ME. Positron emission tomography provides molecular imaging of biological processes. Proc Natl Acad Sci USA 2000;97:9226–9233.

Philippe C, Haeusler D, Mitterhauser M, Ungersboeck J, Viernstein H, Dudczak R, Wadsak W. Optimization of the radiosynthesis of the Alzheimer tracer 2-(4-N-[11C]methylaminophenyl)-6-hydroxybenzothiazole ([11C]PIB). Appl Radiat Isot 2011;69:1212-1217.

Phillips W, Goins B, Bao A. Radioactive liposomes. Rev. Nanomed. Nanobiotechnol. 2009;1:69-83.

Pike VW, Aigbirhio FI. Reactions of cyclotron-produced [^{18}F]fluoride with diaryliodonium salts – a novel single-step route to no-carrier-added [^{18}F]fluoroarenes. J. Chem. Soc., Chem. Commun. 1995:2215-2216.

Poduslo JF, Hultman KL, Curran GL, Preboske GM, Chamberlain R, Marjańska M, Garwood M, Jack CR Jr, Wengenack TM. Targeting vascular amyloid in arterioles of Alzheimer disease transgenic mice with amyloid β protein antibody-coated nanoparticles. J Neuropathol Exp Neurol. 2011;70:653-661.

Pons M, Foradada M, Estelrich J. Liposomes obtained by the ethanol injection method. Int. J. Pharm. 1993;95:51-56.

Pretze M, Pietzsch D, Mamat C. Recent Trends in Bioorthogonal Click-Radiolabeling Reactions Using Fluorine-18. Molecules 2013;18:8618-8665.

Qin S, Fite BZ, Gagnon MK, Seo JW, Curry FR, Thorsen F, Ferrara KW. A physiological perspective on the use of imaging to assess the in vivo delivery of therapeutics. Ann Biomed Eng. 2014;42:280-298.

Qu B, Li X, Guan M, Li X, Hai L, Wu Y. Design, synthesis and biological evaluation of multivalent glucosides with high affinity as ligands for brain targeting liposomes. Eur J Med Chem. 2014;72:110-118.

Re F, Cambianica I, Zona C, Sesana S, Gregori M, Rigolio R, La Ferla B, Nicotra F, Forloni G, Cagnotto A, Salmona M, Masserini M, Sancini G. Functionalization of liposomes with ApoE-derived peptides at different density affects cellular uptake and drug transport across a blood-brain barrier model. Nanomedicine. 2011a;7:551-559.

Re F, Cambianica I, Sesana S, Salvati E, Cagnotto A, Salmona M, Couraud PO, Moghimi SM, Masserini M, Sancini G. Functionalization with ApoE-derived

peptides enhances the interaction with brain capillary endothelial cells of nanoliposomes binding amyloid-beta peptide. J Biotechnol. 2011b;156:341-346.

Reinke AA, Gestwicki JE. Structure-activity relationships of amyloid beta-aggregation inhibitors based on curcumin: influence of linker length and flexibility. Chem Biol Drug Des 2007;70:206-215.

Reinke AA, Gestwicki JE. Insight into amyloid structure using chemical probes. Chem Biol Drug Des 2011;77:399-411.

Rinne JO, Brooks DJ, Rossor MN, Fox NC, Bullock R, Klunk WE, Mathis CA, Blennow K, Barakos J, Okello AA, Rodriguez Martinez de Liano S, Liu E, Koller M, Gregg KM, Schenk D, Black R, Grundman M. 11C-PiB PET assessment of change in fibrillar amyloid-beta load in patients with Alzheimer's disease treated with bapineuzumab: a phase 2, double-blind, placebo-controlled, ascending-dose study. Lancet Neurol. 2010;9:363-372.

Rominger A, Bredel M, Burgold S, Keppler K, Baumann K, Xiong G, Mille E, Gildehaus FJ, Carlsen J, Schlichtiger J, Niedermoser S, Wängler B, Cumming P, Steiner H, Herms J, Haass C, Bartenstein. Lognitudinal Assessment of cerebral β-amyloid deposition in mice overexpressing Swedish mutant β-amyloid precursor protein using ^{18}F-Florbetaben PET. J Nucl Med 2013;54:1127-1134.

Ross TL, Ermert J, Hocke C, Coenen HH. Nucleophilic ^{18}F-fluorination of heteroaromatic iodium salts with no-carrier-added [^{18}F]fluoride. J. Am. Chem. Soc. 2007;129:8018-8025.

Rowe CC, Ackerman U, Browne W, Mulligan R, Pike KL, O'Keefe G, Tochon-Danguy H, Chan G, Berlangieri SU, Jones G, Dickinson-Rowe KL, Kung HP, Zhang W, Kung MP, Skovronsky D, Dyrks T, Holl G, Krause S, Friebe M, Lehman L, Lindemann S, Dinkelborg LM, Masters CL, Villemagne VL. Imaging of amyloid beta in Alzheimer's disease with 18F-BAY94-9172, a novel PET tracer: proof of mechanism. Lancet Neurol. 2008;7:129-135.

Rowe CC, Pejoska S, Mulligan RS, Jones G, Chan JG, Svensson S, Cselényi Z, Masters CL, Villemagne VL. Head-to-head comparison of 11C-PiB and 18F-AZD4694 (NAV4694) for β-amyloid imaging in aging and dementia. J Nucl Med 2013;54:880-886.

Rowe CC, Villemagne VL. Amyloid imaging with PET in early Alzheimer disease diagnosis. Med Clin North Am 2013;97:377-398.

Ryu EK, Choe YS, Lee KH, Choi Y, Kim BT. Curcumin and dehydrozingerone derivatives: synthesis, radiolabeling, and evaluation for β-amyloid plaque imaging. J Med Chem 2006;49:6111-6119.

Ryzhikov NN, Gomzina NA, Fedorova OS, Vasil'ev DA, Kostikov AP, Krasikova RN. Preparation of [18F]Flumazenil, a potential radioligand for PET imaging of cetral benzodiazepine receptors, by isotope exchange. Radiochemistry 2004;46:290-294.

Salvati E, Re F, Sesana S, Cambianica I, Sancini G, Masserini M, Gregori M. Liposomes functionalized to overcome the blood-brain barrier and to target amyloid-β peptide: the chemical design affects the permeability across an in vitro model. Int J Nanomedicine 2013;8:1749-1758.

Sanna MG, Liao J, Jo E, Alfonso C, Ahn MY, Peterson MS, Webb B, Lefebvre S, Chun J, Gray N, Rosen H. Sphingosine 1-phosphate (S1P) receptor subtypes S1P1 and S1P3, respectively, regulate lymphocyte recirculation and heart rate. J Biol Chem 2004;279:13839-13848.

Sauer I, Dunay IR, Weisgraber K, Bienert M, Dathe M. An apolipoprotein E-derived peptide mediates uptake of sterically stabilized liposomes into brain capillary endothelial cells. Biochem. 2005;44:2021-2029.

Scheinin NM, Wikman K, Jula A, Perola M, Vahlberg T, Rokka J, Någren K, Viitanen M, Rinne JO. Cortical ^{11}C-PIB uptake is associated with age, APOE genotype, and gender in "healthy aging". J Alzheimers Dis 2014;41:193-202.

Seo JW, Zhang H, Kukis DL, Meares CF, Ferrara KW. A novel method to label preformed liposomes with ^{64}Cu for positron emission tomography (PET) imaging. Bioconjugate Chem 2008;19:2577–2584.

Seo JW, Qin S, Mahakian LM, Watson KD, Kheirolomoom A, Ferrara KW. Positron emission tomography imaging of the stability of Cu-64 labeled dipalmitoyl and distearoyl lipids in liposomes. J Control Release 2011;151:28-34.

Serrano-Pozo A, Frosch MP, Masliah E, Hyman BT. Neuropathological alterations in Alzheimer disease. Cold Spring Harb Perspect Med 2011;1:a006189.

Shao X, Carpenter GM, Desmond TJ, Sherman P, Quesada CA, Fawaz M, Brooks AF, Kilbourn MR, Albin RL, Frey KA, Scott PJ. Evaluation of [(11)C]N-methyl lansoprazole as a radiopharmaceutical for PET imaging of Tau neurofibrillary tangles. ACS Med Chem Lett 2012;3:936-941.

Shao X, Hoareau R, Runkle AC, Tluczek LJM,. Hockley BG, Henderson BD. Scott PJH. Highlighting the versatility of the Tracerlab synthesis modules. Part 2: fully automated production of [11C]-labeled radiopharmaceuticals using a Tracerlab FXC-Pro. J Label Compd Radiopharm 2011;54:819–838.

Sharma G, Modgil A, Sun C, Singh J. Grafting of cell-penetrating peptide to receptor-targeted liposomes improves their transfection efficiency and transport across blood–brain barrier model. J. Pharm. Sci. 2012;101:2468–2478.

Sharma G, Modgil A, Zhong T, Sun C, Singh J. Influence of short-chain cell-penetrating peptides on transport of Doxorubicin encapsulating receptor-targeted liposomes across brain endothelial barrier. Pharm Res 2014;31:1194-1209.

Shen B, Löffler D, Reischi G, Machulla H-J, Zeller K-P. Nucleophilic substitution of nitro groups by [^{18}F]fluoride in methoxy-substituted ortho-benzaldehydes - A systematic study. J. Fluorine Chem. 2009;130:216-224.

Shoghi-Jadid K, Small GW, Agdeppa ED, Kepe V, Ercoli LM, Siddarth P, Read S, Satyamurthy N, Petric A, Huang SC, Barrio JR. Localization of neurofibrillary tangles and beta-amyloid plaques in the brains of living patients with Alzheimer disease. Am J Geriatr Psychiatry. 2002;10:24-35.

Sim-Selley LJ, Goforth PB, Mba MU, Macdonald TL, Lynch KR, Milstien S, Spiegel S, Satin LS, Welch SP, Selley DE. Sphingosine-1-phosphate receptors mediate neuromodulatory functions in the CNS. J Neurochem. 2009;110:1191-1202.

Snellman A, López-Picón F, Rokka J, Salmona M, Forloni G, Scheinin M, Solin O, Rinne JO, Haaparanta-Solin M. Longitudinal Amyloid Imaging in Mouse Brain with ^{11}C-PIB: Comparison of APP23, Tg2576, and APP$_{swe}$-PS1$_{dE9}$ Mouse Models of Alzheimer Disease. J Nucl Med 2013;54:1434–1441.

Snellman A, Rokka J, Lopez-Picon FR, Eskola O, Salmona M, Forloni G, Scheinin M, Solin O, Rinne JO, Haaparanta-Solin M. In vivo PET imaging of beta-amyloid deposition in mouse models of Alzheimer's disease with a high specific activity PET imaging agent [^{18}F]flutemetamol. EJNMMI Research 2014;4:37 doi:10.1186/s13550-014-0037-3.

Solin O. Couting of positron-emmitting radionuclides on thin-layer chromatograms. Int J Appl Radiat Isot 1983;34:1653-1654.

Solin O, Bergman J, Haaparanta M, Reissell A. Production of ^{18}F from water targets. Specific radioactivity and anionic contaminants. Int J Appl Radiat Isot 1988;10:1065-1071.

Soliven B, Miron V, Chun J. The neurobiology of sphingosine 1-phosphate signaling and sphingosine 1-phosphate receptor modulators. Neurology 2011;76(Suppl 3):S9-S14.

Spitznagle LA, Marino CA. Synthesis of fluorine-18 labeled 21-fluoroprogesterone. Steroids 1977;30:435-438.

Stark B, Pabst G, Prassi R. Long-term stability of sterically stabilized liposomes by freezing and freeze-drying: Effect of cryoprotectants on structure. Eur. J. Pharm. Sci. 2010;41:546-555.

Storey A, Jones C, Bouvet D, Lasbistes N, Fairway S, Williams L, Gibson A, Nairne R, Karimi F, Lånström B. Fluorination process of anilide derivates and benzothiazole fluorinate derivatives as in vivo imaging agents. World Intellectual Property Organization, International publication number WO 2007/020400 A1 22.2.2007.

Sturchler-Pierrat C, Abramowski D, Duke M, Wiederhold K-H, Mistl C, Rothacher S, Ledermann B, Bürki K, Frey P, Paganetti PA, Waridel C, Calhoun ME, Jucker M, Probst A, Staufenbiel M, Sommer B. Two amyloid precursor protein transgenic mouse models with Alzheimer disease-like pathology. Proc. Natl. Acad. Sci. USA 1997;94:13287–13292.

Swahn BM, Sandell J, Pyring D, Bergh M, Jeppsson F, Juréus A, Neelissen J, Johnström P, Schou M, Svensson S. Synthesis and evaluation of pyridylbenzofuran, pyridylbenzothiazole and pyridylbenzoxazole derivatives as ^{18}F-PET imaging agents for β-amyloid plaques. Bioorg Med Chem Lett. 2012;22:4332-4337.

Swomley AM, Förster S, Keeney JT, Triplett J, Zhang Z, Sultana R, Butterfield DA. Abeta, oxidative stress in Alzheimer disease: evidence based on proteomics studies. Biochim Biophys Acta 2014;1842:1248-1257.

Szoka F, Papahadjopoulos D. Procedure for preparation of liposomes with large internal aqueous space and high capture by reverse-phase evaporation. Proc. Natl. Acad. Sci. USA 1978;75:4194-4198.

Takasugi N, Sasaki T, Suzuki K, Osawa S, Isshiki H, Hori Y, Shimada N, Higo T, Yokoshima S, Fukuyama T, Lee VM-Y, Trojanowski JQ, Tomita T, Iwatsubo T. BACE1 activity is modulated by cell-

associated sphingosine-1-phosphate. J. Neurosci. 2011;31:6850–6857.

Tanifum EA, Dasgupta I, Srivastava M, Bhavane RC, Sun L, Berridge J, Pourgarzham H, Kamath R, Espinosa G, Cook SC, Eriksen JL, Annapragada A. Intravenous delivery of targeted liposomes to amyloid-β pathology in APP/PSEN1 transgenic mice. Plos One 2012;7(10):e48515.

Taylor M, Moore S, Mourtas S, Niarakis A, Re F, Zona C, La Ferla B, Nicotra F, Masserini M, Antimisiaris SG, Gregori M, Allsop D. Effect of curcumin-associated and lipid ligand-functionalized nanoliposomes on aggregation of the Alzheimer's Aβ peptide. Nanomedicine 2011;7:541-550.

Teng E, Kepe V, Frautschy SA, Liu J, Satyamurthy N, Yang F, Chen PP, Cole GB, Jones MR, Huang SC, Flood DG, Trusko SP, Small GW, Cole GM, Barrio JR. [F-18]FDDNP microPET imaging correlates with brain Aβ burden in a transgenic rat model of Alzheimer disease: effects of aging, in vivo blockade, and anti-Aβ antibody treatment. Neurobiol Dis. 2011;43:565-575.

Tewson TJ, Welch MJ, Raichle ME. [^{18}F]-Labeled 3-deoxy-3-fluoro-D-glucose: synthesis and preliminary biodistribution data. J Nucl Med 1978;19:1339-1345.

Torchilin VP. Recent advances with liposomes as pharmaceutical carriers. Nat Rev Drug Discov 2005;4:145–160.

Toyama H, Ye D, Ichise M, Liow JS, Cai L, Jacobowitz D, Musachio JL, Hong J, Crescenzo M, Tipre D, Lu JQ, Zoghbi S, Vines DC, Seidel J, Katada K, Green MV, Pike VW, Cohen RM, Innis RB. PET imaging of brain with the beta-amyloid probe, [11C]6-OH-BTA-1, in a transgenic mouse model of Alzheimer's disease. Eur J Nucl Med Mol Imaging 2005;32:593-600.

Urakami T, Akai S, Katayama Y, Harada N, Tsukada H, Oku N. Novel amphiphilic probes for [^{18}F]-radiolabeling preformed liposomes and determination of liposomal trafficking by positron emission tomography. J Med Chem 2007;50:6454-6457.

van Rooy I, Mastrobattista E, Storm G, Hennink WE, Schiffelers RM. Comparison of five different targeting ligands to enhance accumulation of liposomes into the brain. J Control Release 2011;150:30-36.

Villemagne VL, Okamura N. In vivo tau imaging: obstacles and progress. Alzheimers Dement. 2014;10:S254-64.

Wagner A, Vorauer-Uhl K, Kreismayr G, Katinger H. The crossflow injection technique: An improvement of the ethanol injection method. J Liposome Res 2002;12:259–270.

Wagner FM, Ermert J, Coenen HH. Three-step, "one-pot" radiosynthesis of 6-fluoro-3,4-dihydroxy-L-phenylalanine by isotope exchange. J Nucl Med 2009;50:1724-1729.

Webb MS, Harasym TO, Masin D, Bally MB, Maye LD. Sphingomyelin-cholesterol liposomes significantly enhance the pharmacokinetic and therapeutic properties of vincristine in murine and human tumour models Br J Cancer 1995;72:896-904.

Welch MJ, Hawker C, Wooley K. The advantages of nanoparticles for PET. J Nucl Med 2009;50:1743-1746.

Woodbury D, Richardson E, Grigg A, Welling R, Knudson B. Reducing liposome size with ultrasound: Bimodal size distributions. J Liposome Res 2006;16:57–80.

Wu C, Wang Z, Lei H, Duan Y, Bowers MT, Shea JE. he binding of thioflavin T and its neutral analog BTA-1 to protofibrils of the Alzheimer's disease Abeta(16-22) peptide probed by molecular dynamics simulations. J Mol Biol. 2008;384:718-729.

Xu S, Olenyuk B, Okamoto C, Hamm-Alvarez S. Targeting receptor-mediated endocytotic pathways with nanoparticles: Rationale and advances. Adv. Drug Deliv. Rev. 2013;65:121-138.

Yanagisawa D, Shirai N, Amatsubo T, Taguchi H, Hirao K, Urushitani M, Morikawa S, Inubushi T, Kato M, Kato F, Morino K, Kimura H, Nakano I, Yoshida C, Okada T, Sano M, Wada Y, Wada K, Yamamoto A, Tooyama I. Relantionship between the tautomeric structures of curcumin derivatives and their Aβ-binding activities in the context of therapies for Alzheimer's disease. Biomaterials 2010;31:4179-4185.

Yang F, Lim GP, Begum AN, Ubeda OJ, Simmons MR, Ambegaokar SS, Chen P, Kayed R, Glaber CG, Frautschy SA, Cole GM. Curcumin inhibits formation of amyloid β oligomers and fibrils, binds plaques, and reduces amyloid in vivo. J. Biol. Chem. 2005;280:5892-5901.

Yao Xi, Vitek MP, Remaley AT, Levine SJ. Apolipoprotein mimetic peptides.: a new approach for the treatment of asthma. Front Pharmacol. 2012;3:Article 37.

Ying X, Wen H, Lu WL, Du J, Guo J, Tian W, Men Y, Zhang Y, Li RJ, Yang TY, Shang DW, Lou JN,

Zhang LR, Zhang Q. Dual-targeting daunorubicin liposomes improve the therapeutic efficacy of brain glioma in animals. J Control Release 2010;141:183-192.

Zhang W, Oya S, Kung MP, Hou C, Maier DL, Kung HF. F-18 polyethyleneglycol stilbenes as PET imaging agents targeting Aβ aggregates in the brain. Nucl Med Biol 2005;32:799-809.

Zeglis BM, Sevak KK, Reiner T, Mohindra P, Carlin SD, Zanzonico P, Weissleder R, Lewis JS. A pretargeted PET imaging strategy based on bioorthogonal Diels-Alder click chemistry. J Nucl Med 2013;54:1389-1396.

Zimmer ER, Leuzy A, Benedet AL, Breitner J, Gauthier S, Rosa-Neto P. In vivo tracking of tau pathology using positron emission tomography (PET) molecular imaging in small animals. Transl

ORIGINAL PUBLICATIONS